



UNIVERSITY OF
LIVERPOOL

UWB ANTENNAS FOR WIRELESS COMMUNICATIONS

by

Ping Cao

**Submitted in accordance with the requirements for the award of the
degree of Doctor of Philosophy of the University of Liverpool**

September 2013

Copyright

Copyright © 2013 Ping Cao. All rights reserved.

The copyright of this thesis rests with the Author. Copies (by any means) either in full, or of extracts, may not be made without prior written consent from the Author.

Learning is the eye of the mind

There is no end to learning

Lifelong learning

To My Parents: Shouwen Cao and Mulan Bao

To My Brother: Bin Cao

To My Sister: Mingxia Cao

Acknowledgement

First and foremost, I would like to express my deepest thanks to my supervisor, Professor Yi Huang. He has always given me valuable ideas, suggestions and comments with his insightful knowledge and rich research experience which guides me in the right direction. I am very much indebted to his efforts of helping me to complete this dissertation. I also would like to thank Dr. Xu Zhu for supporting and guiding me in my research.

I would like to thank all my brilliant colleagues, Dr. Di Li, Dr. Yang Lu, Miss. Jingwei Zhang, Ms. Neda Khiabani, Ms. Rula. Alrawashdeh, Mr. Sheng Yuan, Ms. Lei Xing, Mr. Qian Xu, Mr. Saqer S. Alja'afreh, Dr. Xin Zheng, Dr. Chattha Hassan, and Dr. Stephen Boyes, *etc.* With all your help and support, my study life becomes happy in all respects. I also would like to thank my friends for their support and friendship that I needed.

Last but not least, I am hugely grateful to my beloved family for their unconditional support and love throughout my PhD, and indeed the whole of my life. Their wisdom, love, excellent advice and support have made me who I am today and I hope that I have made them proud. Thanks my Dad for guiding and believing in me and thanks Mom for your infinite love. Thanks my brother Bin Cao and my sister Mingxia Cao, for all the fun and happiness they bring to my life. Special thanks also go to my uncle Qiang Yan for his generous support and encouragement for me to pursue my goal. Thank you all so much for everything.

Table of Contents

UWB ANTENNAS FOR WIRELESS COMMUNICATIONS.....	i
<i>Copyright.....</i>	<i>i</i>
<i>Acknowledgement.....</i>	<i>iii</i>
<i>Table of Contents.....</i>	<i>iv</i>
<i>Acronyms.....</i>	<i>vii</i>
<i>List of Figures.....</i>	<i>viii</i>
<i>List of Tables.....</i>	<i>xiv</i>
<i>Abstract.....</i>	<i>xv</i>
 CHAPTER 1 INTRODUCTION.....	 1
1.1 Research Motivations.....	1
1.1.1 A Super Wideband Antenna (SWB) Planar Monopole Antenna	2
1.1.2 A Planar UWB Antenna with Quintuple-Band-Notched Characteristics	2
1.1.3 A Planar UWB Reconfigurable Band Rejection UWB Antenna	4
1.1.4 A Planar UWB-MIMO Antenna for Wireless Applications	4
1.2 Organization of the Thesis	5
1.3 Key Contributions.....	6
1.4 List of Publications	8
1.5 References.....	10
 CHAPTER 2 BACKGROUND.....	 12
2.1 Development of UWB/SWB Antennas	12
2.1.1 Definition of UWB.....	12
2.1.2 UWB/SWB Antennas	16
2.2 Review of Band-Notched UWB Antennas	29
2.2.1 Survey on Techniques to Generate Notched Characteristics.....	29
2.2.2 Comparison of Different Approaches	36
2.3 UWB Antennas with Reconfigurable Bands Rejection	40
2.4 UWB-MIMO Antennas	45
2.4.1 Techniques to Reduce Mutual Coupling	45
2.4.2 Design Considerations.....	53
2.5 Summary.....	54
2.6 References.....	55

CHAPTER 3	PLANAR UWB/SWB MONOPOLE ANTENNA	
DESIGN.....		69
3.1	Introduction.....	69
3.2	UWB Planar Monopole Antenna Design.....	70
3.3	SWB Planar Monopole Antenna Design	76
3.3.1	<i>Antenna Configuration.....</i>	76
3.3.2	<i>Effects of the Antenna Parameters on its Performance</i>	77
3.4	Modal Analysis	82
3.4.1	<i>Impedance Performance</i>	82
3.4.2	<i>Current Distribution</i>	83
3.5	Experimental Results and Discussions	85
3.5.1	<i>Reflection Coefficients</i>	85
3.5.2	<i>Radiation Patterns</i>	86
3.5.3	<i>Peak Gains</i>	89
3.6	Summary	90
3.7	References.....	91
CHAPTER 4	DESIGN OF A PLANAR UWB ANTENNA WITH	
BAND-NOTCHED CHARACTERISITICS.....		93
4.1	Introduction.....	93
4.2	Band-Notched Antenna Design	95
4.2.1	<i>M-shaped Resonator (MSR).....</i>	95
4.2.2	<i>Structure of Antenna</i>	97
4.2.3	<i>Parametric Study.....</i>	101
4.3	Theoretical Analysis	107
4.3.1	<i>Current Distribution</i>	107
4.3.2	<i>Equivalent Circuit.....</i>	109
4.4	Results and Discussions.....	114
4.4.1	<i>Frequency-Domain Performance</i>	115
4.4.2	<i>Time-Domain Performance.....</i>	121
4.5	Summary	124
4.6	References.....	125
CHAPTER 5	DESIGN OF A PLANAR UWB ANNTENA WITH	
RECONFIGURABLE BAND REJECTION		126
5.1	Introduction.....	126
5.2	Band-Notched Antenna Design	127
5.2.1	<i>Co-directional Split Ring Resonators (CSRR).....</i>	127
5.2.2	<i>Length and Positions of the Resonator</i>	129
5.3	Antenna Integration with Switches.....	132

5.4	Theoretical Analysis	133
5.4.1	<i>Current Distribution</i>	133
5.4.2	<i>Transmission Line Model</i>	134
5.5	Results and Discussions	137
5.5.1	<i>Frequency-Domain Performance</i>	138
5.5.2	<i>Time-Domain Performance</i>	146
5.6	Summary	148
5.7	References	148

CHAPTER 6 DESIGN OF A UWB-MIMO ANTENNA FOR WIRELESS APPLICATIONS..... 150

6.1	Introduction.....	150
6.2	UWB-MIMO Antenna	151
6.2.1	<i>Antenna Configuration</i>	151
6.2.2	<i>Effects of the Distance between Two Elements</i>	153
6.2.3	<i>Current Distribution</i>	155
6.3	Mutual Coupling Reduction.....	156
6.3.1	<i>Trident-Like Slot Configuration</i>	156
6.3.2	<i>Effectiveness of the Trident-like Slot on its Performance</i>	157
6.4	Theoretical Analysis	159
6.4.1	<i>Current Distribution</i>	159
6.4.2	<i>Equivalent Circuit</i>	160
6.4.3	<i>Parametric Study</i>	162
6.5	Results and Discussions	167
6.5.1	<i>Reflection Coefficients</i>	168
6.5.2	<i>Radiation Characteristics</i>	169
6.5.3	<i>MIMO Characteristics</i>	171
6.6	Summary	173
6.7	References	173

CHAPTER 7 CONCLUSIONS AND FUTURE WORK 175

7.1	Summary	175
7.2	Future Work	177

Acronyms

AWGN	Additive White Gaussian Noise
CMA	Circular Monopole Antenna
CSRR	Co-directional Split Ring Resonator
DGS	Defected Ground Structure
DMN	Decoupling Matching Networks
EBG	Electromagnetics Band Gap
FCC	Federal Communications Commission
MIMO	Multiple-Input-Multiple-Output
MSR	M-shaped Resonator
PICA	Planar Invested Cone Antenna
PMA	Planar Monopole Antenna
SNR	Signal Noise Ratio
SIR	Stepped Impedance Resonator
SIS	Stepped Impedance Stub
SWB	Super Wideband
UWB	Ultra Wideband
WiMAX	Worldwide Interoperability Microwave Access
WLANs	Wireless Local Area Networks

List of Figures

Fig. 1.1 Power spectrum density of UWB and some narrow-band communication systems	3
Fig. 2.1 Illustration of a UWB communication system with its power spectral density	13
Fig. 2.2 FCC emission limits for indoor and outdoor UWB communication systems [4].....	15
Fig. 2.3 The earliest wideband properties antenna (Lodge's biconical antennas) (1898) [6]	16
Fig. 2.4 Some early wideband antennas	17
Fig. 2.5 Some frequency independent antennas	18
Fig. 2.6 The metal-plate monopole antenna: (a) Planar inverted cone antenna (2004) [15], and (b) Leaf-shaped plate antenna (2006) [16]	19
Fig. 2.7 The rectangular metal-plate monopole antenna (a) Offset feed (2001) [17], and (b) Short post and bevelling (2004) [19]	20
Fig. 2.8 The balanced antipodal Vivaldi antenna (a) Convectional microtrip feed (1988) [20], and (b) CPW feed (1993) [21]	21
Fig. 2.9 The printed U-shaped slot antenna (2005) [22]	21
Fig. 2.10 The PICA slot antenna (2008) [23]	22
Fig. 2.11 The elliptical slot antenna (2006) [24]	22
Fig. 2.12 The bow-tie slot antenna (2004) [25]	23
Fig. 2.13 The planar circular asymmetrical dipole antenna (2010) [26]	24
Fig. 2.14 The fractal antenna (2011) [27]	24
Fig. 2.15 The elliptical egg-shaped planar monopole antenna (2011) [29]	25
Fig. 2.16 A compact monopole antenna (2012) [30]	25
Fig. 2.17 The CPW-fed planar monopole antenna: (a) Elliptical (2007) [31], and (b) Trapezoid (2010) [32]	26
Fig. 2.18 The newly developed CPW-fed planar monopole antenna [33]	27
Fig. 2.19 Possible postions of the resonat strucure on UWB antenna.....	29
Fig. 2.20 (a) A CPW UWB antenna integrated with two inverted L slots: On the ground plane (left) and on the radiator(right) [34]	30
Fig. 2.21 The CPW-fed UWB antennas integrated (a) U-shaped slot [35], and (b) Two C-shaped slots [35]	31
Fig. 2.22 A MS-fed UWB antenna integrated with a pair of ML [41].....	32

Fig. 2.23 A UWB antenna with single band-notched function using the slots on the feeding line [42]	32
Fig. 2.24 The UWB antennas integrated with parasitic strips	33
Fig. 2.25 A UWB antenna integrated with an extended strip and a loaded strip [47]	34
Fig. 2.26 A UWB antenna integrated with SRR [49].....	34
Fig. 2.27 The UWB antenna with (a) An open-loop resonator [52], and (b) A dual-gap open-loop resonator [53]	35
Fig. 2.28 A UWB antenna with (a) EBG structure [54], (b) Unit cells of EBG [54] and (b) Equivalent circuit of the EBG [54]	36
Fig. 2.29 An elliptical UWB antenna with switchable stubs [77]	40
Fig. 2.30 A UWB planar monopole antenna with multiple-band-rejection switchable capability [86]	41
Fig. 2.31 A UWB slot antenna with multi-band-rejection switchable capability [79]	42
Fig. 2.32 A UWB circular slot antenna with multi-band-rejection switchable capability [84]	42
Fig. 2.33 3D view of the optimized structure with the neutralization line between the PIFA	46
Fig. 2.34 The structure of a printed diversity monopole antenna [90]	46
Fig. 2.35 The layout of the meander-line monopole antenna array (left), $\lambda/4$ transmission line with its equivalent circuit (middle) and LC- based branch-line coupler (right) [91].....	47
Fig. 2.36 Configuration of (a) The microstrip antenna separated four columns by the fork-like EBG, and (b) A fork-like EBG structure [94]	48
Fig. 2.37 The patch antenna array (a) Top view, (b) Size view, and (c) Unite cell of UC-EBG structure [97]	48
Fig. 2.38 Configuration of two closely-packed PIFAs with slotted ground plane structure [99].....	49
Fig. 2.39 Configuration of the dual-feed PIFA antenna with perpendicular feed [100]	50
Fig. 2.40 Configuration of the cone-shaped radiating MIMO antenna [101]	50
Fig. 2.41 Configuration of a UWB diversity antenna with two notched triangular raidaor [103]	51

Fig. 2.42 Configuration of a UWB-MIMO antenna with two circular disc raidaor elements [104].....	52
Fig. 3.1 Geometry of the circular monopole antenna.....	70
Fig. 3.2 Photograph of the circular monopole antenna	71
Fig. 3.3 Simulated and measured reflection coefficient curves of the CMA.....	72
Fig. 3.4 Simulated reflection coefficient curves of the CMA for various g	72
Fig. 3.5 Simulated reflection coefficients of the CMA for various W_{sub}	73
Fig. 3.6 Simulated total current distributions of the CMA at frequencies of (a) 3 GHz, (b) 6.5 GHz, and (c) 10.5 GHz.....	74
Fig. 3.7 Simulated radiation patterns of the CMA at 3.5 GHz (blue solid line), 6.5 GHz (red break dot line, and 10.5 GHz (black break line).....	75
Fig. 3.8 Simulated gains of the CMA.....	75
Fig. 3.9 Geometry of the proposed monopole antenna	77
Fig. 3.10 Three different models (Ants 1, 2 and 3)	78
Fig. 3.11 Simulated reflection coefficient $ S_{11} $ of Ant 3.....	79
Fig. 3.12 Simulated reflection coefficients $ S_{11} $ of the three antennas	80
Fig. 3.13 The impedance performance of the three antennas (Ants 1, 2 and 3).....	81
Fig. 3.14 The impedance performance of the three antennas (Ants 1, 2 and 3).....	83
Fig. 3.15 Modes at resonate frequencies of the SWB monopole antenna.....	84
Fig. 3.16 Photo of the proposed SWB antenna	85
Fig. 3.17 Simulated and measured reflection coefficients of Ant 3	86
Fig. 3.18 3D-far-field co-polar radiation pattern performance of Ant 3	87
Fig. 3.19 Simulated and measured radiation patterns of the SWB antenna at (a) 3.5, and (b) 12.5 GHz.....	88
Fig. 3.20 Simulated radiation patterns of the SWB antenna at (c) 25, (d) 50, and (e) 150 GHz	88
Fig. 3.21 Simulated and measured peak gains of Ant 3 (2 to 18 GHz).....	89
Fig. 3.22 Simulated peak gains of Ant 3 (20 to 200 GHz).....	90
Fig. 4.1 Geometry of the notch elements: (a) U-shaped slot, (b) Inverted U- shaped slot, and (c) M-shaped resonant	95
Fig. 4.2 Simulated reflection coefficients $ S_{11} $ of the quintuple-band- notched antenna with different L_{total} values	97

Fig. 4.3 Geometry of the proposed antenna: (a) UWB antenna, (b) Single, (c) Dual, (d) Triple, (e) Quadrduple, and (f) Quintuple-band-notched antennas	100
Fig. 4.4 Simulated reflection coefficients $ S_{11} $ of the quintuple-band-notched antenna with different W_3 values	102
Fig. 4.5 Simulated reflection coefficients $ S_{11} $ of the quintuple-band-notched antenna with different L_3	103
Fig. 4.6 Simulated reflection coefficients $ S_{11} $ of the quintuple-band-notched antenna with different L_6 values	104
Fig. 4.7 Simulated reflection coefficients $ S_{11} $ of the quintuple-band-notched antenna with different L_9 values	104
Fig. 4.8 Simulated reflection coefficients $ S_{11} $ of the quintuple-band-notched antenna with different W_{21} values	105
Fig. 4.9 Simulated reflection coefficients $ S_{11} $ of the quintuple-band-notched antenna with different L_{12} values	106
Fig. 4.10 Simulated reflection coefficients $ S_{11} $ of the quintuple-band-notched antenna with different L_{15} values	106
Fig. 4.11 Simulated suface current distributions of the quintuple-band-notched antenna at different frequncies (a) 2.45, (b) 3.54, (c) 5.49, (d) 7.53, (e) 8.47, (f) 3, (g) 6, and (h) 10 GHz	108
Fig. 4.12 Simulated input impedance of the quintuple-band-notched antenna	111
Fig. 4.13 An approximated equivalent circuit of the quintuple-band-notched antenna	111
Fig. 4.14 Transmission line model of the quintuple-band-notched antenna at (a) Passband frequencies, (b) The first notched-band, (c) The second notched band, (d) The third notched band, (e) The fourth notched band, and (f) The fifth notched band	113
Fig. 4.15 Front and back view of the prototyped proposed UWB monopole antenna (a) Without, and (b) With band-notched.....	114
Fig. 4.16 Simulated and measured reflection coefficients $ S_{11} $ of the proposed antenna without band-notched.....	115
Fig. 4.17 Simulated and measured reflection coefficients $ S_{11} $ of the quintuple-band-notched antenna	116
Fig. 4.18 Simulated co-polarized without (red solid line) and with band-notched (red break line), and Measured co-polarized without (blue dot line) and with band-notched (blue dot-dot break line)	

radiation patterns of the proposed antenna at (a) 2.45, (b) 3.54, (c) 5.49, (d) 7.53, and (e) 8.47 GHz	119
Fig. 4.19 Simulated overall/total efficiency of the quintuple band notched antenna	120
Fig. 4.20 Simulated and measured maximum realized gain values of the quintuple-band-notched monopole antenna	120
Fig. 4.21 Simulation setup of the antenna for the time-domain investigation	121
Fig. 4.22 Simulated signals of the antenna with/without notch with single impulse input signal for the side by side case	122
Fig. 4.23 Simulated signals of the antenna with/without notch with single impulse input signal for the face to face case.....	123
Fig. 5.1 Geometries of Four different CSRR filter structures	130
Fig. 5.2 Simulated reflection coefficients $ S_{11} $ of the antenna for different structures	131
Fig. 5.3 Simulated reflection coefficients $ S_{11} $ of the antenna for different values (a) W2, and (b) L2.....	132
Fig. 5.4 Topology of three pairs of switches on the radiator: Ws= 0.8 mm.....	133
Fig. 5.5 Simulated current distributions: (a) S2 OFF at 5.45 GHz, (b) S2 ON at 5.45 GHz (UWB state), and (c) S2 OFF at 8.5 GHz.....	134
Fig. 5.6 Simulated input impedance of the antenna (Structure 3).....	135
Fig. 5.7 Transmission line model for (a) CSRR structures with switches ON (passband), (b) CSRR structures with switch S3 OFF, (c) CSRR structures with switch S2 OFF, and (d) CSRR structures with switches S2 and S3 OFF.....	136
Fig. 5.8 Selected prototypes of the proposed antenna for five switching states.....	137
Fig. 5.9 Simulated and measured reflection coefficients $ S_{11} $ of the proposed antenna for switching States 1-5	141
Fig. 5.10 Simulated reflection coefficients $ S_{11} $ of the proposed antenna for switching States 6-8	142
Fig. 5.11 Simulated co-polarization (red solid line) and cross-polarization (red break line), and measured co-polarization (blue dot line) and cross-polarization (blue dot break line) radiation patterns of the proposed antenna at (a) 2.4 GHz (State 5), (b) 3.57 GHz (c) 5.5 GHz, and (d) 8.5 GHz.....	144
Fig. 5.12 Measured gains of the proposed antenna for five different switching states	145

Fig. 5.13 Simulated overall/total efficiency of the antenna for five different switching states	145
Fig. 5.14 Simulated signals of the antenna with single impulse input signal for switching States 4 and 5 in the side by side case.....	147
Fig. 5.15 Simulated signals of the antenna with single impulse input signal for switching States 4 and 5 in the face to face case	147
Fig. 6.1 Geometry of the proposed UWB-MIMO monopole antenna (Antenna 1): Front view (up) and Back view (down)	152
Fig. 6.2 Simulated and measured S parameters of Antenna 1 (without slots)	153
Fig. 6.3 Simulated S21 of Antenna 1 with different Wd values	155
Fig. 6.4 Simulated current distributions of Antenna 1 at: (a) 3.1, and (b) 10.6 GHz. Port 1 is excited; Port 2 is terminated with a 50 Ω load	156
Fig. 6.5 Geometry of the modified UWB-MIMO monopole antenna with the trident-like slot (Antenna 2)	157
Fig. 6.6 Simulated S parameters of Antenna 2	159
Fig. 6.7 Simulated surface current distributions of Antenna 2 with at the frequencies of: (a) 3.1 GHz, (b) 10.6 GHz.....	160
Fig. 6.8 The approximate equivalent circuit of Antenna 2.....	161
Fig. 6.9 Simulated S parameters of Antenna 2 for different W1 values	163
Fig. 6.10 Simulated S parameters of Antenna 2 for different L1 values.....	164
Fig. 6.11 Simulated S parameters of Antenna 2 for different L2 values.....	165
Fig. 6.12 Simulated S parameters of Antenna 2 for different W3 values	166
Fig. 6.13 Prototype of the modified UWB-MIMO antenna (Antenna 2).....	168
Fig. 6.14 Simulated and measured S parameters of Antenna 2 (with slots).....	169
Fig. 6.15 Measured radiation patterns of Antenna 2 at the frequencies of.....	170
Fig. 6.16 Simulated and measured gains of the antenna with and without slot	171
Fig. 6.17 Simulated and measured envelope correlation coefficient of Antenna 2	172

List of Tables

Table 2-1 Comparison of various SWB antennas	28
Table 2-2 Comparison of multiple band-notched UWB antennas	37
Table 2-3 UWB antennas with reconfigurable band-rejection.....	43
Table 2-4 Summarized states of the art on UWB-MIMO antennas	52
Table 2-5 Design consideration for UWB-MIMO antennas	54
Table 3-1 Optimized parameters of the SWB antenna in Fig. 3.9	78
Table 3-2 Comparion of the analyze performanes for three antennas	83
Table 4-1 Numerical and theoretical predictions for the band-notched frequency	97
Table 4-2 Dimensions in mm of the antenna shown in Fig. 4.3(a)	100
Table 4-3 Dimensions in mm of MSRs for the quintuple-band-notched antenna shown in Figs. 4.3(b-f).....	101
Table 4-4 Calculated fidelity factor for UWB antenna without and with band-notched function.....	123
Table 4-5 Comparison with the design in [75].....	125
Table 5-1 Numerical and theoretical predictions for the band-notched frequency	130
Table 5-2 Switch combinations and operational frequency bands for each state.....	139
Table 5-3 Calculated fidelity factor of the UWB antenna for switching States 4 and 5	146
Table 6-1 Summary of the effects of the slot parameters in mm on the S parameters of Antenna 2	167

Abstract

This thesis focuses on four inter-related research topics on the design and analysis of compact planar ultra wide-band (UWB) monopole antennas for future wireless communications, namely, a planar super-wide-band (SWB) monopole antenna, a planar UWB antenna with band-notched characteristics, a planar UWB antenna with reconfigurable band-rejection features, and a planar UWB multiple-input and multiple-output (MIMO) antenna.

A novel Mickey-mouse shaped planar monopole antenna with SWB performance is proposed and investigated. Three different techniques for bandwidth enhancement are implemented. The antenna is evolved from the traditional circular monopole antenna and has achieved an impedance bandwidth of more than 100:1 and a stable radiation patterns over a wider bandwidth.

The design of a compact planar UWB monopole antenna ($22 \times 34 \text{ mm}^2$), incorporated with five m-shaped resonators (MSRs) at different positions, to achieve quintuple-band-notched performance is presented. The frequency-domain performance (in term of reflection coefficients, realized gain, efficiency, and radiation pattern), and time-domain performance (in term of pulse responses and fidelity), are investigated by simulation and measurement. The results show that the proposed UWB antenna has approximately omnidirectional radiation patterns and excellent band-notched behaviours and good time domain performance with the fidelity of more than 85.5% in the pulse response.

A planar UWB monopole antenna with reconfigurable band-notched characteristics is also introduced. The band rejection is realized by incorporating two co-directional split ring resonators (CSRR) on the radiator element. Switches are added to the CSRR structures to achieve the

reconfigurability. The proposed antenna can operate at different switching states including a UWB state, single and dual band-notched states with good rejection behaviours. Good radiation patterns and gain values are also obtained for different switching states. This compact wideband antenna can be very good candidate for a wide range of mobile portable applications.

A compact planar UWB-MIMO antenna ($60 \times 45 \text{ mm}^2$) is presented for wireless applications. The wideband isolation of more than 15 dB is achieved by etching a new trident-like slot on the ground plane of the antenna. An equivalent circuit have been introduced for analysis and the diversity performances are studied. The results show that the proposed MIMO antenna is a very good candidate for wireless applications.

The study of these four special antennas has demonstrated that, using various techniques, the planar monopole antenna can be an excellent choice for a wide range of wireless communication applications.

CHAPTER 1 INTRODUCTION

1.1 Research Motivations

Many emerging wireless communication systems are aimed at providing higher data-rate transmission and more versatile services. The dramatically advancement in the wireless communication systems and the substantially increasing demand from the consumers have pushed the radio system approaching its physical limit.

Ultra-wideband (UWB) is a fast emerging technology and has become one of the most promising solutions to fulfil the requirements with uniquely attractive features such as high data rates, coexistence with existing narrowband systems, low-power consumption for the future wireless communication systems. Since the Federal Communications Commission (FCC) in the United States approved the unlicensed use of the UWB spectrum between 3.1 and 10.6 GHz, in 2002 [1], both industry and academic have paid much attention and effort in developing commercial UWB systems. The rapid development of UWB systems requires novel UWB antenna designs. Among different UWB antennas proposed in the past [2-9], the planar monopole

antenna (PMA) has attracted the most attention due to its low profile, low cost, simple fabrication, omni-directional radiation pattern and ease of integration with RF front end [10,11].

1.1.1 A Super Wideband Antenna (SWB) Planar Monopole Antenna

Various wideband antennas have been interesting subjects and have found important applications in military and civilian systems. The PMA has been a good candidate for such applications. There has been a question of how wide the bandwidth of a PMA could be. Can we make a PMA a SWB antenna? SWB technology could possibly be a potential approach to offer high-resolution sensing applications such as the ground-penetrating radar and through wall sensing. SWB radio technology has unique advantages as compared to narrowband technology, and also comprised all UWB technology features but with more channel capacity, higher precision and supper resolution in communications and ranging. Therefore, design of a compact planar monopole antenna with SWB performance is the first research topic in the thesis.

1.1.2 A Planar UWB Antenna with Quintuple-Band-Notched Characteristics

Congestion in the spectrum is becoming a serious problem in the RF and microwave spectrum, which may cause significant interference among the users and degrade the performance system involved. Since the UWB systems use a wideband of the spectrum, which could easily be interfered by the existing nearby communication systems such as the Wireless Local Area Networks (WLANs) operating at the bands of 2.45 GHz (2.4-2.484 GHz), 5.25

GHz (5.15-5.35 GHz) and 5.75-GHz (5.725-5.825 GHz), the Worldwide Interoperability for Microwave Access (WiMAX) systems operating in the 2.35 GHz (2.3-2.4 GHz), 2.6 GHz (2.5-2.69 GHz), 3.35 GHz (3.3-3.4 GHz), 3.5 GHz (3.4-3.6 GHz), 3.7 GHz (3.6-3.8 GHz) and 5.8 GHz (5.725-5.85 GHz) bands, downlink of X-band satellite communication system operating at the band of 7.25-7.75 GHz and ITU band of 8.01-8.5 GHz respectively. The relative power-spectrum density (PSD) in the UWB and some existing narrowband communication systems is shown in Fig. 1.1.

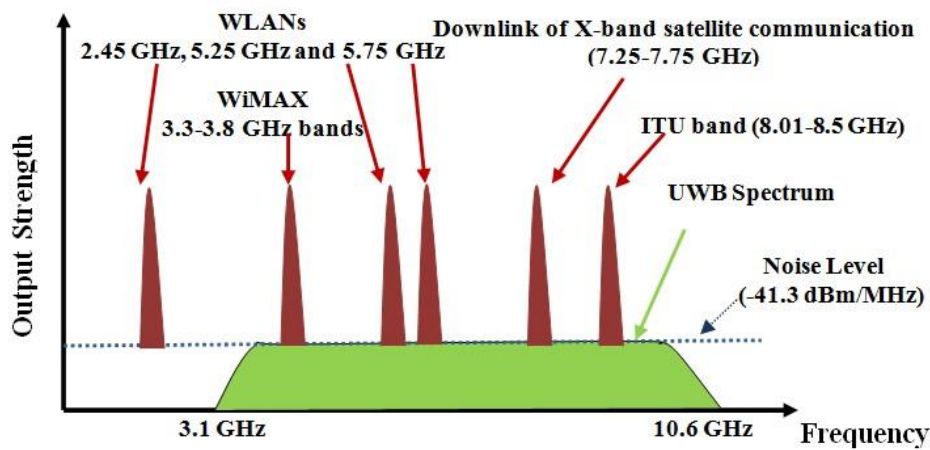


Fig. 1.1 Power spectrum density of UWB and some narrow-band communication systems

Whilst one solution to this problem is to insert a band-stop filter by means of the lumped element filters, however this would increase the size, cost and complexity of the system. An alternative solution is to design an UWB antenna which incorporates an integrated band-notched filter. Many researchers have been proposed to achieve band-rejection operations for UWB antenna; however most of designs are suffered from at least one of the following limitations: 1) limited number of rejection bands; 2) poor rejection at the notch frequency; 3) relative larger size. Therefore, the design of a compact planar

UWB monopole antenna with multiple-band-notched characteristics and good level of rejections is the second research topic in the thesis.

1.1.3 A Planar UWB Reconfigurable Band Rejection UWB Antenna

Antennas are required to support multiple standards and application since the demand of compactness of the systems and devices. To achieve this, reconfigurable antennas, incorporating switches become a promising solution. In the meantime, for the future UWB system, there is a need for band rejection capabilities to avoid interfering with nearby narrow band communication systems such as WLANs and WiMAX, *etc.* In this condition, a planar UWB antenna with reconfigurable band-notched capability could be useful.

1.1.4 A Planar UWB-MIMO Antenna for Wireless Applications

As mentioned that UWB technology has become one of the most promising technologies for future high data rate communications since the FCC released the UWB frequency range of 3.1-10.6 GHz for license free applications in 2002 [1], but this technology is limited to short range communications due to the low allowable transmitted power of -43 dBm/MHz. On the other hand, MIMO technology takes advantage of using multiple antennas at the terminals, which can be used to enhance the communication performance in terms of capability, improved signal quality and reliability in rich scattering environments. Thus, the combination of MIMO and UWB technologies may extend the communication range as well as offer higher reliability. However, the requirement for the compactness of MIMO enabled terminals may introduce strong mutual coupling between the closely packed antenna elements,

which can dramatically degrade the MIMO system performance. Therefore, the fourth research topic of the thesis is to design a planar UWB-MIMO antenna with compact structure and an optimised minimum mutual coupling that cover the entire range of the UWB band.

1.2 Organization of the Thesis

This thesis is organised in seven chapters as follows:

Chapter 2 reviews the development of the UWB/SWB antennas in past decades. The state-of-the-art technology of band-notched UWB antennas is also presented. Previous work on wideband to band-rejection reconfigurable antennas and UWB-MIMO antennas for wireless applications are also compared and summarised.

Chapter 3 presents a new compact planar monopole antenna with SWB performance. Additionally, the radiation mechanism of the planar SWB monopole antenna is also investigated.

In Chapter 4, the operating principles of the M-shaped resonators (MSRs) are studied. The use of the MSRs to create a UWB monopole antenna with quintuple-band-notched characteristics is proposed. The performances of the proposed antenna in the frequency-domain and time-domain are also investigated.

In Chapter 5, a new UWB monopole antenna is presented to achieve reconfigurable band-rejection characteristics. The band-rejections are realised by incorporating two complementary split ring resonators (CSRRs) printed on the radiating element. To give a narrow reconfigurable stop band operation, the CSRRs are integrated with three pairs of the switches. The proposed design concept is verified using both numerically and experimentally methods.

Chapter 6 presents a compact UWB-MIMO antenna for wireless applications. A novel approach to enhance the wideband isolation of the two antenna ports/elements is introduced and investigated. The proposed design concept is verified using both numerically and experimentally methods.

Finally, Chapter 7 finalises the thesis, reviews the work undertaken and draws main conclusions of the research, it is finished by suggesting some future work.

1.3 Key Contributions

The major contributions in this thesis are highlighted in the following sections.

Chapter 3: A Compact Super Wideband (SWB) Planar Monopole Antenna

A novel compact Mickey-mouse shaped planar monopole antenna with SWB performance is proposed and investigated. Three different techniques for bandwidth enhancement are implemented. The SWB antenna is evolved from the traditional circular monopole antenna and has achieved an impedance bandwidth of more than 50:1 and exhibited a wide band pattern characteristics, the usable spherical patterns are sustained in a bandwidth wider than 10:1 (the work was published in [12]).

Chapter 4: A Compact UWB Antenna with Quintuple-Band-Notched Characteristics

UWB antennas with band-notched features are necessary to reduce potential interferences between UWB systems and other existing communication

systems. A newly compact planar UWB monopole antenna with quintuple-band-notched characteristics is proposed and investigated. The size of the antenna is $22 \times 34 \text{ mm}^2$, which is about 10% smaller compared to the design in the literature; the band-notched functions are successfully achieved by integrating five half/one-wavelength MSR structures into the radiator, feed-line, and ground plane. And excellent levels of rejection in the notched bands are achieved. It can be also confirmed that the proposed antenna has limited effect on the time-domain performances (the work was submitted as listed in Section 1.4.1).

Chapter 5: A UWB Antenna with Reconfigurable Band-Rejection Characteristics

A novel planar UWB monopole antenna with reconfigurable narrow band-rejection characteristic is proposed and studied. Both the numerical and experiment results are confirmed that the proposed antenna has a capability of switching independently ON and OFF for different states including a UWB state, single and dual band-notched states with better band-rejection behaviours compared to designs in the literature. It is evident that the performances have verified the proposed design concept (the work was submitted as listed in Section 1.4.2).

Chapter 6: A Compact UWB-MIMO Antenna for Wireless Applications

A novel compact UWB-MIMO antenna ($60 \times 45 \text{ mm}^2$) is proposed for wireless applications. The size of the antenna is about 30% smaller than one reported in the literature [106], where similar performances is demonstrated. A new isolation technique is firstly introduced to reduce the mutual coupling between two closely-placed antenna elements. The isolation of more than 15

dB is achieved for the operating frequency from 2.3 to 12 GHz. The numerical and experimental results are indicated that the antenna has a very good diversity performance (the work was submitted as list in Section 1.4.3).

1.4 List of Publications

1. **P. Cao**, Y. Huang, J. W. Zhang, R. Alrawashdeh and X. Zhu, “A UWB planar monopole antenna with quintuple-band-notched characteristics,” *submitted to IET Microwaves, Antennas & Propagation*. 2013.
2. **P. Cao**, Y. Huang, R. Alrawashdeh, J. W. Zhang and X. Zhu, “A UWB monopole antenna with reconfigurable band-notched characteristics,” *submitted to International Journal of Antennas and Propagation*. 2013.
3. **P. Cao**, Y. Huang, J. W. Zhang, N. Khiabani and X. Zhu, “A UWB-MIMO monopole antenna for wireless communications,” *submitted to IET Microwaves, Antennas & Propagation*. 2013.
4. **P. Cao**, Y. Huang, J. W. Zhang and R. Alrawashdeh, “A compact super wideband monopole antenna,” in *7th European Conference on Antennas and Propagation (EuCAP)*, Sweden, pp. 3107-3110, 2013.
5. **P. Cao**, Y. Huang and J. W. Zhang, “A UWB monopole antenna for GPR application,” in *6th European Conference on Antennas and Propagation (EuCAP)*, Prague, pp. 2837-2840, 2012.
6. **P. Cao**, Y. Huang, J. W. Zhang and Y. Lu, “A comparison of planar monopole antennas for UWB applications,” in *Antennas and Propagation Conference (LAPC)*, Loughborough, pp. 1-4, 2011.
7. Y. Huang, Y. Lu, S. Boyes, **P. Cao** and T. Loh, “Ground plane effects and measurements of portable planar broadband antennas,” invited paper

- to *International Conference on Electromagnetics in Advanced Applications, IEEE-APS Topical Conference on Antennas and Propagation in Wireless Communications*, Torino, Italy, pp. 12-17 Sep., 2011.
8. Y. Lu, Y. Huang, H. T. Chattha and **P. Cao**, “Reducing ground-plane effects on UWB monopole antennas,” *IEEE Antennas and Wireless Propagation Letters*, vol. 10, pp. 147-150, 2011.
 9. J. W. Zhang, Y. Huang, **P. Cao** and H. T. Chattha, “Broadband unidirectional dipole antennas for wireless applications,” in *Antennas and Propagation Conference (LAPC)*, Loughborough, pp. 1-4, 2011.
 10. J. W. Zhang, Y. Huang, and **P. Cao**, “Harvesting RF energy with rectenna arrays,” in *6th European Conference on Antennas and Propagation (EuCAP)*, Prague, pp. 365-367, 2012.
 11. J. W. Zhang, Y. Huang and **P. Cao**, “A wideband cross dipole rectenna for wireless harvesting,” in *7th European Conference on Antennas and Propagation (EuCAP)*, Sweden, pp. 3063-3067, 2013.
 12. R. Alrawashdeh, Y. Huang and **P. Cao**, “A conformal U-shaped loop antenna for biomedical applications,” in *7th European Conference on Antennas and Propagation (EuCAP)*, Sweden, pp. 157-160, 2013.
 13. R. Alrawashdeh, Y. Huang, **P. Cao**, and L. Eng, “A new small conformal antenna for capsule endoscopy,” in *7th European Conference on Antennas and Propagation (EuCAP)*, Sweden, pp. 220-223, 2013.

1.5 References

- [1] Federal Communications Commission, "Revision of Part 15 of the commission's rules regarding ultra-wideband transmission systems, first report and order," *ET Docket 98-153, FCC 02-48*, pp. 1-118, Feb.14, 2002.
- [2] N. P. Agrawall, G. Kumar, and K. P. Ray, "Wide-band planar monopole antennas," *IEEE Trans. on Antennas and Propagation*, vol. 46, pp. 294-295, 1998.
- [3] E. S. Angelopoulos, A. Z. Anastopoulos, D. I. Kaklamani, A. A. Alexandridis, F. Lazarakis, and K. Dangakis, "Circular and elliptical CPW-fed slot and microstrip-fed antennas for ultra-wideband applications," *IEEE Antennas and Wireless Propagation Letters*, vol. 5, pp. 294-297, 2006.
- [4] H. D. Chen and H. T. Chen, "A CPW-fed dual-frequency monopole antenna," *IEEE Trans. on Antennas and Propagation*, vol. 52, pp. 978-982, 2004.
- [5] Y. Lu, Y. Huang, Y. C. Shen, and H. T. Chattha, "A further study of planar UWB monopole antennas," in *Antennas & Propagation Conference, 2009. LAPC. Loughborough*, pp. 353-356, 2009.
- [6] L. Paulsen, J. B. West, W. F. Perger, and J. Kraus, "Recent investigations on the volcano smoke antenna," in *IEEE Antennas and Propagation Society International Symposium*, vol. 3, pp. 845-848, 2003.
- [7] P. Cao, Y. Huang, J. W. Zhang, and Y. Lu, "A comparison of planar monopole antennas for UWB applications," in *Antennas and Propagation Conference (LAPC), Loughborough*, pp. 1-4, 2011.

- [8] K. C. L. Chan; Y. Huang, X. Zhu, “A planar elliptical monopole antenna for UWB applications,” in *IEEE/ACES Inter. Conference on Wireless Communications and Applied Computational Elec.*, Hawaii, U.S.A., pp. 182-185, Apr. 3-7, 2005.
- [9] J. X. Liang, C. C. Chian, X. D. Chen, and C. G. Parini, “Study of CPW-fed circular disc monopole antenna for ultra-wideband applications,” in *IEE Proc. Microwaves, Antennas and Propagation*, pp. 520-526, Dec. 2005.
- [10] Z. N. Chen, et al, “Planar antennas,” *IEEE Microwave Magazine*, vol. 7, issue 6, pp. 63-73, Dec. 2006.
- [11] Y. Huang and Kevin Boyle, “Antennas from theory to practice,” *John Wiley and Sons*, 2008.
- [12] P. Cao, Y. Huang, J. W. Zhang, and R. Alrawashdeh, “A compact super wideband monopole antenna,” in *7th European Conference on Antennas and Propagation (EuCAP)*, Sweden, pp. 3107-3110, 2013.

CHAPTER 2 BACKGROUND

2.1 Development of UWB/SWB Antennas

2.1.1 Definition of UWB

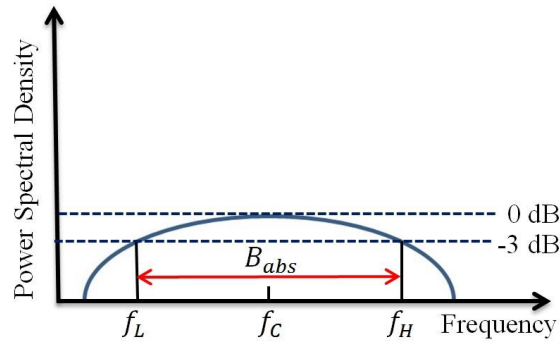
An ultra-wideband (UWB) signal is characterized by its very large bandwidth compare to the conventional narrowband systems. Commonly, a UWB signal is defined as a signal with a fractional bandwidth of larger than 20% or an absolute bandwidth of at least 500 MHz [1]. The B_{abs} can be calculated as the difference between the upper cut-off frequency f_H and the lower cut-off frequency f_L of the -3 dB emission point, as shown in Fig 2.1. The absolute bandwidth and the fractional bandwidth are then given in Equations (2.1) and (2.2), respectively.

$$B_{abs} = f_H - f_L \quad (2.1)$$

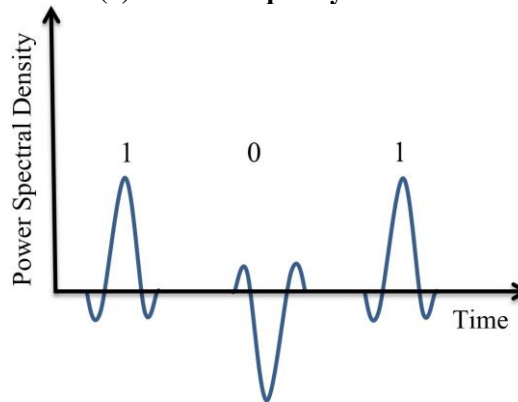
$$FBW = \frac{B_{abs}}{f_c} = \frac{2(f_H - f_L)}{(f_H + f_L)} = \frac{1}{Q} \quad (2.2)$$

where f_c is the centre frequency and Q is defined as quality factor, which is inversely proportional to the half power fractional bandwidth of the antenna.

In general, an antenna is a resonate device. If the antenna can be well matched to its feed across a certain frequency range, that frequency range is defined as it impedance bandwidth. The impedance bandwidth can be specified in terms of return loss (S parameters) over a frequency range. Generally, in the wireless communications, the antenna is required to provide a return loss great than 10 dB over its frequency bandwidth.



(a) In the frequency domain



(b) In the time domain

Fig. 2.1 Illustration of a UWB communication system with its power spectral density

The frequency-domain and time-domain behaviours of a UWB communication system are illustrated in Fig. 2.1. Signals which occupy an extremely wide bandwidth in the frequency domain are usually very short pulses in the order of sub-nanosecond in the time domain. Thus, the most significant difference between traditional radio transmissions and UWB radio transmissions is that the traditional systems employ carrier-wave modulation, while UWB system transmits information by generating radio energy as very narrow pulses occupying a large spectrum.

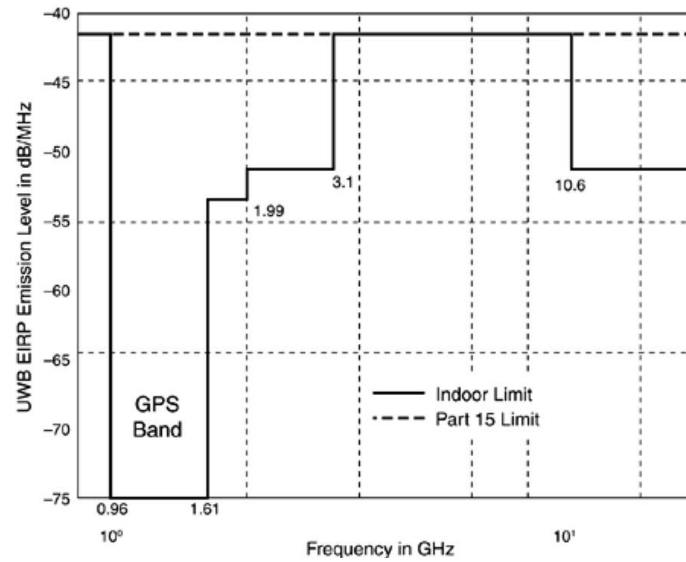
The suitability of UWB signals for high-speed data communications can be obtained from the Shannon capacity formula [2]. For an ideal additive white Gaussian noise (AWGN) channel with limited bandwidth, the maximum achievable data rate can be calculated by.

$$C = B \log_2(1 + SNR) \quad (2.3)$$

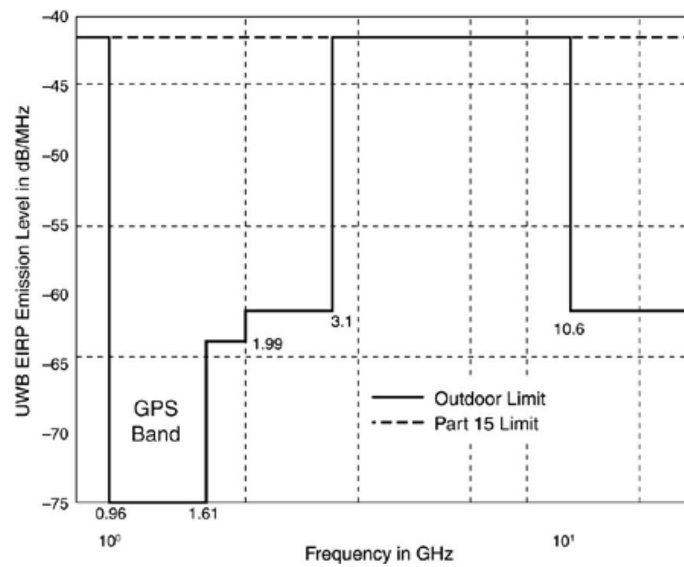
where C denotes the channel capacity (maximum transmit data rate), B stands for the bandwidth of the channel. SNR is the signal-to-noise ratio (SNR) over the entire channel bandwidth Equation (2.3) indicates that it becomes possible to transmit more information from transmitter to the receiver by increasing the bandwidth occupation or transmission power. However the transmission power in a wireless communication system is limited because of the regulation limit or due to the fact that many portable devices and systems are battery powered and the potential interference should also be avoided. Therefore, a wide frequency bandwidth is the solution to increase its channel capacity.

Since UWB systems can operate over an ultra-wide frequency spectrum, they will overlap with some allocated wireless systems, which may cause significant interference. In February 2002, the FCC approved that a UWB spectral mask specified of 7.5 GHz of usable frequency range from 3.1 to 10.6 GHz for communication devices and protected existing system operating within this spectrum by limiting the equivalent isotropically radiated power

(EIRP) level to -41.3dBm/MHz (known as Part 15 Limit) [3]. Fig. 2.2 shows the spectral masks of FCC's regulation for UWB communication systems [4].



(a) Indoor limits



(b) Outdoor limits

Fig. 2.2 FCC emission limits for indoor and outdoor UWB communication systems [4]

2.1.2 UWB/SWB Antennas

UWB antennas usually are referred to as the antenna with an actual frequency range from 3.1 to 10.6 GHz with a ratio bandwidth of 3.4:1, which the antenna with a ratio bandwidth not less than 10:1 is generally called the SWB antenna [5]. In this section, the developments of UWB/SWB antennas are reviewed.

The earliest antenna with wideband properties was the biconical antennas made by Sir Oliver Lodge in [6], as shown in Fig. 2.3. At the early stage, the antennas were based on three-dimensional structures with bulky volumes such as biconical/conical antennas [7], spheroidal antenna [8-9], omni-directional and directional coaxial horn antenna [10]. Some of the very early wideband antennas are shown in Fig. 2.4.

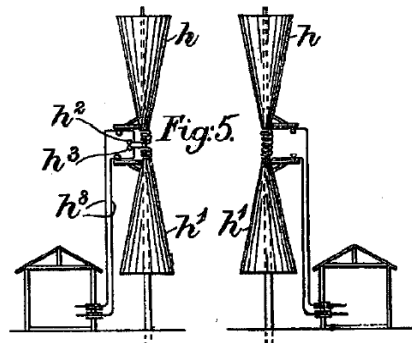
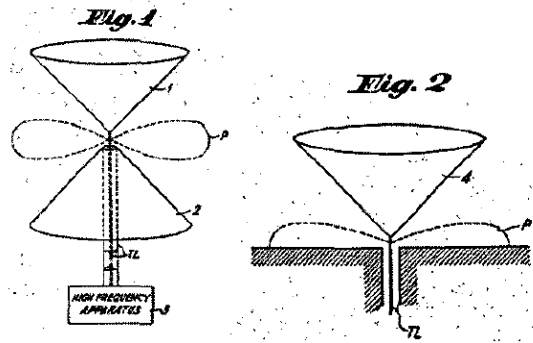
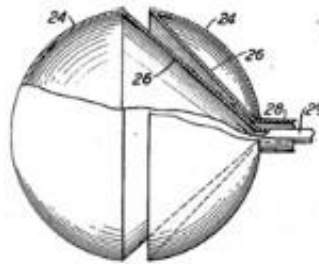


Fig. 2.3 The earliest wideband properties antenna (Lodge's biconical antennas) (1898)

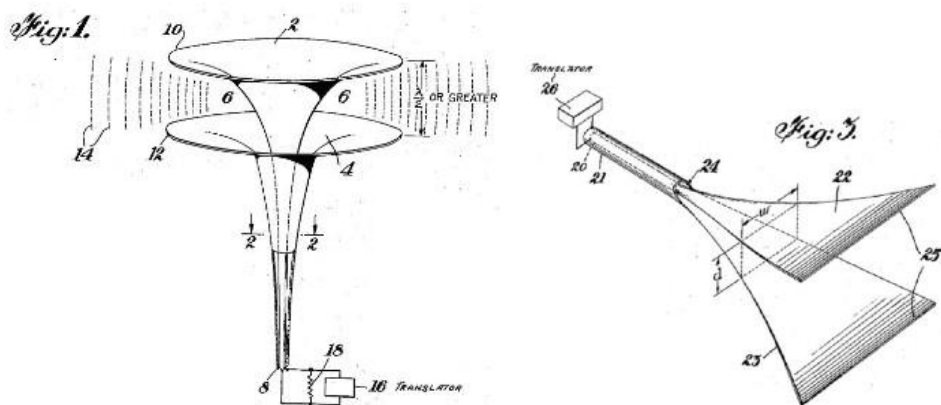
[6]



(a) Biconical (left)/conical(right) antennas (1939) [7]



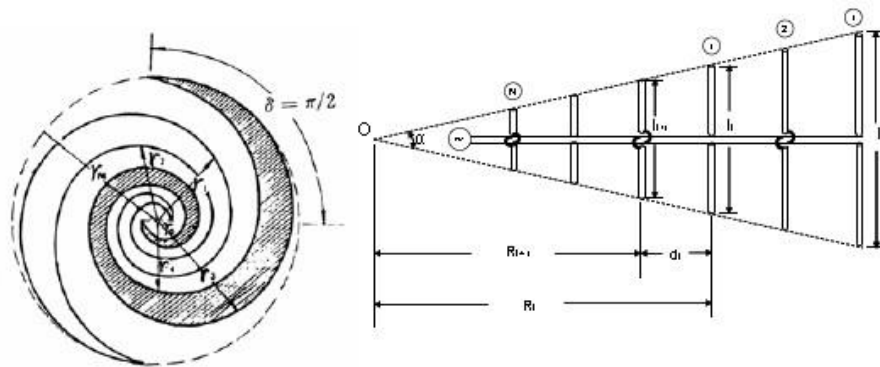
(b) A spheroidal antenna (1941) [8, 9]



(c) A omni-directional (left), and directional (right) coaxial horn (1948) [10]

Fig. 2.4 Some early wideband antennas

In the late 1950 and early 1960, a family of antennas with a ratio bandwidth more than 10:1 were first developed by Rumsey et al, which were called as the frequency independent antenna [5]. Classical shapes of such antennas include the equiangular spiral antenna and the planar log-periodic dipole antennas, as shown in Fig. 2.5.



(a) An equiangular spiral antenna (left) and (b) Log-periodic dipole antenna (right)
(1959) [5]

Fig. 2.5 Some frequency independent antennas

From 1990s, many new-style SWB antennas have been proposed, which can be summarized as three types [11]: The SWB metal-plate monopole antennas, printed slot antennas and planar monopole antennas. The details of these types of the SWB antennas are reviewed and compared below.

2.1.2.1 SWB Metal-plate Monopole Antennas

The first wideband-metal-plate monopole was proposed by G. Dubost in [12]. Its impedance bandwidth has been widened with an optimized structure of metal-plate monopole, such as discs or elliptical monopole antenna [13], trapezium monopole antenna [14], inverted cone monopole and leaf-shaped monopole antenna. In [15], the planar inverted cone antenna consists of a single flat element vertically mounted above a ground plane as shown in Fig.

2.6(a). The antenna achieved an impedance bandwidth ratio of more than 10:1 and a radiation pattern bandwidth of 4:1. Later on in [16], the leaf-shaped plate monopole antenna comprised of three circular holes with the dielectric layer, which provides the impedance bandwidth ratio better than 20:1 from 1.3 to 29.7 GHz, as shown in Fig. 2.6(b). In the meantime, the radiation pattern bandwidth has extended due to the introduction of three circular holes.

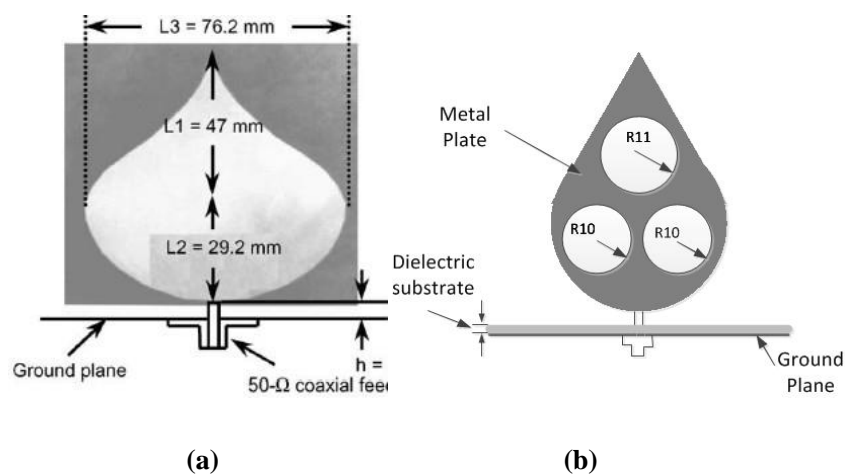


Fig. 2.6 The metal-plate monopole antenna: (a) Planar inverted cone antenna (2004) [15], and (b) Leaf-shaped plate antenna (2006) [16]

In addition, the rectangular metal-plate monopole has been well investigated due to the simplest structure and a steady radiating pattern, but the impedance bandwidth is only about 2:1 in the early time. Since then, many methods have been suggested in order to realize the wideband properties, such as the antennas with an offset feed [17], double/three feeds [18] and combining the short post and bevelling technique [19]. In [17], by changing the location of the feeding, the impedance bandwidth improved to 6:1, as shown in Fig. 2.7(a). In [19], the bandwidth further enhanced to 10:1 by combining the short post and bevelling technique, as shown in Fig. 2.7(b). The drawback of these metal-plate monopole antennas always needs a perpendicular metal ground plane.

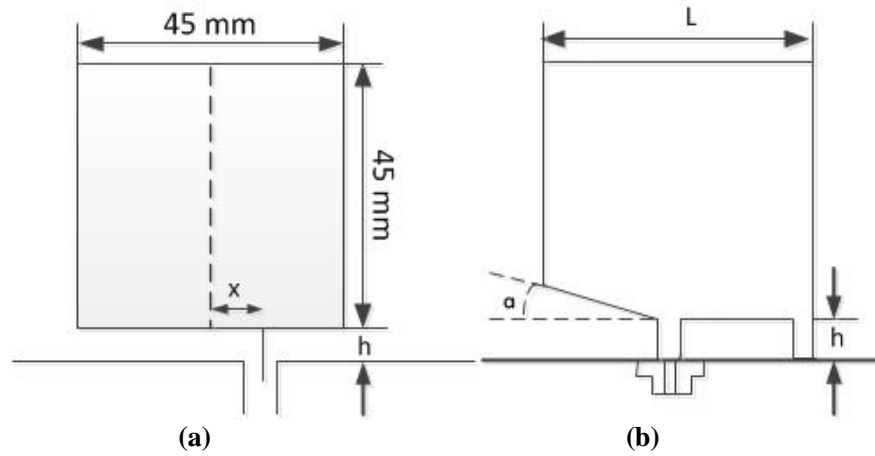


Fig. 2.7 The rectangular metal-plate monopole antenna (a) Offset feed (2001) [17], and (b) Short post and bevelling (2004) [19]

2.1.2.2 SWB Slot Antennas

SWB slot type antennas were also proposed and investigated [20-26] in the past decades. These antennas can be mainly divided in two categories, such as SWB tapered slot and wide-slot antennas.

SWB Tapered-slot Antennas

The conventional Vivaldi antenna typically has a bandwidth of less than 3:1, limited by the feed line to radiating slot transition. One of the well-known balanced antipodal Vivaldi tapered slot antenna with wide-bandwidth was introduced in [20]; the transition was done by tapering the micro-strip to symmetric double sided slot line with a very wideband capability. Thus the antenna has a ratio bandwidth of 15:1 (from 1.3 to 20 GHz) and achieved the cross-polarization to be less than -17 dB, as shown in Fig. 2.8(a). In [21], another type of balanced antipodal Vivaldi antenna using CPW feeding provided a ratio bandwidth of 18:1 (1 to 18 GHz), as shown in Fig. 2.8(b).

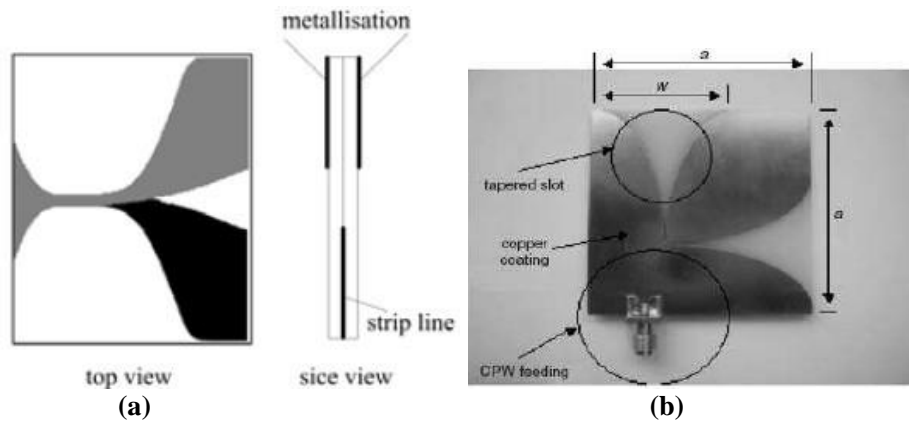


Fig. 2.8 The balanced antipodal Vivaldi antenna (a) Conventional microstrip feed (1988) [20], and (b) CPW feed (1993) [21]

SWB Wide-slot Antennas

In recent years, various SWB printed wide-slot antennas have been reported to use different slot shapes [22-25]. As stated in [22], the printed slot antenna using U-shaped microstrip feeding was studied by adding a tuning rectangular copper pad in one side of the microstrip (to improve the impedance bandwidth of the antenna). By properly tuning the physical size of the copper pad, The antenna achieved a fractional bandwidth of more than 135.7%, covering frequencies from 2.3 to 12 GHz and a gain variation from 2 to 7 dBi was obtained, as shown in Fig. 2.9.

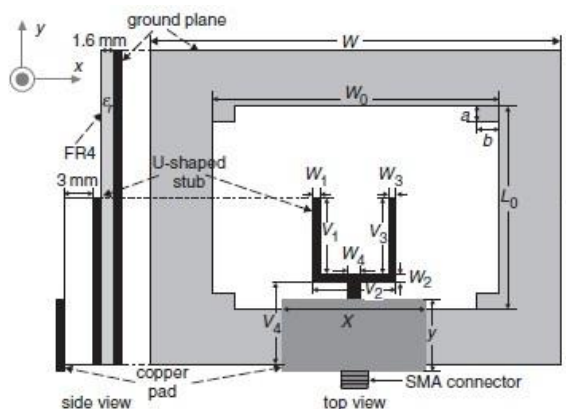


Fig. 2.9 The printed U-shaped slot antenna (2005) [22]

The impedance bandwidth of slot antenna was further improved. As shown in Fig. 2.10, the design of using Planar Invested Cone Antenna (PICA) like structures was proposed and the antenna achieves a ratio bandwidth of 13:1, covering frequencies from 2.2 to 30 GHz [23].

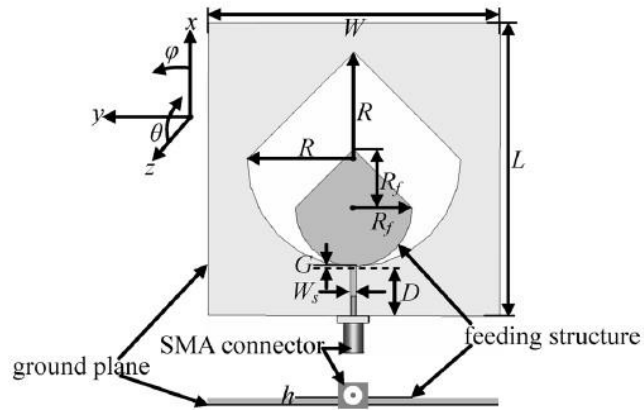


Fig. 2.10 The PICA slot antenna (2008) [23]

Apart from Microstrip line-fed, the CPW-fed printed wide-slot antennas also have been designed to demonstrate a wide bandwidth capability. For instance, in ref [24], the elliptical slot antenna with an elliptical patch as the feed has a ratio bandwidth about 15:1, covering frequencies from 1.3 GHz to 20 GHz, as shown in Fig. 2.11.

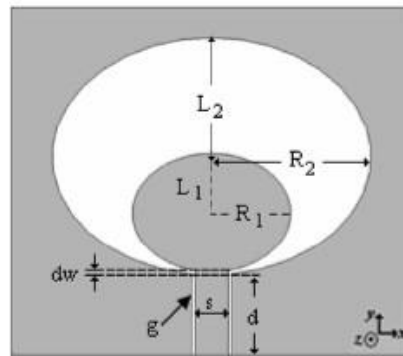


Fig. 2.11 The elliptical slot antenna (2006) [24]

Another type of printed slot antenna is printed bow-tie slot antenna and the bow-tie slot is added under the bow-tie slot antenna [25], which has a simple configuration, wider bandwidth, lower cross-polarization levels and higher gain performance, as shown in Fig. 2.12.

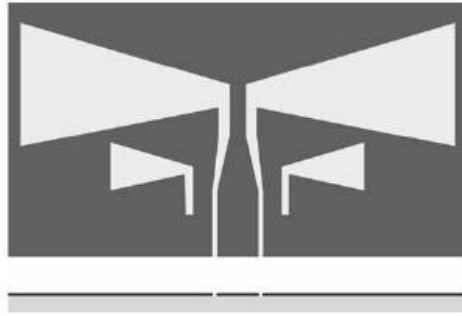


Fig. 2.12 The bow-tie slot antenna (2004) [25]

2.1.2.3 SWB Planar Monopole Antennas

During the past few year, many planar monopole antennas fed by the microstrip (MS)-line [26-29] and the CPW [30-32] have been also proposed for SWB applications. Because of this attractive features such as low profile, low-cost, ease of fabrication and omni-directional radiation pattern. Various planar monopole antennas fed by the MS line and CPW are reviewed as follows:

SWB Microstrip-fed Monopole Antennas

In [26], a planar circular asymmetrical dipole antenna, fed by a microstrip was studied. It was performed on two planar substrates having different dielectric permittivity. The prototype on the substrate with lower permittivity shows much larger bandwidth, and it has a ratio bandwidth of 21.9:1, covering frequencies from 0.79 to 17.46 GHz, as shown in Fig. 2.13.

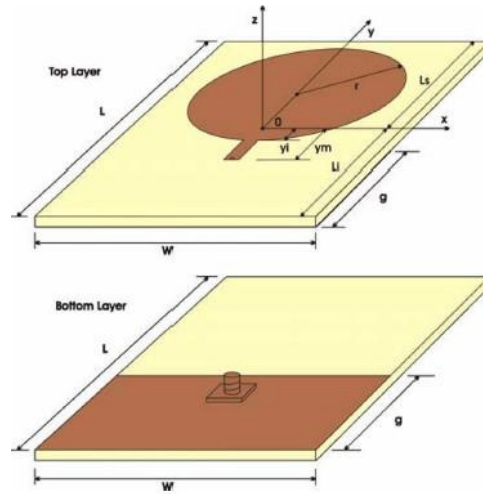


Fig. 2.13 The planar circular asymmetrical dipole antenna (2010) [26]

In [27], a wideband monopole fractal antenna with Hilbert fractal slot patterned ground plane was also investigated, as shown in Fig. 2.14. The radial arrow fractal slots cause the path lengths of the surface currents on the radiator to have the multiband behavior. The antenna has a wide bandwidth ranging from 1.65 to 14.6 GHz or a ratio bandwidth about 14:1 for $S_{11} < -10$ dB and a stable gain performance about 3 dBi across the desired band were obtained. Recently, another circular-hexagonal fractal antenna was proposed in [28] with a much wider bandwidth ranging from 2.18 to 44.5 GHz.

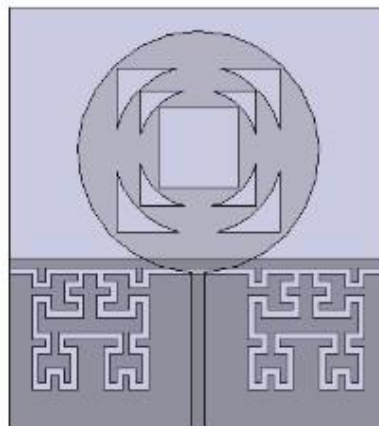


Fig. 2.14 The fractal antenna (2011) [27]

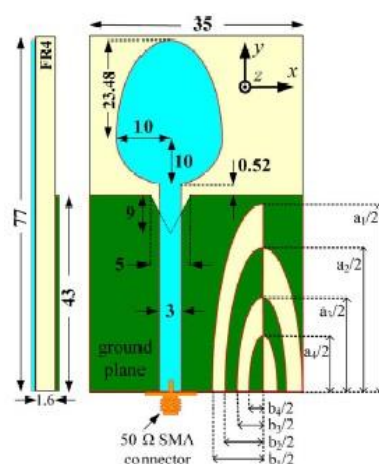


Figure 1 shows the schematic diagram of the proposed antenna. The diagram includes two views: a Bottom View and a Top View. The Bottom View is a rectangle with width W and length L , featuring a central rectangular slot of width w_{GS} and height l_{GS} . The Top View shows the antenna's profile with a total width w_0 and a central slot of width w_{c1} . The antenna has a vertical stem of width w_{t1} and a horizontal base of width w_{t2} . The total height is l_0 , with a central slot of height l_{c2} . The antenna is labeled "Switching Elements".

25

Recently, in [30], a compact implementation of a microstrip-fed monopole antenna for the SWB communications was proposed, as shown in Fig. 2. 16. The proposed antenna possessed a broad frequency range from 3 to 33 GHz or a ratio bandwidth of 11:1, but also implemented with switchable dual band-notched characteristics.

SWB CPW-fed Monopole Antennas

Apart from Microstrip line-fed, the CPW-fed monopole antennas with SWB performamne have also been investigated. A compact CPW-fed monopole antenna composed of an elliptical monopole patch and a coplanar trapeziform ground plane was introduced in [31], as shown in Fig. 2.17(a). The results demonstrate that this antenna achieves a ratio impedance bandwidth of 21.6:1, covering frequency range from 0.41 to 8.86 GHz, with a good gain and omnidirectional radiation performance as well.

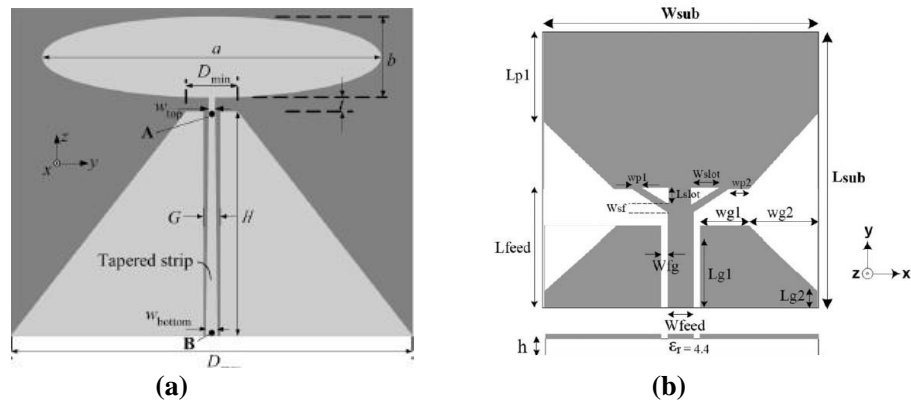


Fig. 2.17 The CPW-fed planar monopole antenna: (a) Elliptical (2007) [31], and (b) Trapezoid (2010) [32]

Fig. 2.17(b) shows another CPW-fed monopole antenna which was proposed for the same purpose in [32]. The impedance bandwidth of the proposed antenna reaches 174% and has a -10 dB impedance bandwidth covering frequency range from 2.76 to 40 GHz or a ratio bandwidth of 14. 5:1,

More recently, in [33], a SWB antenna with the impedance bandwidth from 5 to 150 GHz or a ratio bandwidth of 30:1 was successfully developed, as shown in Fig. 2.18.

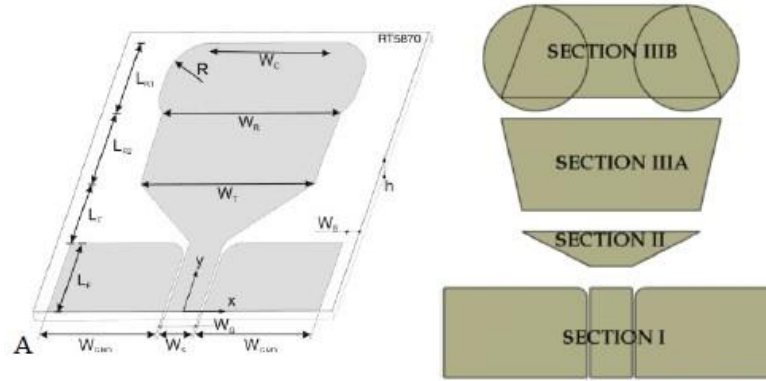


Fig. 2.18 The newly developed CPW-fed planar monopole antenna [33]

A comparison of several reviewed SWB antennas in term of bandwidth, size, radiation patterns and gain performance is made and compared in Table 2-1. All the antennas have been achieved with a ratio bandwidth of more than 10:1 band, it can be observed that the metal plate monopole antennas always needs a perpendicular metal ground plane, which lead to a large size. SWB printed slot antennas may achieve relatively higher gain. In addition, it can be noted that SWB planar monopole antennas may have the smallest volume and widest bandwidth. And the antenna in [33] achieved the widest frequency range from 5 to 150 GHz with a ratio bandwidth of 30:1, However this antenna does not cover the some important bands operating at frequencies less than 5 GHz, such as, the lower band of UWB, Bluetooth, WiMAX2500, and LTE2600. There is also a question on what the widest achievable bandwidth for such a planar monopole antenna. The work will be presented in Chapter 3.

Table 2-1 Comparison of various SWB antennas

Antenna Type	Bandwidth (GHz) (S11 <-10 dB)	Ratio Bandwidth (S11 <-10 dB)	Size (λ^2)	Gains (dBi)
Trapezoidal metal plate monopole [14]	1.07 - 12.2	11.4:1	0.89×0.89	0.5- 4.5
Leaf-shaped plate monopole [16]	1.3 - 29.7	22.8:1	0.35×0.35	3-5
Tapered slot antenna [21]	1 - 18	18:1	0.43×0.32	3.2-9
CPW-fed rectangular slot antenna [24]	1.3 - 20	15:1	0.39×0.39	-----
A circular-hexagonal Fractal antenna [28]	2.18-44.5	20.4:1	0.33×0.23	2-3
MS-fed elliptical egg-shape planar monopole antenna[29]	1.44-18.8	12:1	0.37×0.21	1-7
CPW-fed planar monopole antenna [33]	5-150	30:1	0.25×0.28	-----

Note: λ is the wavelength of the lowest useable frequency

2.2 Review of Band-Notched UWB Antennas

2.2.1 Survey on Techniques to Generate Notched Characteristics

Several designs have been proposed to use planar UWB antennas to obtain the band-notched function [34-75]. Among the proposed methods, the most widely used approaches can be classified into few groups according to the resonator structures positions on the antenna such as on or next to the radiator or other side of the substrate or the feed line or the top edge of the ground plane, as shown in Figs. 2.19(a) to (c), respectively. In the literature, various techniques have been applied to obtain the single band-notched characteristics of UWB antennas. The details of these techniques can be summarised as follows.

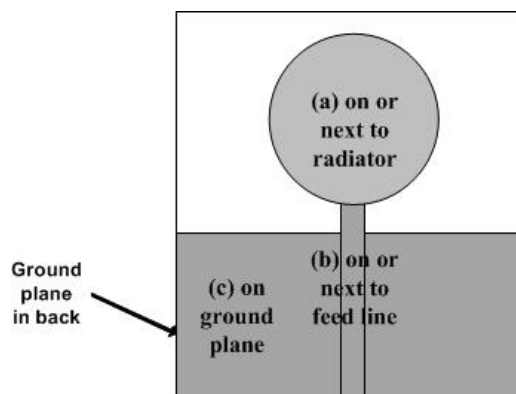


Fig. 2.19 Possible positions of the resonator structure on UWB antenna

2.2.1.1 Inserting slots

UWB antennas having different slots or cuts, e.g., L shape [34], U shape [35-38], C shapes [35, 39], V shape [40], meandered grounded stubs [41], and CPW slot [42] on the various radiating elements or the ground plane or the feed

line were demonstrated to create band notched functions. Generally speaking, the notched frequency is determined by the total length of the slot or cut which is approximately half or quarter wavelength. Some of these designs are now described in detail below.

In [34], a CPW-fed compact elliptical monopole UWB with a narrow frequency rejection was presented. The frequency band-notched at 5.65 GHz was achieved by inserting two inverted half-wavelength L slots near the CPW feeding on the ground plane/radiator of the antenna, respectively, as shown in Fig. 2.20(a). The principle of this approach was to stop the current flow at the introduction of the inverted L slots, which the radiation of the antenna could be suppressed and a notched frequency could be created.

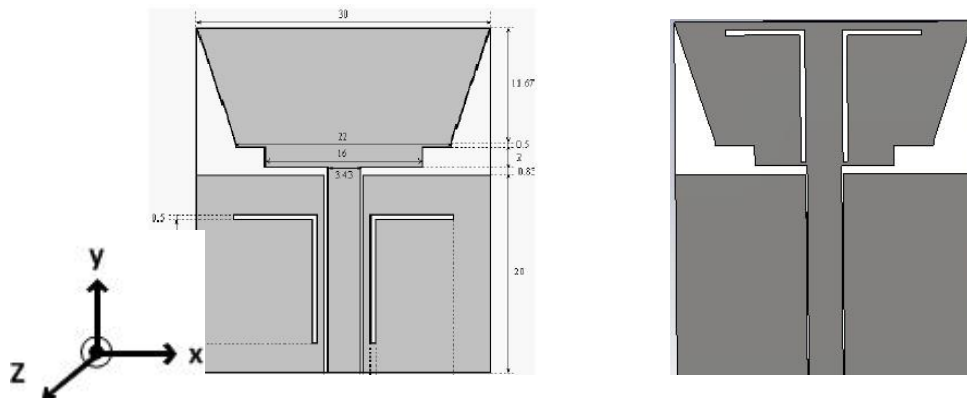


Fig. 2.20 (a) A CPW UWB antenna integrated with two inverted L slots: On the ground plane (left) and on the radiator(right) [34]

The radiation patterns of the antenna were investigated for both cases at 5 GHz, as shown in Fig. 2.20(b). It can be seen that the patterns had limited effect for the slots on the radiator/ground pane. The pattern in YOZ plane tends to have slightly more directional at around 90 degrees from the y-direction for the case of the slots on the radiator than the ground plane.

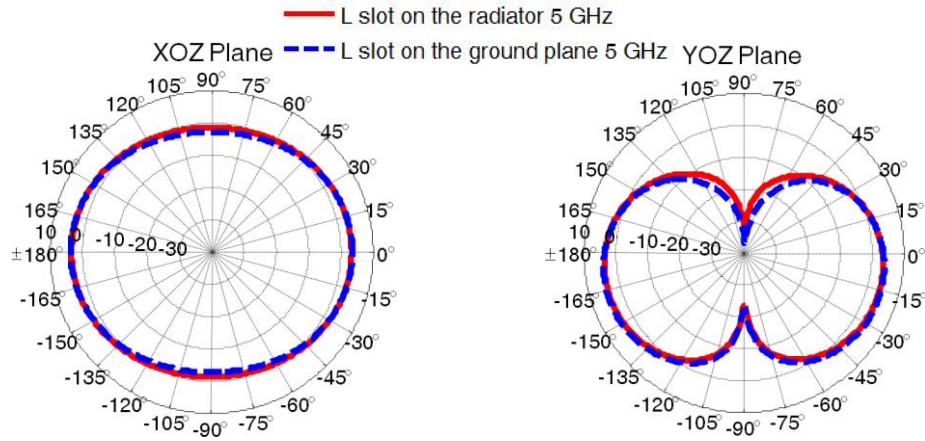


Fig. 2.20 (b) Simulated radiation patterns of the slot on the radiator and ground plane

A CWP-fed compact elliptical UWB monopole antenna with a U-shaped and C-shaped slot in the patch was introduced in [35], as shown in Figs. 2.21(a) and (b), respectively. The band rejection was caused by the presence of a slot having a length of approximately $\lambda/2$ at the frequency of 5.8 GHz and the values of gain reduction were 10 dB and 5 dB, respectively.

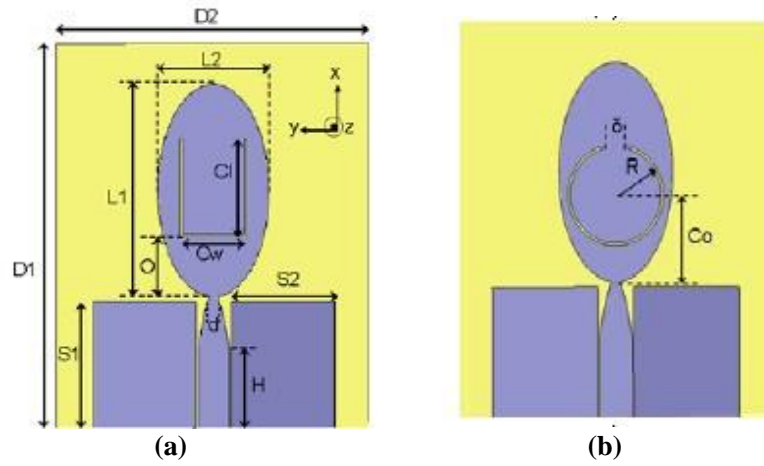


Fig. 2.21 The CPW-fed UWB antennas integrated (a) U-shaped slot [35], and (b) Two C-shaped slots [35]

Ref. [41] introduced the use of a pair of meander grounded stubs to design a deep single band-notched UWB planar monopole antenna, as shown in Fig. 2.22. The results showed that the single band notch was achieved from 5.15 to 5.825 GHz with gain suppression of 9 dB.

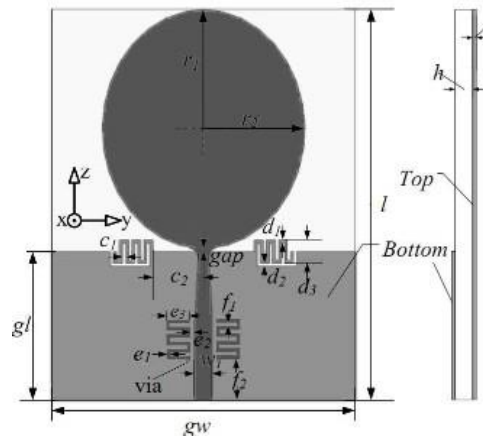


Fig. 2.22 A MS-fed UWB antenna integrated with a pair of ML [41]

A compact UWB monopole antenna [42] in Fig. 2.23 obtained the frequency band-notched function by inserting a CPW resonant cell on the feeding line. Measured results indicated that the antenna has a notched band from 5.10 to 5.94 GHz.

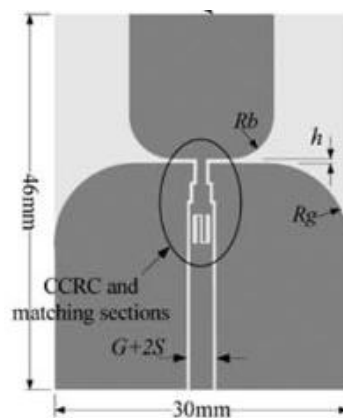


Fig. 2.23 A UWB antenna with single band-notched function using the slots on the feeding line [42]

2.2.1.2 Parasitic Element

The parasitic strips have also been used to achieve band rejection function [43-46]. For example, in [43], a UWB antenna with band-notched function was investigated by placing a pair of parasitic elements in the radiating aperture of the planar antenna at the top and bottom layer, as shown in Fig. 2.24(a). The results showed that the antenna exhibits a 10 dB return loss bandwidth from 3 to 11 GHz with 9 dB gain suppression at the rejection bands.

Another example is a CPW-fed UWB elliptical monopole [44] with two resonating inverted L-shaped stubs are collected to the radiator, as shown in Fig. 2.24(b). The band-notched was realized at the center frequency of 5.5 GHz with only 5 dB gain suppression.

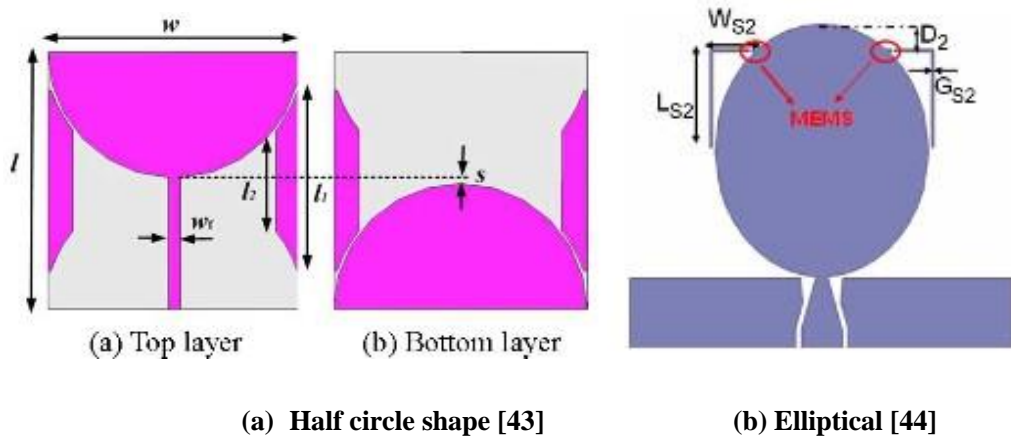


Fig. 2.24 The UWB antennas integrated with parasitic strips

More recently, in [47], a wide band-notched function was achieved by using an extended strip and a loaded strip for a half circle radiator shaped UWB antenna, as shown in Fig. 2.25. The results showed a good band-notched performance in 5-6 GHz with gain suppression better than 10 dB.

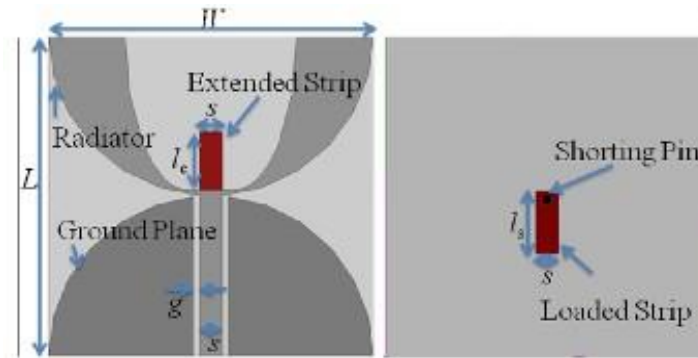


Fig. 2.25 A UWB antenna integrated with an extended strip and a loaded strip [47]

2.2.1.3 Split-Ring-Resonant (SRR) or Complementary SRR (CSRR)

SRR, originally proposed by Pendry [48], can be considered as an electronically small size resonator with a very high quality (Q) factor [49], which is able to produce a band-notch property for UWB antennas [49, 50]. Ref. [49] introduced a UWB antenna with a modified SRR slot-type structure on the path for rejecting unwanted frequency band, as shown in Fig. 2.26. The results showed that the antenna has a notched band at the center frequency of 5.2 GHz. The value of gain suppression was about 9 dB. In addition, [51] was successfully achieved a single band-notched function for WLAN band at 5.7 GHz.

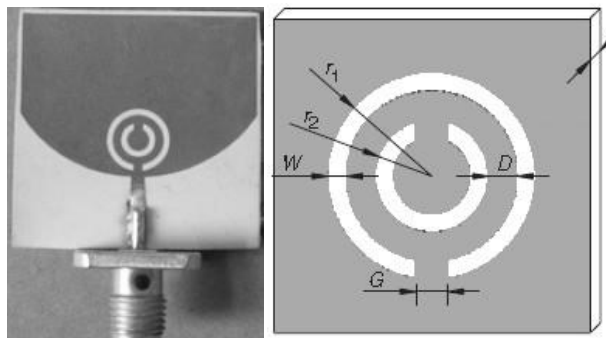


Fig. 2.26 A UWB antenna integrated with SRR [49]

2.2.1.4 Open-loop resonant

An open-loop resonator was placed onto the other side of the substrate and a dual-gap open-loop resonator was inserted into the radiating element of a UWB monopole antenna, were studied in [52-53], and shown in Figs. 2.27(a) and (b), respectively. By printing the open-loop on the reverse side of the substrate, the antenna yielded almost 11 dB gain suppression at the notched center frequency of 5.2 GHz. For the case of etching the dual-gap open loop resonator into the radiator, the notch band was achieved at 4.2 GHz with 5.8 dB gain suppression.

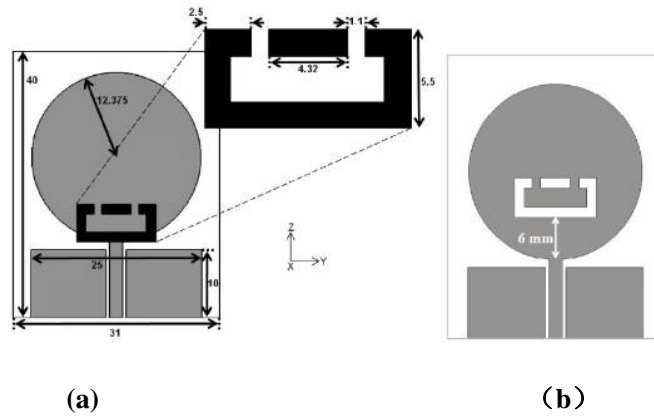


Fig. 2.27 The UWB antenna with (a) An open-loop resonator [52], and (b) A dual-gap open-loop resonator [53]

2.2.1.5 Electromagnetics Band Gap (EBG)

EBG structures have also been used in the design of UWB antennas with a stop band characteristic [54-55]. Using the band-gap characteristic of the mushroom-like EBG structure on a simple UWB antenna was presented in [54], as shown in Fig. 2.28. An EBG consists of metallic patches and short pins named vias that connect patches into the ground plane. The inductor L is a result of the currents flowing through the vias, and the capacitor is due to the gap effect between the adjacent patches as shown in Fig. 2.28(c). The antenna

had a notch band at 5.5 GHz. The gain value was not presented in the paper. It had limited band-notched performance due to the dielectric loss of the substrate.

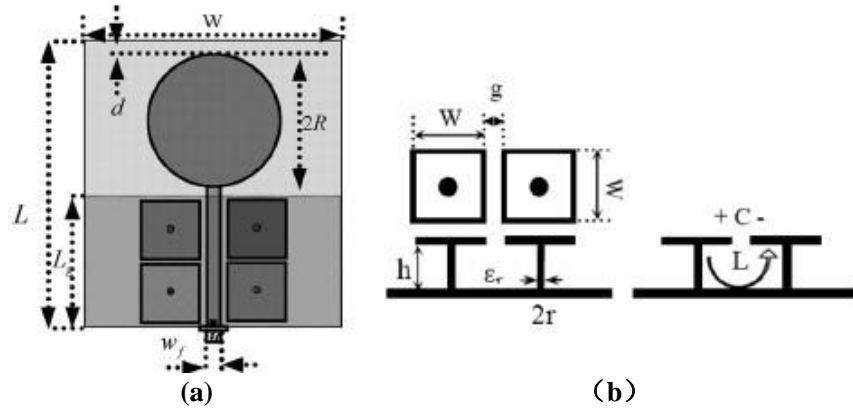


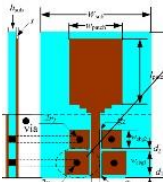
Fig. 2.28 A UWB antenna with (a) EBG structure [54], (b) Unit cells of EBG [54] and (b) Equivalent circuit of the EBG [54]

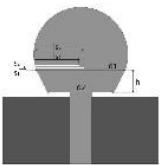
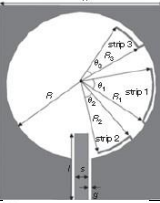
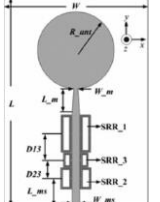
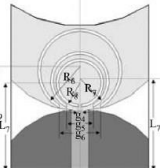
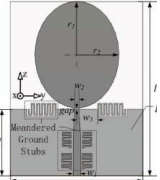
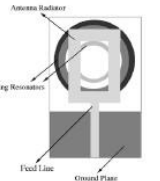
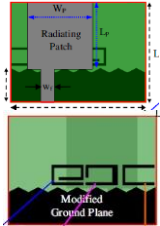
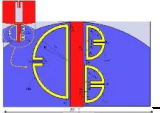
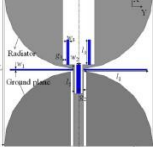
Though lots of band-notched UWB antennas have been reported in [33-54], most of them were designed to achieve one band-notched function with a reasonable rejection performance. In order to mitigate the interference by several existing narrow band communication systems, a wide variety of multiple band-notched UWB antennas have been designed and reported in [55-75]. These designs with two [55-64], three [65-71], four [72-74], and five [75] band-notched functions were achieved by utilizing some of the described techniques. The details of these designs are summarized in Section 2.2.2.

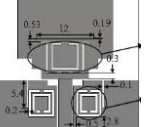
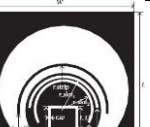
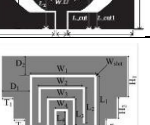
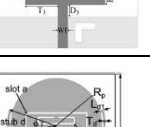
2.2.2 Comparison of Different Approaches

In terms of techniques, size, bandwidth, gain suppression, and notch bands, a comprehensive comparison between the two, three, four, and five band-notched antennas in open literature is listed in Table 2-2.

Table 2-2 Comparison of multiple band-notched UWB antennas

Ref .	Antenna Layout	Techniques	Analyzed Parameters	Gain Suppression (dB)	Notch Bands (GHz)
[55]		EBG	Size: 34×42.5 mm ² BW: 2.27-10.83 GHz	7.5 5.2	3.37-3.87 5.32-6.15
[56]					

[63]		Open-ended thin slits	Size: $35 \times 35 \text{ mm}^2$ BW: 3-11 GHz	8 6	5.15-5.35 5.725-5.825
[64]		Strips	Size: $24 \times 29 \text{ mm}^2$ BW: 3 - 11 GHz	17 18	3.0-3.6 5.1-6.1
[65]		SRRs	Size: $54 \times 47 \text{ mm}^2$ BW: 2.1-10.5 GHz	9 7 7.5	2.24-2.62 3.78-4.03 5.94-6.4
[66]		Closed-loop slots	Size: $25 \times 30 \text{ mm}^2$ BW: 3.02-11 GHz	14 8 7	3.3-3.6 5.15-5.35 5.725-5.825
[67]		Meandered lines	Size: $30 \times 39.3 \text{ mm}^2$ BW: 2.68 -11.15 GHz	7 6 5.8	3.3-3.6 5.15-5.35 5.725-5.825
[68]		Closed-loop ring resonators	Size: $33 \times 30 \text{ mm}^2$ BW: 2.8-11 GHz	7 5 5	3.3-3.7 5.15-5.35 5.725-5.825
[69]		Parasitic strips	Size: $30 \times 22 \text{ mm}^2$ BW: 2.92-15.7 GHz	6 8 7	2.26-3.71 5.15-5.37 5.78-5.95
[70]		Capacitive load loop (CLL)	Size: $27 \times 34 \text{ mm}^2$ BW: 2.8-11 GHz	8 8 6	3.3-3.6 5.15-5.35 5.725-5.825
[71]		QW-stubs and open-ended slots	Size: $28 \times 28.5 \text{ mm}^2$ BW: 2.8-11 GHz	25 7 17	3.15-3.62 5.1-5.38 5.72-6.12

[72]		CSRR	Size: $31 \times 31 \text{ mm}^2$ BW: 2.8-11.4 GHz	7 4.5 3.5 6	3.3-3.6 5.0-5.4 5.7-6.0 7.6-8.6
[73]		Two C-shaped slots and inverted U-shaped	Size: $26 \times 28 \text{ mm}^2$ BW: 3.1-12 GHz	8 5 6 4	5.1-5.43 5.78-5.98 7.2-7.79 8.03-8.83
[74]		U-shaped slot	Size: $30 \times 31 \text{ mm}^2$ BW: 2.8-12 GHz	10 6 7 7.5	3.5-3.6 4.5-4.8 5.15-5.35 5.725-5.825
[75]		C-shape slots and Open-circuit stubs	Size: $26 \times 31.8 \text{ mm}^2$ BW: 2.45-12 GHz	5 6 3 3 6	3.27-3.57 5.01-5.45 5.55-6.05 7.05-7.45 7.83-8.19

From the summary above, it shows that there were many UWB antenna techniques/designs capable of achieving band-notched characteristics in the open literature. However, in those literatures only the antenna in [75] can achieve most number of notches. The antenna incorporated with four C-shaped slots and open circuit stubs was successfully realized with five-band-notched functions throughout the UWB band. Nevertheless, there are several limitations of this antenna: 1). the size of the antenna is not compact enough. 2). the rejection performance at the notched frequency bands is to be improved (gain suppressions are less than 10 dB for the notched bands). Thus, there is desire to design the UWB-PMA with a more compact size and a very good level of rejection over the notched bands to mitigate the potential interference. The work will be presented in Chapter 4.

2.3 UWB Antennas with Reconfigurable Bands Rejection

In Section 2.2, UWB antennas with fixed band-notched characteristics have been reviewed. In this Section, several UWB antennas with reconfigurable band rejection operation incorporating with the switches have been proposed [76-86] and are summarized in Table 2-3.

In [77], the CPW-fed elliptical UWB monopole antenna was achieved to reject at 5.5 GHz by using MEMS switches to connect and disconnect the stubs into the radiator, as shown in Fig.2.29. The switching ON and OFF at single band rejection was proposed in [78] where a parasitic patch was added in the back of the rectangular monopole with an ideal switch to obtain the band notch.

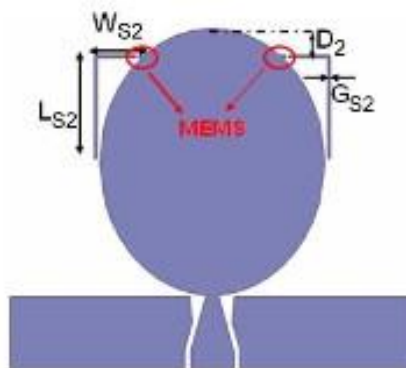


Fig. 2.29 An elliptical UWB antenna with switchable stubs [77]

The UWB planar monopole antennas with multiple-band-notched reconfigurable capability was also proposed in [80, 82, 86]. For instance, In [86], a CPW-fed antenna with a capability to operate in UWB band or narrow rejection bands operation was investigated, as shown in Fig. 2.30. The radiation element consisting of dual monopole elements is to enhance the antenna wideband performance. The band rejection operation of WIMAX and WLAN was achieved by defecting the ground plane with dielectric slits and

can be dynamically switching on/off by controlling the surface currents paths along the slits with eight PIN diodes. The PIN diodes effectively short circuit to the dielectric slits without affecting between the band notches.

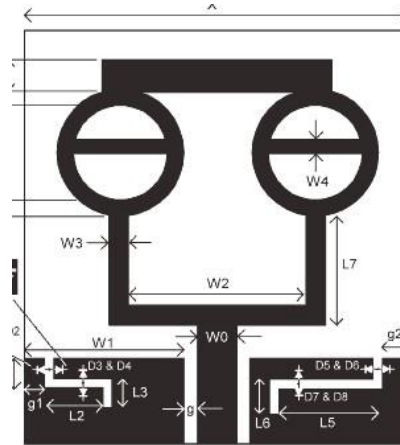


Fig. 2.30 A UWB planar monopole antenna with multiple-band-rejection switchable capability [86]

In the literature, many papers also discussed UWB slot antennas with multiple modes bands-notched reconfigurable ability by incorporating ideal switches or PIN diodes [79, 81, 83-85].

Ref. [79] presented a reconfigurable multi-band-rejection wide slot antenna. Two ideal switches on stepped impedance stub (SIS) and stepped impedance resonator (SIR) were used to obtain a dual rejection band between 5.5 and 8.8 GHz, as shown in Fig. 2.31. The gain values of the antenna were dropped to -5.6 and -3.8 dBi at the notched frequencies, respectively.

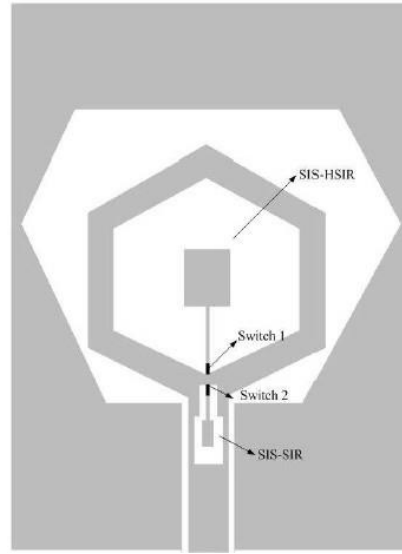


Fig. 2.31 A UWB slot antenna with multi-band-rejection switchable capability [79]

Furthermore in [84], a circular slot with tree arms on a radiating patch was introduced to improve the bandwidth of antenna and also to realize the switching functions, as shown in Fig. 2.33. By biasing two PIN diodes, the antenna achieved a UWB mode in the frequency range of 3.12-12.51 GHz, two single bands of 3.12-3.84 GHz and 5-6.07 GHz and a dual-band of 3.12-3.84 GHz and 4.9-6.02 GHz.

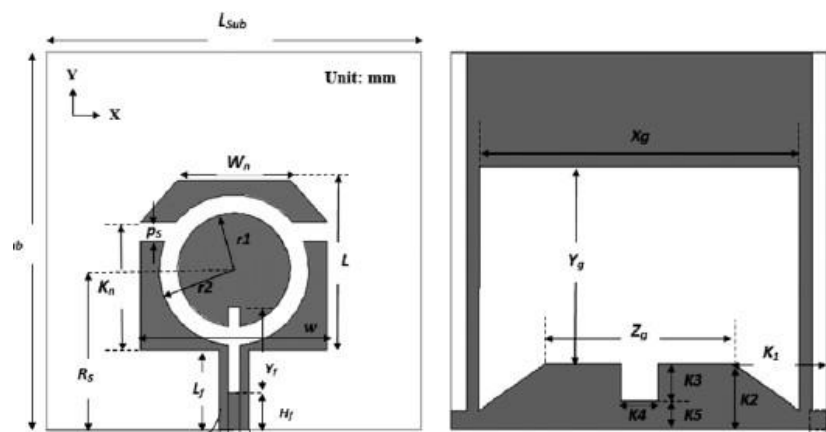
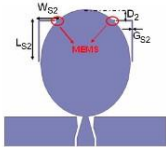
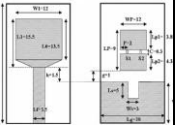
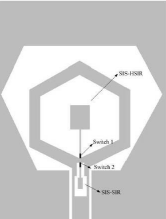


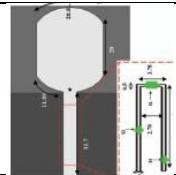
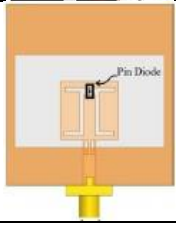
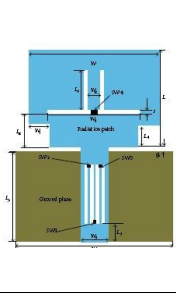
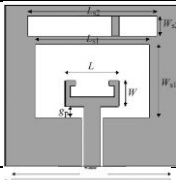
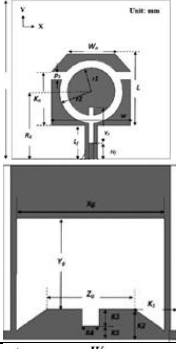
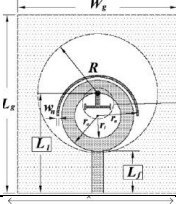
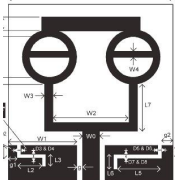
Fig. 2.32 A UWB circular slot antenna with multi-band-rejection switchable capability [84]

In addition, a summarized state of art of UWB antennas with reconfigurable band-rejection operation in the literature are listed in Table 2-3, which detailing in the antenna size, switching bands, switching type and number of switch. From among of designs/techniques, the antennas [77-78] were limited to one rejection band at a time and were thus not suitable for terminals which require rejecting more than one service band. Although the antennas reported in [79-86] have the capability to switch and reject more than two service bands, most of these designs suffered from the limitations such as the poor rejection at the notch frequency and a large number of the switches required for integration. For example in [86], the antenna incorporated eight PIN diodes, the large number of switches will introduce significant losses. Therefore, there is a desire for UWB reconfigurable band-notched antenna with a compact size and very good level of rejection at the desired frequencies. The work will be presented in Chapter 5.

Table 2-3 UWB antennas with reconfigurable band-rejection

Ref.	Antenna Layout	Antenna Structure	Size (mm ²)	Switching Bands (GHz)	Switching Type	Number of Switch
[77]		Elliptical monopole antenna	28 × 40	State 1: 5-6	MEMs	1
[78]		Rectangular monopole antenna	28 × 43	State: 5.15-5.825	Ideal Switch (Copper)	1
[79]		Hexagon slot antenna	24 × 32	State 1: 5-6.2 State 2: 8.7-9.5 State 3: 2.9-11	Ideal Switch (Copper)	2

UWB Antennas for Wireless Communications

[80]		C-shaped slots	30×26	Mode 1: 3.1-10.6 Mode 2: 3.08 Mode 3: 2.5 Mode 4: 4	PIN diode	3
[81]		Square slot antenna	20×20	Mode 1: 5.03-5.94 Mode 2: 3.04-11.7	PIN diode	1
[82]		Folded stepped impedance resonator	30×32	Case 1: 5.5, 6.8, 11.5 Case 2: 5.5, 11.5 Case 3: 8.7 Case 4: 8.7 Case 5: 6.8, 8.7 Case 6: 6.8, 8.7 Case 7: 6.8 Case 8: 3-14	Ideal Switch (Copper)	4
[83]		CPW fed slot antenna	29×34	Mode 1: 3.43-3.7 Mode 2: 3.01-10.4	Ideal Switch (Copper)	1
[84]		Rectangular parasitic strips	20×30	Mode 1: 3.12-3.84 Mode 2: 5-6.07 Mode 3: 3.12-3.82 4.9-6.06 Mode 4: 3.12-12.51	PIN diode	2
[85]		Circular slot antenna	40×45	State 1: 3-3.6 State 2: 2.9-4 State 3: 3-3.8 & 2.9-3.4 State 4: 2.6-10.6	PIN diode	2
[86]		CPW monopole antenna	28×30	State 1: 3.38 State 2: 5.55 State 3: 3.15 & 5.7 State 4: 3.1-10.8	PIN diode	8

2.4 UWB-MIMO Antennas

2.4.1 Techniques to Reduce Mutual Coupling

In diversity and MIMO systems, sufficient isolation between antennas is required. Reducing mutual coupling between antenna elements results in degraded radiation efficiency due to the leakage of the transmitted power from the excited antenna to the port of non-excited antenna, which the antennas couple strongly to each other and to the ground plane by sharing the surface currents. For many years, numerous studies have been done to find techniques to reduce the mutual coupling and increase the isolation between antenna elements. Most of these techniques are only suitable for narrowband MIMO systems [87-103]. These techniques are discussed in the next section.

2.4.2.1 Using Decoupling and Matching Networks (DMN)

A decoupling network can be simple. The technique of using a neutralized or suspended line between two antennas operating in the same frequency band can reduce the mutual coupling [87-90]. For example, in [87], the authors have inserted a suspended neutralization line physically connected to the two PIFAs element (operating in the UMTS band 1920-2170 MHz), as shown in Fig. 2.33. The introduction of the neutralization line was used to cancel out the existing mutual coupling since the line stores a certain amount of the current/signal delivered from one antenna element to the other antenna element. In other words, an additional path was created to compensate for the electrical currents on the PCB from one antenna to another. Thus, the antenna achieved the mutual coupling below -18 dB at frequency of 1.96 GHz.

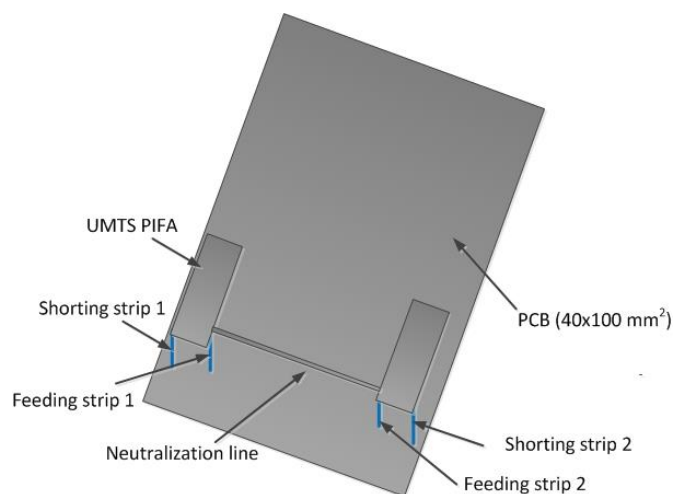


Fig. 2.33 3D view of the optimized structure with the neutralization line between the PIFA

Recently, a novel printed diversity monopole antenna was presented for Wi-Fi/WiMAX applications in [90], based on the same concept, but with much more complex neutralization line integration. The configuration of the antenna is shown in Fig. 2.34. The antenna comprises two crescent shaped radiators placed symmetrically with respect to a defected ground plane and neutralization lines were connected between them to achieve an impedance bandwidth of 2.4-4.2 GHz and the mutual coupling of less than -17 dB.

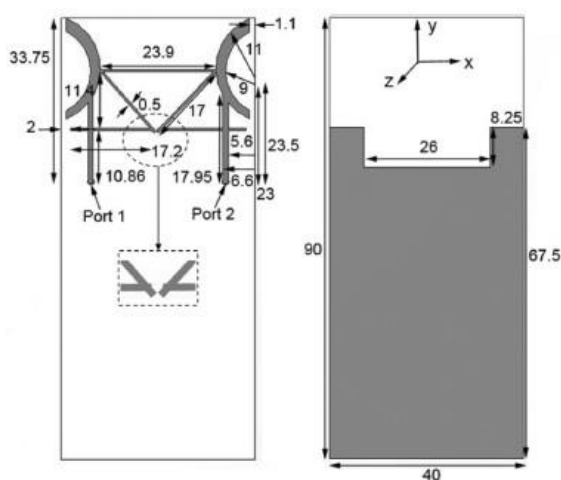


Fig. 2.34 The structure of a printed diversity monopole antenna [90]

A decoupling technique, using the circuit approach to improve the isolation of a compact dual-element antenna was investigated in [91]. As shown in Fig. 2.45, an LC components based branch line hybrid coupler (using the passive inductors and capacitors) was used and designed at 710 MHz to decouple the antenna elements. A series inductance and two parallel capacitances were placed instead of each $\lambda/4$ section of the branch line coupler. The isolation between the ports is better than 35 dB with match ports at 710 MHz. In addition, a similar approach was also demonstrated in [92].

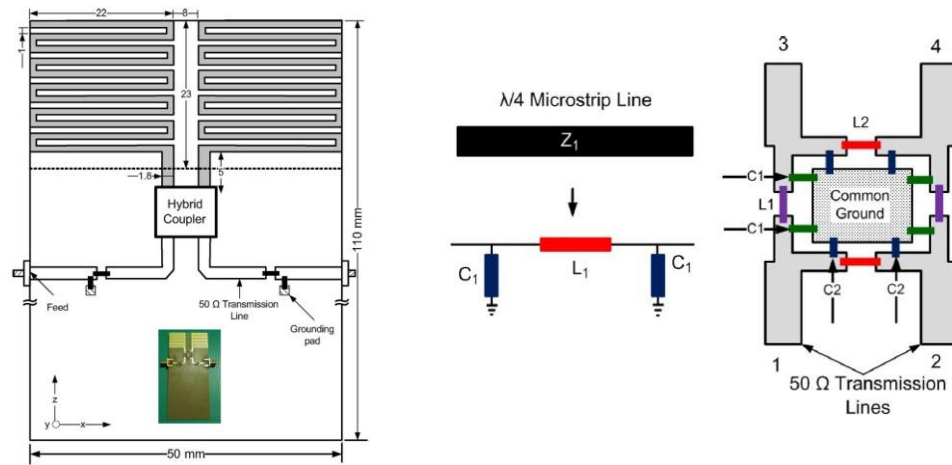


Fig. 2.35 The layout of the meander-line monopole antenna array (left), $\lambda/4$ transmission line with its equivalent circuit (middle) and LC-based branch-line coupler (right) [91]

2.4.2.2. Using Electromagnetic Band Gap (EBG) Structures

As stated in [93], an electromagnetic band gap (EBG) structure behaves as a high electromagnetic impedance surface (parallel resonant LC circuits). It acts as electric filters and has the ability of suppressing surface wave propagation in a frequency band which helps to enhance the ports isolation in printed antennas. In recent year, several of the narrow band MIMO antennas have been designed using this structure to reduce the mutual coupling [94-97].

In [94], four columns of fork-like EBG patches were inserted between the E-plane coupled antennas to reduce the mutual coupling, as shown in Fig. 2.36. When the EBG structure was employed, a 6.51 dB mutual coupling reduction was achieved at 5.2 GHz.

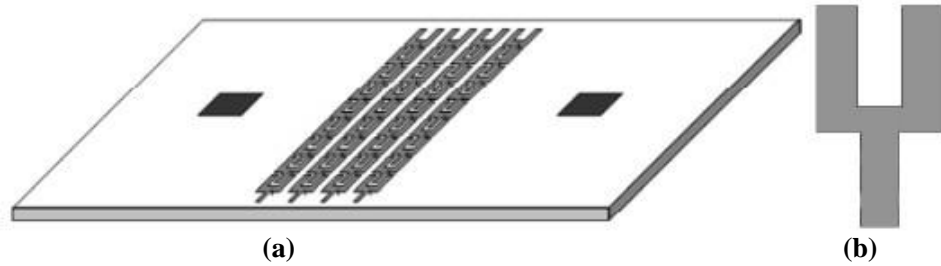


Fig. 2.36 Configuration of (a) The microstrip antenna separated four columns by the fork-like EBG, and (b) A fork-like EBG structure [94]

Recently, in [97], a configuration of uni-planar compact UC-EBG structures was used for both mutual coupling reduction and miniaturization purposes, as shown in Fig. 2.37. The antenna array with the UC-EBG superstrate has a relatively larger directivity, which was capable of suppressing the surface waves within a certain frequency band. The results showed about 10 dB reductions in mutual coupling at 5.75 GHz.

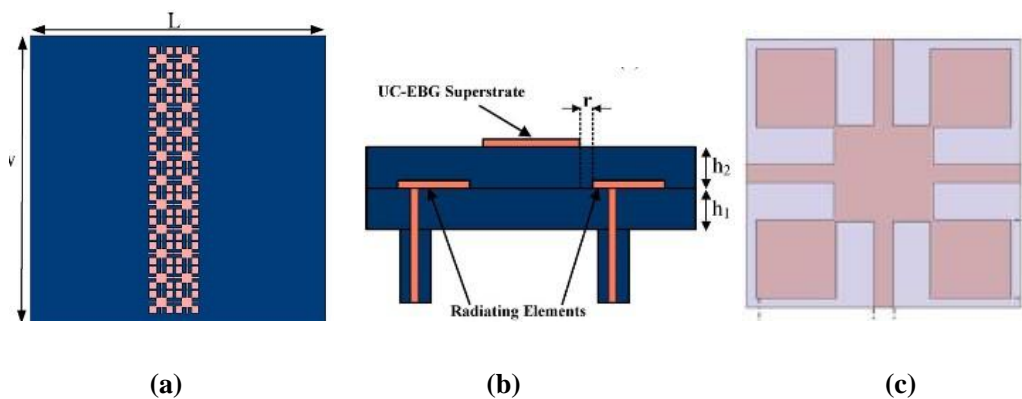


Fig. 2.37 The patch antenna array (a) Top view, (b) Size view, and (c) Unite cell of UC-EBG structure [97]

2.4.2.3. Using Defected Ground Structure (DGS)

Another well-known method to reduce the mutual coupling between two antennas elements is the introduction of resonate defects such as slots, slits and stubs on the ground plane [98-101].

In [98], the ground plane structure consisting of five pairs of slits etched into the middle of a ground plane of two closely packed PIFAs was investigated, as shown in Fig. 2.38. The structure behaves as a band-stop filter based on a parallel resonator (a combination of capacitance and inductance) which effectively suppresses the surface current waves, and thus it provides a lower mutual coupling between the antennas. The isolation was improved by 12 dB at 2.53 GHz. In [99], it has been demonstrated that the meander line embedded ground plane provides better isolation as compared with slitted ground plane.

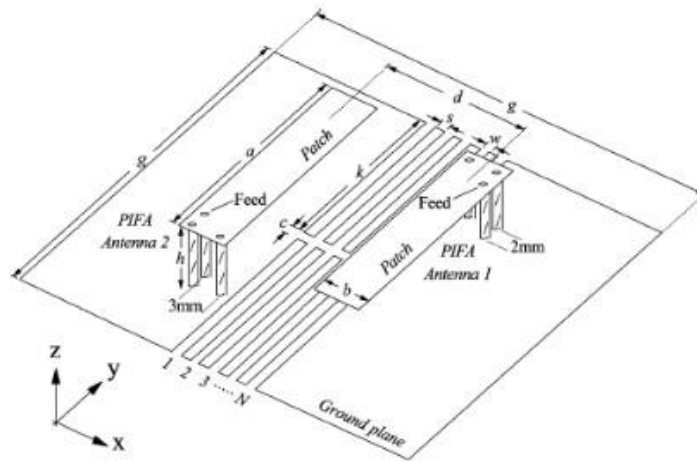


Fig. 2.38 Configuration of two closely-packed PIFAs with slotted ground plane structure [99]

Recently, a dual-feed planar PIFA using two isolated feeding port on common radiating plate was proposed in [100], as shown in Fig. 2.39. To reduce the mutual coupling an approach of removing the most of the conductor

to reduce the current flow on the ground plane between the two ports was implemented. The results showed that the antenna has an operation bandwidth from 2.4 to 2.7 GHz with more than 12 dB improvement in isolation.

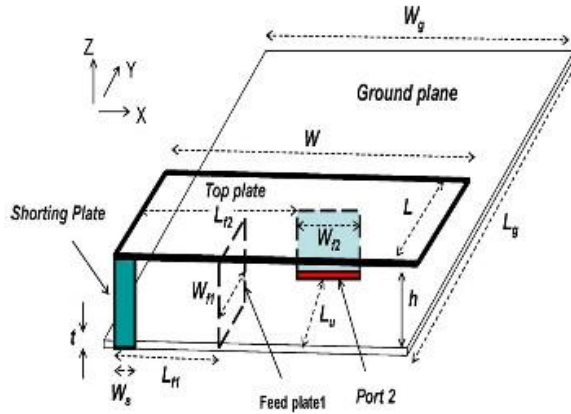


Fig. 2.39 Configuration of the dual-feed PIFA antenna with perpendicular feed [100]

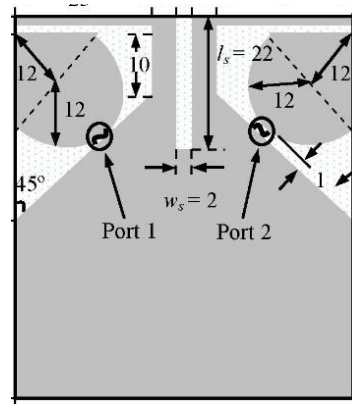


Fig. 2.40 Configuration of the cone-shaped radiating MIMO antenna [101]

In [101], a cone-shaped diversity antenna with size of $60 \times 62 \text{ mm}^2$ was designed as shown in Fig. 2.40. A slot was introduced at the upper center portion of the ground lane for improving the isolation and the impedance matching. The results showed that the antenna can operate frequency bandwidth from 3.1 to 5.8 GHz for $S_{21} < -20 \text{ dB}$; the gain variation is about 2 dB.

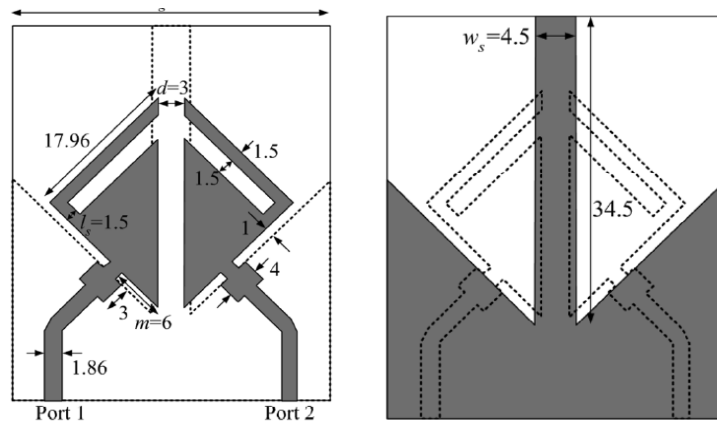


Fig. 2.41 Configuration of a UWB diversity antenna with two notched triangular radiators [103]

2.4.2.4. Using Spatial and Angular Variations

The technique of using spatial and angular variations relative to the antenna elements of array is very commonly used to reduce mutual coupling [102-103]. For instance, in [103], a compact ($45 \times 37 \text{ mm}^2$) diversity antenna with two notched triangular radiators was presented, as shown in Fig. 2.41. The antenna elements were fed orthogonally and were designed for the lower band of UWB, i.e. 3.1- 4.8 GHz. The isolation between two antenna elements is greater than 20 dB across the band.

2.4.2.5. Inserting stubs

The method of inserting stubs is mainly found in the literature for UWB-MIMO antennas [104-112]. For instance, a two element diversity planar antenna, with an inverted-Y shaped stub on the ground plane to improve the isolation, was proposed in [104], as shown in Fig. 2.42. The 10 dB return loss bandwidth was achieved from 3.2 to 10.6 GHz and isolation of more than 15 dB.

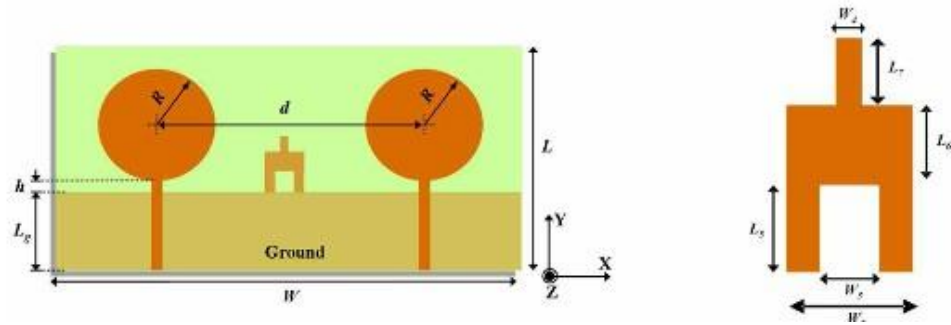
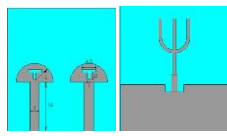
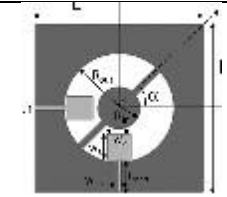
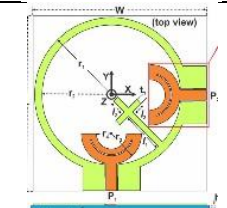


Fig. 2.42 Configuration of a UWB-MIMO antenna with two circular disc radiators elements [104]

In addition, a summarized state of art of MIMO-UWB antennas is listed in Table 2-4, which detailing in the antenna size, bandwidth (BW), gain variation (GV), radiation efficiency (RE) and isolation.

Table 2-4 Summarized states of the art on UWB-MIMO antennas

Ref.	Antenna Layout	Antenna Structure	Technique	Analyzed Parameters and Performances
[104]		Two circular disc radiator	Inserting an inverted-Y shaped stub	<ul style="list-style-type: none"> Size : $40 \times 68 \text{ mm}^2$ BW: 3.1-10.6 GHz GV: 2.5 dB Isolation: 15 dB
[105]		Circular shaped radiator	Separation distance	<ul style="list-style-type: none"> Size : $38 \times 91 \text{ mm}^2$ BW: 2.8-8.0 GHz GV: 2.5 dB Isolation: 17 dB
[106]		Two Y-shaped radiators	Inserting three stubs	<ul style="list-style-type: none"> Size : $64 \times 60 \text{ mm}^2$ BW: 2.27-10.2 GHz GV: 1.5 dB Isolation: 20 dB
[107]		Two square shaped radiators	Inserting cross shape stub	<ul style="list-style-type: none"> Size : $62 \times 64 \text{ mm}^2$ BW: 3.3-10.5 GHz GV: 3 dB Isolation: 18 dB

[108]		Two semicircular radiating elements	Using a fork-shaped slot	<div>✚</div> Size : $35 \times 40 \text{ mm}^2$ <div>✚</div> BW: 4.4 -10.7 GHz <div>✚</div> GV: 1.8 dB <div>✚</div> Isolation: 20 dB
[110]		An annular slot antenna for pattern diversity	Placing two shorts	<div>✚</div> Size : $80 \times 80 \text{ mm}^2$ <div>✚</div> BW: 3 -12 GHz <div>✚</div> RE: 60% <div>✚</div> Isolation: 15 dB
[111]		An annular slot and orthogonal feeding	A cross-shaped strip between the U-shaped stubs	<div>✚</div> Size : $58 \times 58 \text{ mm}^2$ <div>✚</div> BW: 2.8 -11 GHz <div>✚</div> RE: 70% <div>✚</div> GV: 2 dB <div>✚</div> Isolation: 14 dB

2.4.2 Design Considerations

Section 2.4.1 shows that many MIMO antennas have been proposed for UWB applications in open literature [87-111]. In [87-103], various decoupling techniques were employed to enhance isolation of two closed-placed ports/elements and most of these designs/techniques were only suitable for a relatively narrow band not for the entire UWB band. For those designs reported in [104-111], which could cover the entire UWB band with good isolation, most were not compact enough for small devices. For example, in [105] and [107], the UWB-MIMO antennas were designed with the sizes of 38 by 91 mm^2 and 62 by 64 mm^2 , and the mutual coupling coefficients of less than -17 dB and -18 dB, respectively. In addition, the MIMO antenna proposed in [106] was achieved probably the widest bandwidth from 2.27 to 10.6 GHz with a size of 64 by 60 = 3840 mm^2 and an isolation of 20 dB. There is still a huge demand for MIMO antennas with an even more compact size and an optimised minimum mutual coupling to cover the whole UWB band and ISM 2.45 GHz (i.e. roughly from 2.4 to 10.6 GHz). The detailed specifications of the desired

UWB-MIMO antenna are given in Table 2-5. The work will be presented in Chapter 6.

Table 2-5 Design consideration of the UWB-MIMO antennas

Parameters	Values
Operating Bandwidth	At least 3.1-10.6 GHz
Gain Variation	No more than 4 dB
Radiation Efficiency	Higher than 70%
Isolation	Not less than 15 dB
Correlation Coefficient	No greater than 0.5
Design Profile	Compact, printed and easy to fabricate

2.5 Summary

In this Chapter, the development of UWB/SWB antennas has been reviewed. In the field of UWB antennas with band-notched operation, it shows that quite a few UWB antennas with band-notched behaviours have been achieved and published in the literature. Only one proposed antenna, [75] can achieve quintuple-band-notched characteristics. However, this antenna has limited gain suppression. In the field of UWB antennas with reconfigurable band-rejection, most of them have with one fixed rejection band at a time and a few can switch with multi-mode band-rejection functions, but with limited band-notched performance. In the field of the UWB-MIMO antennas for wireless communications, most of the proposed designs are only able to operate over a narrow band not for the entire UWB band [87-103]. For those which could cover the entire UWB band [104-111], most antennas have not designed with a compact size for small devices [105-107,110]. To address the problems identified there is a need to further investigate planar UWB antennas for future wireless commutations which is the main objective of this study.

2.6 References

- [1] Federal Communications Commission, *First Report and Order 02-48*, Feb. 2002.
- [2] C. E. Shannon, "A mathematical theory of communication," *Bell Syst. Tech. J.*, vol. 27, pp. 379-423, 623-656, July & Oct. 1948.
- [3] Federal Communications Commission, "Revision of Part 15 of the commission's rules regarding ultra-wideband transmission systems, first report and order," *ET Docket 98-153, FCC 02-48*, pp. 1-118, Feb.14, 2002.
- [4] S. Zafar, G. Sinan and G. Ismail, "Ultra-wideband positioning systems: theoretical limits", *Ranging Algorithms, and Protocols*, Cambridge University Press, 2008.
- [5] V. Rumsey. "Frequency independent antennas," *Academic Press. New York*, 1966.
- [6] O. Lodge, "Electric telegraphy," *U. S. Patent No. 609*, 154 Aug. 16, 1898.
- [7] P. S. Carter, "Wide band short wave antenna and transmission line system," *U. S. Patent 2, 181, 870*, Dec. 1939.
- [8] S. A. Schelkunoff, "Ultra short wave radio system," *U.S. Patent 2,235,506*, March 18, 1941.
- [9] S. A. Schelkunoff, "Advanced antenna theory," *New York: John Wiley and Sons*, pp. 160, 1952.
- [10] L. N. Brillouin, "Broad band antenna," *U. S. Patent 2,454,766*, Nov. 1948.

- [11] S. S. Zhong, X. R. Yan and X. L. Liang, "UWB planar antennas technology," *Frontiers of Electric and Electronic Engineering in China*, 3(2), pp. 136-144, 2008.
- [12] G. Dubost and S. Zisler. "Antennas a large band," *New York: Masson*, pp. 128-129, 1976.
- [13] N. P. Agrawall, G. Kumar, and K. P. Ray, "Wide-band planar monopole antennas," *IEEE Trans. on Antennas and Propagation*, vol. 46, pp. 294-295, 1998.
- [14] J. A. Evans and M. J. Amunann, "Planar trapezoidal and pentagonal monopoles with impedance bandwidths in excess of 10:1," in *IEEE Antennas and Propagation Society International Symposium*, vol. 3, pp. 1558-1561, 1999.
- [15] S. Y. Suh, W. L. Stutaman and W. A. Davis, "A new ultra-wideband printed monopole antenna: the planar inverted cone antenna (PICA)," *IEEE Trans. on Antennas and Propagation*, vol. 52, no. 5, pp. 1361-1364, May 2004.
- [16] X. F. Bai, S. S. Zhong, and X.-L. Liang, "Leaf-shaped monopole antenna with extremely wide bandwidth," *Microwave and Optical Technology Letters*, vol. 48, pp. 1247-1250, 2006.
- [17] P. V. Anob, K. P. Ray, and G. Kumar, "Wideband orthogonal square monopole antennas with semi-circular base," in *IEEE Antennas and Propagation Society International Symposium*, vol.3, pp. 294-297, 2001.
- [18] E. Antonino-Daviu, M. Cabedo-Fabres, M. Ferrando-Bataller, and A. Valero-Nogueira, "Wideband double-fed planar monopole antennas," *Electronics Letters*, vol. 39, pp. 1635-6, 2003.

- [19] M. J. Ammann and C. Zhi-Ning, "A wide-band shorted planar monopole with bevel," *IEEE Trans. on Antennas and Propagation*, vol. 51, pp. 901-903, 2003.
- [20] E. Gazit, "Improved design of the Vivaldi antenna," *Microwaves, Antennas and Propagation, IEE Proceedings H*, vol. 135, pp. 89-92, 1988.
- [21] J. D. S. Langley, P. S. Hall, and P. Newham, "Novel ultra-wide-bandwidth Vivaldi antenna with low cross polarization," *Electronics Letters*, vol. 29, pp. 2004-2005, 1993.
- [22] D. C. Chang, J. C. Liu and M. Y. Liu, "Improved U-shaped stub rectangular slot antenna with tuning pad for UWB applications," *Electronics Letters*, vol. 41, pp. 1095-1097, 2005.
- [23] S. Cheng, P. Halbjorner and A. Rydberg, "Printed slot planar inverted cone antenna for ultra-wideband Applications," *IEEE Antennas and Wireless Propagation Letters*, vol. 7, pp. 18-21, 2008.
- [24] E. S. Angelopoulos, A. Z. Anastopoulos, D. I. Kaklamani, et al., "Circular and elliptical CPW-fed slot and microstrip-fed antennas for ultra-wideband applications," *IEEE Antennas and Wireless Propagation Letters*, vol.5, no. 1, pp. 294-297, Dec. 2006.
- [25] J. W. Niu and S. S. Zhong, "A CPW-fed broadband slot antenna with linear tape," *Microwave and Optical Technology Letters*, vol. 41, pp. 218-221, 2004.
- [26] S. Barbarino and F. Consoli, "Study on super-wideband planar asymmetrical dipole antennas of circular shape," *IEEE Trans. on Antennas and Propagation*, vol. 58, pp. 4074-4078, 2010.

- [27] H. Oraizi and S. Hedayati, "Wideband monopole fractal antenna with Hilbert fractal slot patterned ground plane," in *41st European Microwave Conference (EuMC)*, pp. 242-245, 2011.
- [28] M. A. Dorostkar, M. T. Islam, and R. Azim, "Design of a novel super wide band circular-hexagonal fractal antenna," *Progress in Electromagnetics Research*, vol. 139, pp. 229-245, 2013.
- [29] C. Ke-Ren, C. Sim, and R. Jeen-Sheen, "A compact monopole antenna for super wideband applications," *IEEE Antennas and Wireless Propagation Letters*, vol. 10, pp. 488-491, 2011.
- [30] M. Almalkawi, M. Westrick, and V. Devabhaktuni, "Compact super wideband monopole antenna with switchable dual band-notched characteristics," in *Microwave Conference Proceedings (APMC), Asia-Pacific*, pp. 723-725, 2012.
- [31] S. S. Zhong, X. L. Liang and W. Wang, "Compact elliptical monopole antenna with impedance bandwidth in excess of 21:1," *IEEE Trans. on Antennas and Propagation*, vol. 55, pp. 3082-3085, 2007.
- [32] M. Akbari, M. Koohestani, C. Ghobadi, and J. Nourinia, "Compact CPW-FED printed monopole antenna with super-wideband performance," *Microwave and Optical Technology Letters*, vol. 53, pp. 1481-1483, 2011.
- [33] D. Tran, A. Szilagyi, I. E. Lager, P. Aubry, L. P. Ligthart, and A. Yarovoy, "A super wideband antenna," in *5th European Conference on Antennas and Propagation (EuCAP)*, Rome, pp. 2656-2660, 2011.
- [34] E. Pancera, D. Modotto, A. Locatelli, F. M. Pigozzo, and C. De Angelis, "Novel design of UWB antenna with band-Notch capability," *European Conference on Wireless Technologies*, pp. 48-50, 2007.

- [35] S. Nikolaou, B. Kim, Y. S. Kim, J. Papapolymerou, and M. M. Tentzeris, "CPW-fed ultra-wideband (UWB) monopoles with band rejection characteristic on ultra-thin organic substrate," *Proceedings of APMC 2006*, CD-Rom: FROF-26, pp. 12-15, Dec. 2006.
- [36] T. Dissanayake and K. P. Esselle, "Prediction of the notch frequency of slot loaded printed UWB antennas," *IEEE Trans. on Antennas and Propagation*, vol. 55, pp. 3320-3325, 2007.
- [37] Z. A. Zheng, and Q. X. Chu, "A CPW-Fed ultrawideband antenna with dual notched bands," in. *IEEE International Conference on Ultra-Wideband ICUWB 2009*, pp. 645-648, 2009.
- [38] E. Antonino-Daviu, et al., "Modal analysis and design of band-notched UWB planar monopole antennas," *IEEE Trans. on Antennas and Propagation*, vol. 58, pp. 1457-1467, 2010.
- [39] C. Qing-Xin and Y. Ying-Ying, "A compact ultra-wideband antenna with 3.4/5.5 GHz dual band-notched characteristics," *IEEE Trans. on Antennas and Propagation*, vol. 56, pp. 3637-3644, 2008.
- [40] Y. Kim and D. H. Kwon, "CPW-fed planar ultra wideband antenna having a frequency band notch functions," *Electronics Letters*, vol. 40, pp. 403-405, 2004.
- [41] L. Liu, Y. F. Weng, S. W. Cheung, T. I. Yuk, and T. Peter, "Deep band-notched characteristic using meander lines for UWB monopole antennas," *PIERS Proceedings, Kuala Lumpur, Malaysia*, pp. 27-30, March, 2012.
- [42] S. W. Qu, et al., "A band-notched ultra-wideband printed monopole antenna," *IEEE Antennas and Wireless Propagation Letters*, vol. 5, pp. 495-498, 2006.

- [43] A. M. Abbosh and M. E. Bialkowski, "Design of UWB planar band-notched antenna using parasitic elements," *IEEE Trans. on Antennas and Propagation*, vol. 57, pp. 796-799, 2009.
- [44] S. Nikolaou, N. D. Kingsley, G. E. Ponchak, J. Papapolymerou, M. M. Tentzeris, "UWB elliptical monopoles with a reconfigurable band notch using MEMS switches actuated without bias lines," *IEEE Trans. on Antennas and Propagation*, vol.57, no.8, pp. 2242-2251, Aug. 2009.
- [45] K. S. Ryu and A. A. Kishk, "UWB antenna with single or dual band-notches for lower WLAN band and upper WLAN band," *IEEE Trans. on Antennas and Propagation*, vol. 57, pp. 3942-3950, 2009.
- [46] K. H. Kim, et al., "Band-notched UWB planar monopole antenna with two parasitic patches," *Electronics Letters*, vol. 41, pp. 783-785, 2005.
- [47] C. Y. Huang, W. C. Hsia, and J.-S. Kuo, "Planar ultra-wideband antenna with a band-notched characteristic," *Microwave and Optical Technology Letters*, vol. 48, pp. 99-101, 2006.
- [48] J. B. Pendry, A. J. Holden, D. J. Robbins, and W. J. Stewart, "Magnetism from conductors and enhanced nonlinear phenomena," *IEEE Transactions on Microwave Theory and Techniques*, vol. 47, pp. 2075-2084, 1999.
- [49] J. Kim, et al., "5.2 GHz notched ultra-wideband antenna using slot-type SRR," *Electronics Letters*, vol. 42, pp. 315-316, 2006.
- [50] L. Li, Z. L. Zhou, J. S. Hong, and B. Z. Wang, "Compact dual-band-notched UWB planar monopole antenna with modified SRR," *Electronics Letters*, vol. 47, pp. 950-951, 2011.

- [51] J. Nam-I, K. Dang-Oh, and K. Che-Young, "A compact band notched UWB antenna for mobile applications," *PIERS Online*, vol. 6, no. 2, 2010.
- [52] J. R. Kelly, P. S. Hall, and P. Gardner, "Planar band-notched UWB antenna," in *3rd European Conference on Antennas and Propagation (EuCAP), Berlin*, pp. 1636-1639, 2009.
- [53] J. R. Kelly, P. S. Hall, P. Gardner, and F. Ghanem, "Integrated narrow/band-notched UWB," *Electronics Letters*, vol. 46, pp. 814-816, 2010.
- [54] M. Yazdi and N. Komjani, "Design of a band-notched UWB monopole antenna by means of an EBG structure," *IEEE Antennas and Wireless Propagation Letters*, vol. 10, pp. 170-173, 2011.
- [55] F. Xu, Z.-X. Wang, X. Chen, and X.-A. Wang, "Dual band-notched UWB antenna based on spiral electromagnetic-bandgap structure," *Progress in Electromagnetics Research B*, vol. 39, pp. 393-409, 2012.
- [56] K. S. Ryu and A. A. Kishk, "UWB antenna with single or dual band-notches for lower WLAN band and upper WLAN band," *IEEE Trans. on Antennas and Propagation*, vol. 57, pp. 3942-3950, 2009.
- [57] M. Abdollahvand, G. Dadashzadeh, D. Mostafa, "Compact dual band-notched printed monopole antenna for UWB application," *IEEE Antennas and Wireless Propagation Letters*, vol. 9, pp. 1148-1151, 2010.
- [58] Q. X. Chu and Y. Y. Yang, "A compact ultra-wideband antenna with 3.4/5.5 GHz dual band-notched characteristics," *IEEE Trans. on Antennas and Propagation*, vol. 56, pp. 3637-3644, 2008.

- [59] W. S. Chen and K. Y. Ku, "Band-rejected design of the printed open slot antenna for WLAN/WiMAX Operation," *IEEE Trans. on Antennas and Propagation*, vol. 56, pp. 1163-1169, 2008.
- [60] J. Wen and C. Wenquan, "A novel UWB antenna with dual notched bands for WiMAX and WLAN Applications," *IEEE Antennas and Wireless Propagation Letters*, vol. 11, pp. 293-296, 2012.
- [61] Y. Sung, "UWB monopole antenna with two notched bands based on the folded stepped impedance resonator," *IEEE Antennas and Wireless Propagation Letters*, vol. 11, pp. 500-502, 2012.
- [62] L. Xiong and P. Gao, "Dual-band planar monopole antenna for Bluetooth and UWB applications with WIMAX and WLAN band-notched," *Progress in Electromagnetics Research Letters*, vol. 28, pp. 183-194, 2012.
- [63] D. Zhou, S. Gao, et al., "A simple and compact planar UWB antenna with single or dual-band-notched," *Progress in Electromagnetics Research*, vol. 123, pp. 47-65, 2012.
- [64] F. Zhu, S. Gao, J. Z. Li, and J. D. Xu, "Planar asymmetrical ultra-wideband antenna with improved multiple band-notched characteristics," *Electronics Letters*, vol. 48, pp. 615-617, 2012.
- [65] Y. Zhang, W. Hong, C. Yu, Z. Q. Kuai, Y. D. Don, and J. Y. Zhou, "Planar ultra-wideband antennas With multiple notched bands based on etched slots on the patch and/or split ring resonators on the feed line," *IEEE Trans. on Antennas and Propagation*, vol. 56, pp. 3063-3068, 2008.
- [66] T. Ming-Chun, S. Q. Xiao; T. W. Deng, D. Wang, J. Guan; B. Z. Wang; G. Ding. Ge, "Compact UWB antenna with multiple band-notches for WiMAX and WLAN," *IEEE Trans. on Antennas and Propagation*, vol. 59, no. 4, pp. 1372-1376, April 2011.

- [67] Y. F. Weng, S. W. Cheung, and T. I. Yuk, "Triple band-notched UWB antenna using meandered ground stubs," in *Antennas and Propagation Conference (LAPC), 2010*, Loughborough, pp. 341-344, 2010.
- [68] M. Almalkawi and V. Devabhaktuni, "Ultra-wideband antenna with triple band-notched characteristics using closed-loop ring resonators," *IEEE Antennas and Wireless Propagation Letters*, vol. 10, pp. 959-962, 2011.
- [69] M. T. Islam, R. Azim, and A. T. Mobashsher, "Triple band-notched planar UWB antenna using parasitic strips," *Progress in Electromagnetics Research*, vol. 129, pp. 161-179, 2012.
- [70] L. Chia-Ching, J. Peng, and R. W. Ziolkowski, "Single, dual and tri-band-notched Ultra-wideband (UWB) antennas using capacitively Loaded Loop (CLL) Resonators," *IEEE Trans. on Antennas and Propagation*, vol. 60, pp. 102-109, 2012.
- [71] F. G. Zhu, S. Gao, et al., "Multiple band-notched UWB antenna with band-rejected elements integrated in the feed line," *IEEE Trans. on Antennas and Propagation*, vol. 61, pp. 3952-3960, 2013.
- [72] Y. Q. Cao, J. X. Wu, H. C. Yang, "Design of CPW-fed monopole antenna with quadruple band-notched function for UWB application," *2011 International Conference on Computational Problem-Solving (ICCP)*, pp. 353-356, 2011.
- [73] X. Y. Li, L. S. Yan, W. Pan, and B. Luo, "A compact printed quadruple band-notched UWB antenna," *International Journal of Antennas and Propagation*, vol. 12, 2013.
- [74] Z. H. Wu, F. Wei, X. W. Shi, and W.-T. Li, "A compact quad band-notched UWB monopole antenna loaded one lateral l-shaped slot," *Progress in Electromagnetics Research*, vol. 139, pp. 303-315, 2013.

- [75] J. Xu, D. Y. Shen, X. P. Zhang, and K. Wu, "A compact disc UltrawideBand (UWB) antenna with quintuple band rejections," *IEEE Antennas and Wireless Propagation Letters*, vol. 11, pp. 1517-1520, 2012.
- [76] P. S. Hall, P. Gardner, J. Kelly, E. Ebrahimi, M. R. Hamid, F. Ghanem, F. J. Herraiz-Martinez, and D. Segovia-Vargas, "Reconfigurable antenna challenges for future radio systems," *2009 3rd European Conference on Antennas and Propagation*, vol. 1-6, pp. 902-908, 2009.
- [77] S. Nikolaou, N. D. Kingsley, G. E. Ponchak, J. Papapolymerou, and M. M. Tentzeris, "UWB elliptical monopoles with a reconfigurable band notch using MEMS switches actuated without bias lines," *IEEE Trans. on Antennas and Propagation*, vol. 57, pp. 2242-2251, 2009.
- [78] A. H. Khidre, H. A. El Sadek, and H. F. Ragai, "Reconfigurable UWB printed monopole antenna with band rejection covering IEEE 802.11a/h," *IEEE in Antennas and Propagation Society International Symposium*, 2009. APSURSI '09. pp. 1-4, 2009.
- [79] Y. Li, W. Li, and Q. Ye, "Compact reconfigurable UWB antenna integrated with stepped impedance stub loaded resonators and switches," *Progress in Electromagnetics Research C*, vol. 27, pp. 239-252, 2012.
- [80] M. E. Zamudio, Y. Tawk, J. Costantine, S. E. Barbin, and C. G. Christodoulou, "Reconfigurable filter embedded into an antenna for UWB cognitive radio environment," in *2011 IEEE-APS Topical Conference on Antennas and Propagation in Wireless Communications (APWC)*, pp. 714-717, 2011.
- [81] A. Valizade, C. Ghobadi, J. Nourinia, M. Ojaroudi, "A novel design of reconfigurable slot antenna with switchable band notch and

- multiresonance functions for UWB applications,” *IEEE Antennas and Wireless Propagation Letters*, vol. 11, pp. 1166-1169, 2012.
- [82] Y. S. Li, W.X. Li, and Q. B. Ye, “A CPW-fed circular wide-slot UWB antenna with wide tunable and flexible reconfigurable dual notch bands,” *The Scientific World Journal*, vol. 2013, pp. 1-10, 2013.
- [83] D. Thiripurasundari and D. S. Emmanuel, “CPW fed slot antenna with reconfigurable rejection bands for UWB application,” *Radio electronics and Communications Systems*, vol. 56, pp. 278-284, 2013.
- [84] N. Tasouji, J. Nourinia, C. Ghobadi, and F. Tofigh, “A novel printed UWB slot antenna with reconfigurable band-notch characteristics,” *IEEE Antennas and Wireless Propagation Letters*, vol. 12, pp. 922-925, 2013.
- [85] A. A. Kalteh, G. R. DadashZadeh, M. Naser-Moghadasi, and B. S. Virdee, “Ultra-wideband circular slot antenna with reconfigurable notch band function,” *IET Microwaves, Antennas & Propagation*, vol. 6, 2012.
- [86] M. Naser-Moghadasi, M. R. Harty, M. S. M. Seyed Momeni and B. S. Virdee, “Novel compact UWB antenna with reconfigurable dual-band notches using pin diode switches actuated without $\lambda_g/4$ DC bias lines,” *Microwave and Optical Technology Letters*, 54, pp. 2392-2397, 2012.
- [87] A. Diallo, C. Luxey, P. Le-Thuc, R. Staraj, and G. Kossiavas, “Study and reduction of the mutual coupling between two mobile phone PIFAs operating in the DCS1800 and UMTS bands,” *IEEE Trans. on Antennas and Propagation*, vol. 54, pp. 3063-3074, 2006.
- [88] S. W. Su and C. T. Lee, “Printed two monopole-antenna system with a decoupling neutralization line for 2.4 GHz MIMO applications,” *Microwave and Optical Technology Letters*, vol. 53, pp. 2037-2043, 2011.

- [89] A. Chebihi, C. Luxey, A. Diallo, P. Le Thuc, and R. Staraj, "A novel isolation technique for closely spaced PIFAs for UMTS mobile phones," *IEEE Antennas and Wireless Propagation Letters*, vol. 7, pp. 665-668, 2008.
- [90] S. Chan Hwang, R. A. Abd-Alhameed, Z. Z. Abidin, N. J. McEwan, and P. S. Excell, "Wideband printed MIMO/diversity monopole antenna for WiFi/WiMAX applications," *IEEE Trans. on Antennas and Propagation*, vol. 60, pp. 2028-2035, 2012.
- [91] R. A. Bhatti, Y. Soongyu, and P. Seong-Ook, "Compact antenna array with port decoupling for LTE-standardized mobile phones," *IEEE Antennas and Wireless Propagation Letters*, vol. 8, pp. 1430-1433, 2009.
- [92] S.-C Chen, Y-S Wang, and S-J Chung, "A decoupling technique for increasing the port isolation between two strongly coupled antennas," *IEEE Trans. on Antennas and Propagation*, vol. 56, issue 12, pp. 3650-3658, 2008.
- [93] Y. Fan and Y. Rahmat-Samii, "Mutual coupling reduction of microstrip antennas using electromagnetic band-gap structure," in *IEEE Antennas and Propagation Society International Symposium, 2001*. vol. 2, pp. 478-481, 2001.
- [94] Y. Li, F. Mingyan, C. Fanglu, S. Jingzhao, and F. Zhenghe, "A novel compact electromagnetic-bandgap (EBG) structure and its applications for microwave circuits," *IEEE Transactions on Microwave Theory and Techniques*, vol. 53, pp. 183-190, 2005.
- [95] E. Rajo-Iglesias, O. Quevedo-Teruel, and L. Inclan-Sanchez, "Study of mutual coupling reduction in single and stacked multilayer patch antennas by using planar EBG structures," in *IEEE Antennas and Propagation Society International Symposium*, pp. 393-396, 2007.

- [96] E. Michailidis, C. Tsimenidis, and G. Chester, "Mutual coupling reduction in a linear two element patch array and its effect on theoretical MIMO capacity," in *Antennas and Propagation Conference. LAPC 2008*. Loughborough, pp. 457-460, 2008.
- [97] H. S. Farahani, M. Veysi, M. Kamyab, and A. Tadjalli, "Mutual coupling reduction in patch antenna arrays using a UC-EBG superstrate," *IEEE Antennas and Wireless Propagation Letters*, vol. 9, pp. 57-59, 2010.
- [98] C. Chi-Yuk, C. Chi-Ho, R. D. Murch, and C. R. Rowell, "Reduction of mutual coupling between closely-packed antenna elements," *IEEE Trans. on Antennas and Propagation*, vol. 55, pp. 1732-1738, 2007.
- [99] F. Jolani, A. M. Dadgarpour, and G. Dadashzadeh, "Reduction of mutual coupling between dual-element antennas with new PBG techniques," *13th International Symposium on Antenna Technology and Applied Electromagnetics and the Canadian Radio Science Meeting, ANTEM/URSI 2009*, pp. 1-4, 2009.
- [100] H. T. Chattha, Y. Huang, S. J. Boyes, and X. Zhu, "Polarization and pattern diversity-based dual-feed planar inverted-F antenna," *IEEE Trans. on Antennas and Propagation*, vol. 60, pp. 1532-1539, 2012.
- [101] L. Liu, H. Zhao, T. S. P. See, and Z. N. Chen, "A printed ultra-wideband diversity antenna," in *The 2006 IEEE 2006 International Conference on Ultra-Wideband*, pp. 351-356, 2006.
- [102] K. L. Wong, S. W. Su, and Y. L. Kuo, "A printed ultra-wideband diversity monopole antenna," *Microwave and Optical Technology Letters*, vol. 38, pp. 257-259, 2003.
- [103] T. S. P. See, A. M. L. Swee, and Z. N. Chen, "Correlation analysis of UWB MIMO antenna system configurations," *IEEE International Conference on Ultra-Wideband. ICUWB 2008*, pp. 105-108, 2008.

- [104] A. I. Najam, Y. Duroc, and S. Tedjni, "UWB-MIMO antenna with novel stub structure," *Progress in Electromagnetics Research C*, vol. 19, pp. 245-257, 2011.
- [105] M. Jusoh, M. F. B. Jamlos, M. R. Kamarudin, and M. F. B. A. Malek, "A MIMO antenna design challenges for UWB application," *Progress in Electromagnetics Research B*, vol. 36, pp. 357-371, 2012.
- [106] H. Seokjin, L. Jaewon, and C. Jaehoon, "Design of UWB diversity antenna for PDA applications," *10th International Conference on Advanced Communication Technology, ICACT 2008*, pp. 583-585, 2008.
- [107] C. Yong, L. Wen-jun, C. Chong-hu, C. Wei, and L. Yong, "Printed diversity antenna with cross shape stub for ultra-wideband applications," *11th IEEE Singapore International Conference on Communication Systems, ICCS 2008*, pp. 813-816, 2008.
- [108] K. M. Prasanna and S. K. Behera, "Compact two-port UWB MIMO antenna system with high isolation using a fork-shaped structure," *International Conference on Communications and Signal Processing (ICCSP)*, pp. 726-729, 2013.
- [109] C. Yong, L. Wen-jun, and C. Chong-hu, "Printed diversity antenna for ultra-wideband applications," in *IEEE International Conference on Ultra-Wideband (ICUWB), 2010*, pp. 1-4, 2010.
- [110] M. Gallo, E. Antonino-Daviu, M. Ferrando-Bataller, M. Bozzetti, J. M. Molina-Garcia-Pardo, and L. Juan-Llacer, "A broadband pattern diversity annular slot antenna," *IEEE Trans. on Antennas and Propagation*, vol. 60, pp. 1596-1600, 2012.
- [111] B. P. Chacko, G. Augustin, and T. A. Denidni, "Uniplanar slot antenna for ultra wideband polarization-diversity applications," *IEEE Antennas and Wireless Propagation Letters*, vol. 12, pp. 88-91, 2013.

CHAPTER 3 PLANAR UWB/SWB MONOPOLE ANTENNA DESIGN

3.1 Introduction

Due to the importance of the planar UWB antennas, in this Chapter, investigations on a simple circular microstrip-fed planar UWB monopole antenna using both the numerical and experimental approaches are firstly conducted. Several bandwidth enhancement techniques, such as adding two ears to the radiator and truncated/smoothed the ground plane, are then implemented to achieve SWB performance. The former and latter are used to improve the bandwidth of the circular monopole antenna (CMA) at lower and higher frequencies, respectively. The aim is to design a planar SWB monopole antenna with a small size and stable radiation patterns.

3.2 UWB Planar Monopole Antenna Design

A circular monopole antenna (CMA) is chosen as a basic structure due to the fact that it has a wide operating bandwidth, the satisfactory radiation properties (nearly omni-directional radiation patterns) and simple structures. The CMA used was based on [1], and has been re-designed to operate over a bandwidth of 2.45 to 10.6 GHz (including UWB and ISM 2.45 bands). The geometry of the CMA is shown in Fig. 3.1. The antenna is simulated and fabricated on FR4 substrate which has relative permittivity $\epsilon_r = 4.3$ with a thickness of 1.5 mm. The CMA with a radius of R and a $50\ \Omega$ microstrip-fed line are printed on the same side of the FR4 substrate. L_{sub} and W_{sub} denote the length and the width of the substrate, respectively. The width of the microstrip feed line is fixed at $W_f = 2.8$ mm to achieve $50\ \Omega$ impedance matching. The conducting ground plane with a length of $L_{gnd} = 19.7$ mm is placed on the back side of the substrate. g is the feed gap between the feed point and the ground plane.

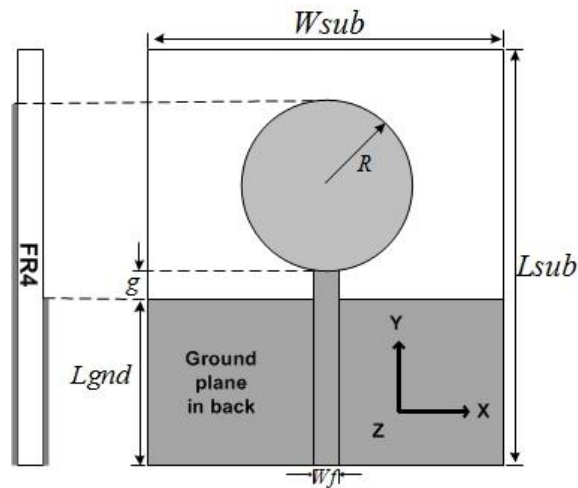


Fig. 3.1 Geometry of the circular monopole antenna

The photograph of the circular monopole antenna is shown in Fig. 3.2 with the optimum design values, *i.e.* $W_{sub} = 42$ mm, $L_{sub} = 45$, $R = 10$ mm, $g = 0.4$ mm and $L_{gnd} = 19.7$ mm. The reflection coefficients $|S_{11}|$ of the CMA are investigated as presented in Fig. 3.3. Both the simulated and measured results are in reasonable agreement, while the difference between them is probably due to fabrication errors and the SMA connector was not taking into account during the simulation analysis. An important feature is that the antenna can operate from 2.45 to 10.6 GHz with the reflection coefficient less than -10 dB.

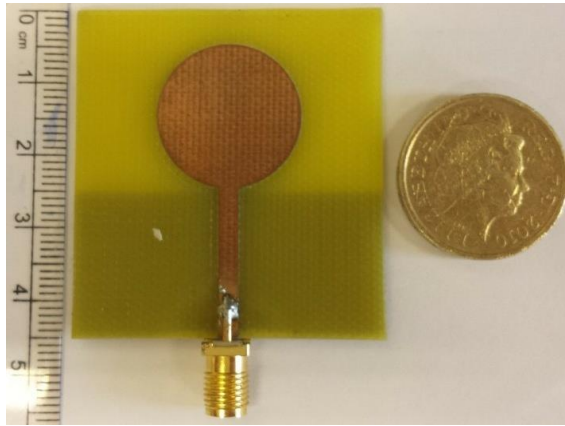


Fig. 3.2 Photograph of the circular monopole antenna

In addition, the effects of the feeding gap g and the width of the ground plane W_{sub} on the impedance characteristic of the CMA are investigated, as shown Figs. 3.4 and 3.5, respectively.

From Fig. 3.4, it can be observed that the resonant frequency slightly decreases as the feeding gap increases. But the impedance bandwidth is significantly affected, which the impedance matching of the antenna is getting worse. The optimum feeding gap is found to be at $g = 0.4$ mm. In practice, the gap size may not be a parameter for antenna designers to change.

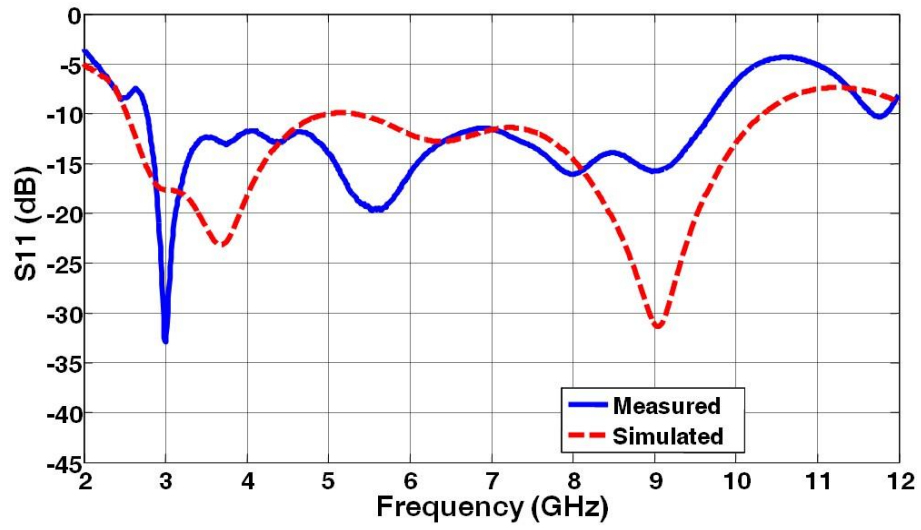


Fig. 3.3 Simulated and measured reflection coefficient curves of the CMA

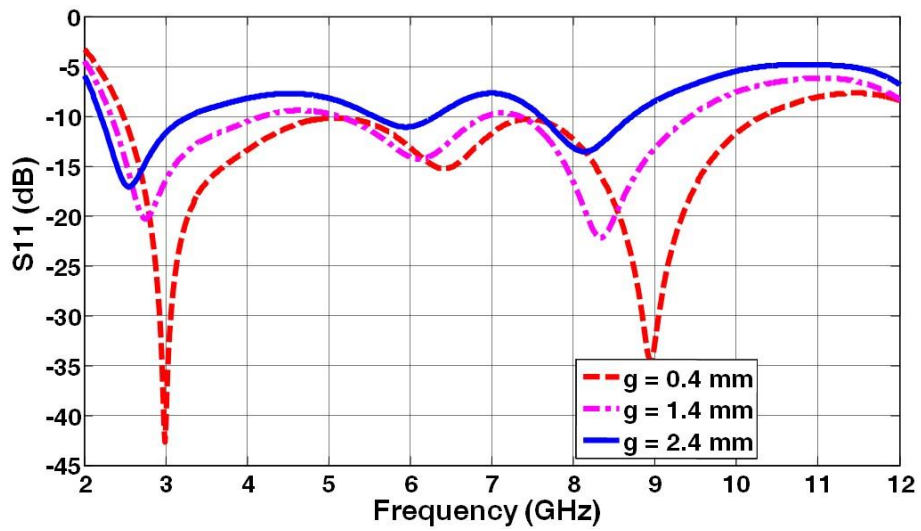


Fig. 3.4 Simulated reflection coefficient curves of the CMA for various g

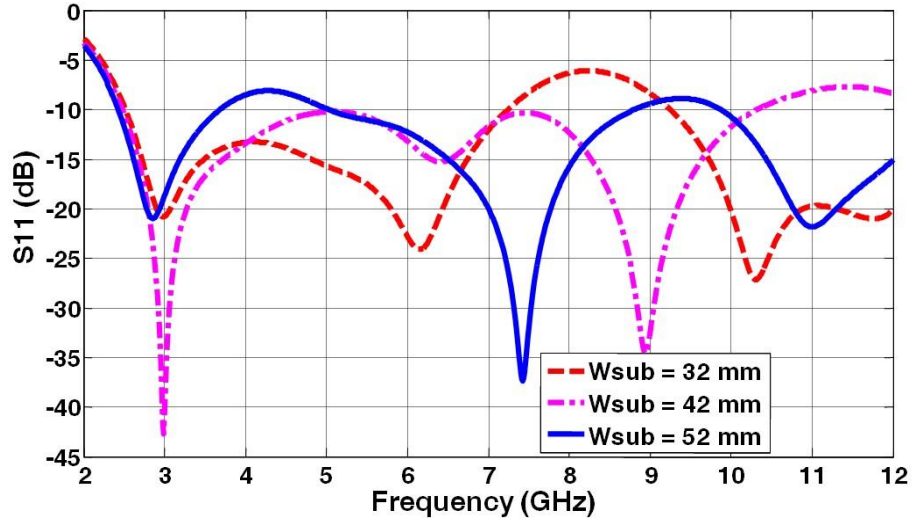


Fig. 3.5 Simulated reflection coefficients of the CMA for various W_{sub}

The width of the ground plane W_{sub} is another design parameter affecting the antenna operation. The simulated reflection coefficients $|S_{11}|$ of the CMA with various ground-plane widths W_{sub} (varying from 32 to 52 mm), are obtained and shown in Fig. 3.5. The ground length L_{gnd} is fixed at 19.7 mm. It can be observed that the -10 dB bandwidth is sensitive to the ground plane width. The impedance matching becomes worse when the width of the ground is either too wide or too narrow. The optimum width of the ground plane is found to be $W_{sub} = 42$ mm.

Moreover, the current distributions of the CMA are also investigated to understand its behaviour. Fig. 3.6 shows the current distributions of the CMA close to the measurement resonance frequencies as depicted in Fig. 3.6. The current pattern near the first, second and third resonance at the frequencies of 3, 6.5, and 10 GHz corresponding to the first, second and third order harmonics, are shown in Figs. 3.6(a), (b) and (c), respectively. It can be also observed that the surface current is mainly concentrates on three areas: the feed point of the radiator, the edge of the radiator and the top edge of the ground plane. At the first resonance frequency, the antenna operates in a standing wave due to the wavelength is bigger than the antenna dimension, the EM wave can be easily

couple into the antenna structures [1]. With the increase of the frequency, the antenna tends to operate in a hybrid mode of travelling and stranding waves. However, the impedance mismatching accuses at high frequencies around 10 GHz, as shown in Fig. 3.3. This is because the ground plane on the other side of the substrate cannot form a good slot with the circular radiator to support travelling waves.

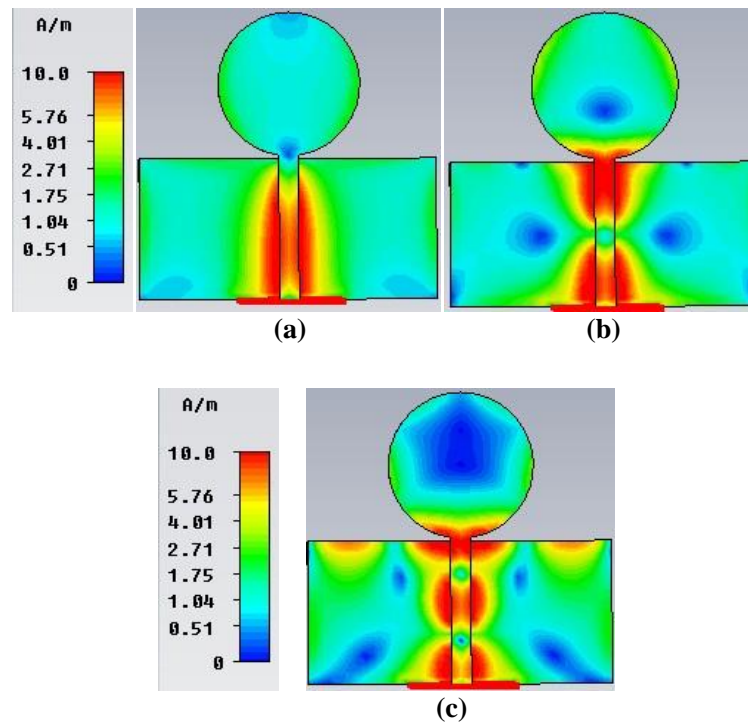


Fig. 3.6 Simulated total current distributions of the CMA at frequencies of (a) 3 GHz, (b) 6.5 GHz, and (c) 10.5 GHz

Similar to other planar monopole antennas investigated in [1-2], it is found from above studies that -10 dB bandwidth of the microstrip-fed CMA is mainly dependent on the feeding gap g and the width of the ground plane W_{sub} .

The simulated radiation patterns of the CMA at 3.5, 6.5 and 10.5 GHz are depicted in Fig. 3.7. It can be seen that the XOZ plane pattern is a good omnidirectional at lower frequency of 3 GHz as well as at higher frequencies of 6.5 and 10.5 GHz. In the YOZ plane, the pattern is look like a donut shape at 3.5

GHz, which two nulls at y-direction. With the increase of the frequency to 6.5 and 10.5 GHz, the pattern tends to have more directional at around 45 degrees from the y-direction.

The simulated gains of the CMA from 3 to 11 GHz are also illustrated in Fig. 3.8. It can be seen that the gains vary within the range from 1.6 to 4 dBi and reach the maximum vales at 10 GHz.

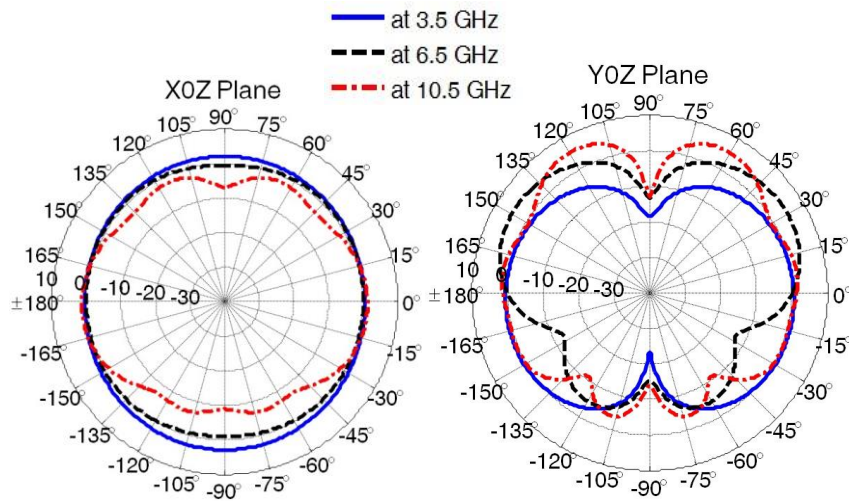


Fig. 3.7 Simulated radiation patterns of the CMA at 3.5 GHz (blue solid line), 6.5 GHz (red break dot line, and 10.5 GHz (black break line)

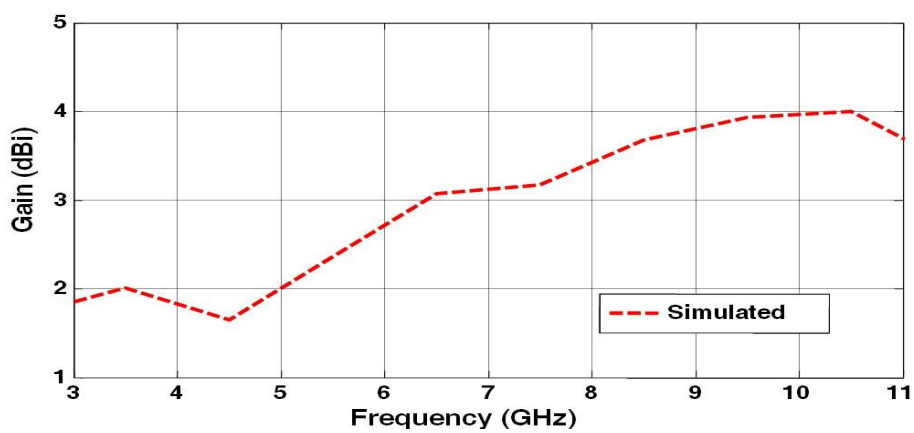


Fig. 3.8 Simulated gains of the CMA

To further enhance the impedance bandwidth of the CMA, several techniques are used and the detailed of the designs are illustrated in the next section.

3.3 SWB Planar Monopole Antenna Design

Various techniques have been proposed to broaden the bandwidth of the planar antenna and improve their performance such as bevelling the edges [3-5], offset feeding [6], slotted ground plane [7-9], and smooth rounded elements[10-11].

In this Section, the techniques of incorporating a pairs of ears at the top of the radiator and truncated and smoothed ground plane to enhance the bandwidth of the circular monopole antenna are presented. The former and latter are used to improve the bandwidth at the lower and higher frequencies, respectively. It can be found that much wider bandwidth can be achieved. It is worth mentioning that the size of the proposed SWB is the same as the circular antenna (refer to Fig. 3.1).

3.3.1 Antenna Configuration

The geometry of the proposed antenna is shown in Fig. 3.9. The antenna radiator is fed by a microstrip line with the characteristic impedance is 50 ohms; the length of the feedline is denoted as L_f and its width (W_f) is fixed at 2.8 mm. It is fabricated on an inexpensive FR 4 substrate with a thickness of 1.5 mm and relative permittivity of 4.3. The overall size of the substrate is $L_{sub} \times W_{sub}$ and the electrical dimension of the antenna is $0.29 \times 0.26 \lambda^2$ (λ is the wavelength of the lowest useable frequency). The optimised parameters of the proposed antenna are listed in Table 3-1.

To achieve the impedance matching and broaden the bandwidth, several techniques are implemented. A pair of ears with radius of $R1$ is firstly placed at the top of the CMA radiator with a distance Lr (between the top of the feedline and the centre of the ear). It can be found that a much enhanced impedance bandwidth can be achieved especially at lower frequencies. As stated in Section 3.1, the ground plane is an important part of the impedance matching network. Thus, to further enhance the matching over a wide frequency range, a one-step staircase slot ($W1 \times L1$) is embedded in the ground plane. In addition, a smoothed ground plane is introduced. The idea behind this is to reduce the electromagnetic coupling between the radiator and the ground plane and help to achieve a much better impedance matching [12].

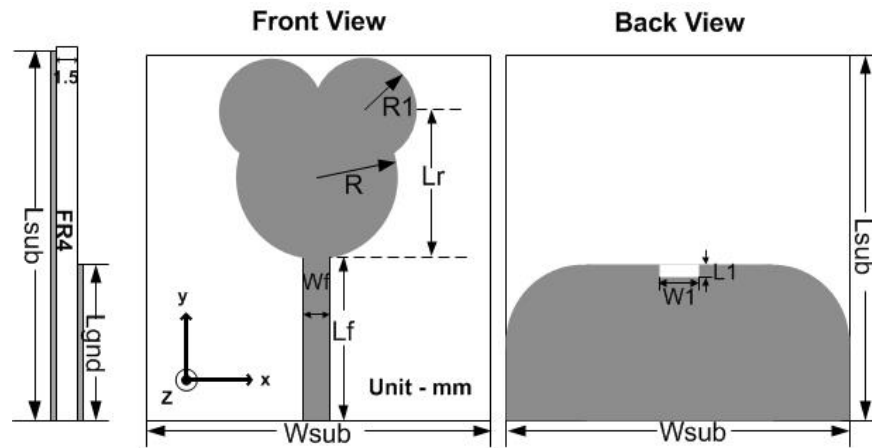


Fig. 3.9 Geometry of the proposed monopole antenna

3.3.2 Effects of the Antenna Parameters on its Performance

During the antenna development process, three different antennas are defined as shown in Fig. 3.10: Ant 1, the conventional circular monopole antenna; Ant 2, the antenna with Mickey-mouse shaped radiator and a one-step

staircase slot in the ground plane, and Ant 3 with a top-corner rounded ground plane.

Table 3-1 Optimized parameters of the SWB antenna in Fig. 3.9

Antenna Parameters	Values (mm)	Antenna Parameters	Values (mm)
W_{sub}	42	W_f	2.8
L_{sub}	45	W_l	3
L_{gnd}	19.7	L_l	1
L_f	21.4	R	10
L_r	18		

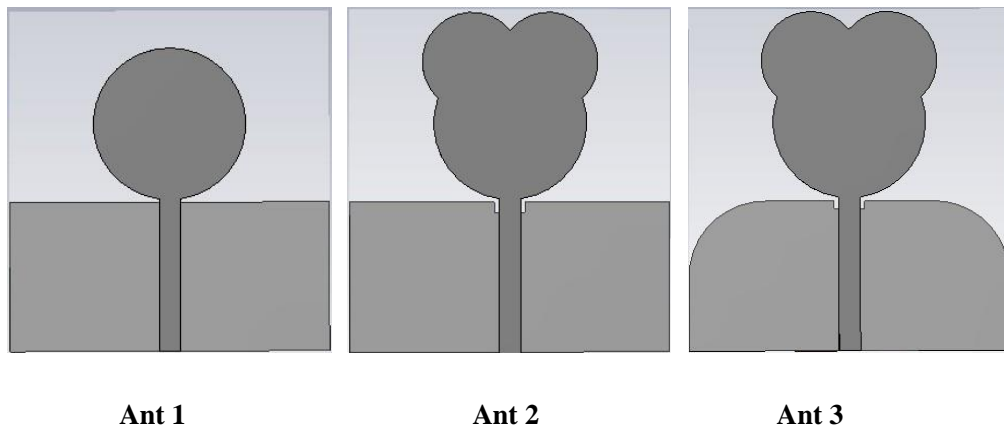
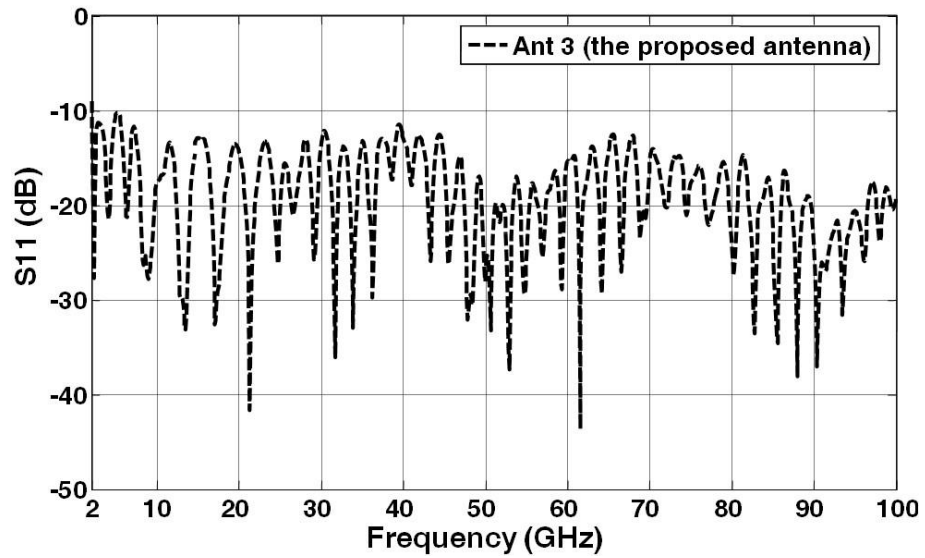


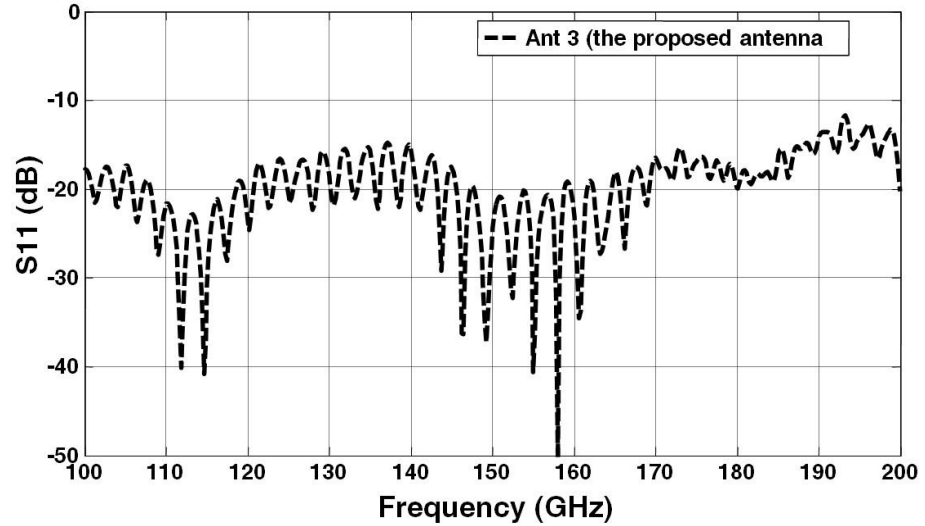
Fig. 3.10 Three different models (Ants 1, 2 and 3)

To study of the impedance and matching characteristics, the simulated reflection coefficients of Ant 3 is depicted in Fig. 3.11. The simulation is computed and shown here only up to 200 GHz and its impedance bandwidth is actually much wider than what is presented here (due to the memory limitation of the computer). For comparison, the corresponding impedance bandwidths of the three different antennas are plotted together in Fig. 3.12. It is apparent that the -10 dB impedance bandwidth is improved from 8 to 20 GHz and beyond (to more than 150 GHz). By comparing with the design in [33], the proposed SWB

antenna is able to produce a ratio bandwidth of 100:1 rather than 30:1, and it can cover much lower frequencies with a comparable size.



(a) Frequency from 2 to 100 GHz



(b) Frequency from 100 to 200 GHz

Fig. 3.11 Simulated reflection coefficient $|S_{11}|$ of Ant 3

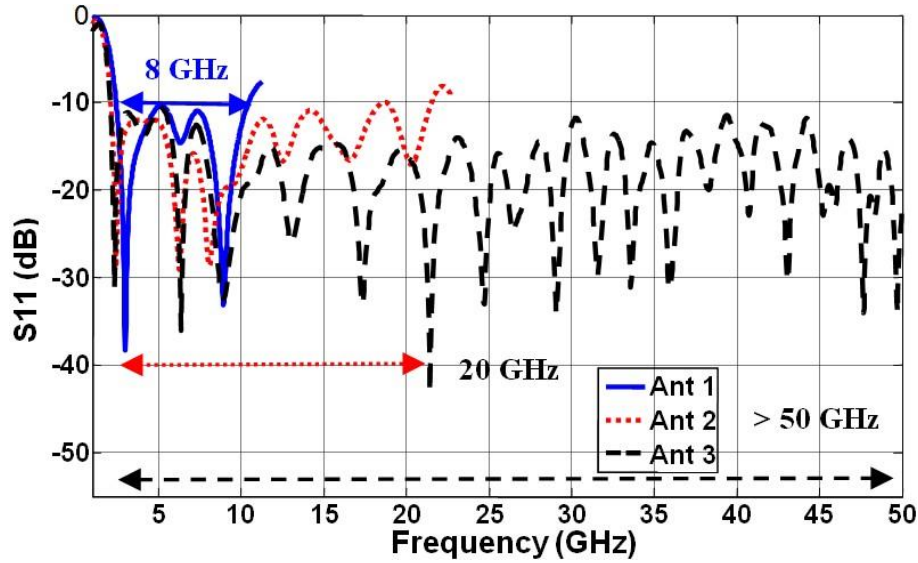
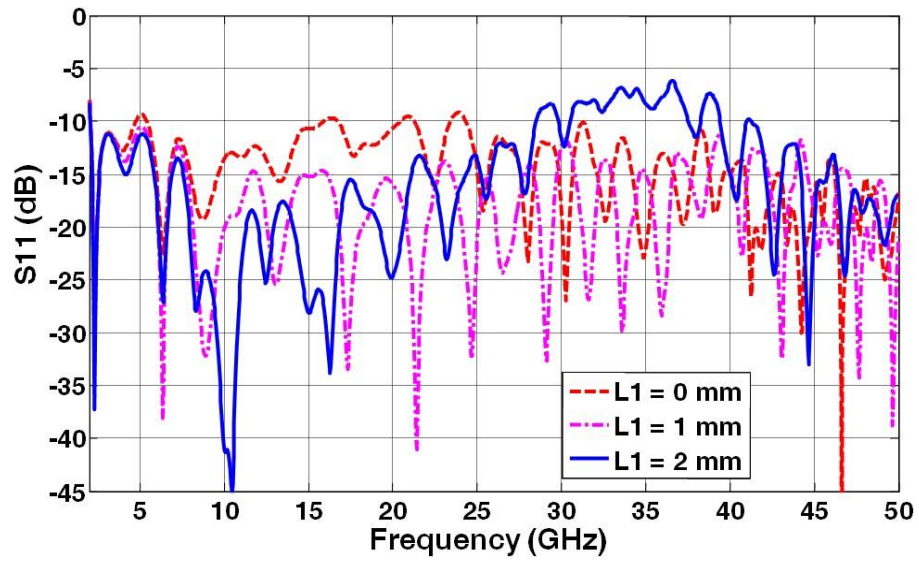


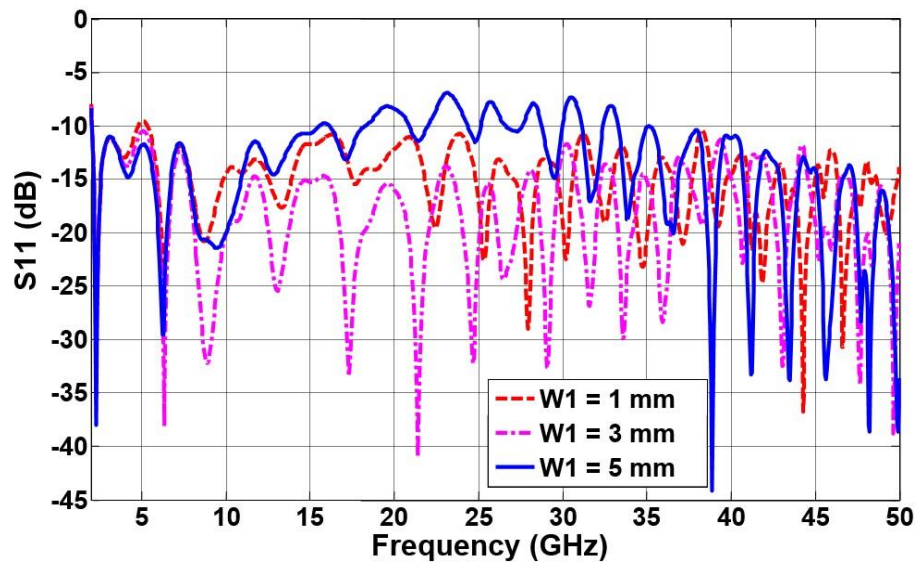
Fig. 3.12 Simulated reflection coefficients $|S_{11}|$ of the three antennas

As the simulation results show that the ground plane acts as impedance matching of the antenna. Modifying the ground plane has significantly improved the return loss of the antenna, especially at higher frequencies. Therefore, a parametric study on the geometrical parameters of the slotted ground (refer to Fig. 3.9) of the SWB antenna are carried out.

By varying the lengths and the widths of the slots on the ground plane, it is possible to tune the impedance matching, as shown in Fig. 3.13. The effects of varying L_1 on the reflection coefficients of the SWB antenna are depicted in Fig. 3.13(a). L_1 is chosen to be 0, 1, and 2 mm, respectively. It can be clearly seen that the total achievable bandwidth may shrink significantly by increasing the length of the slotted ground. Similarly, Fig. 3.13(b) illustrates the effects of varying width of slotted ground L_1 on the reflection coefficients of the SWB antenna. The width of the slotted ground plane of 5 mm has a significant effect on the impedance matching. This is due to that the width of the slot may have brought the antenna to much more capacitive and far away from the resonance point, especially at the higher frequency. The optimum value of W_1 is chosen to be 3 mm.



(a) Length of the slot



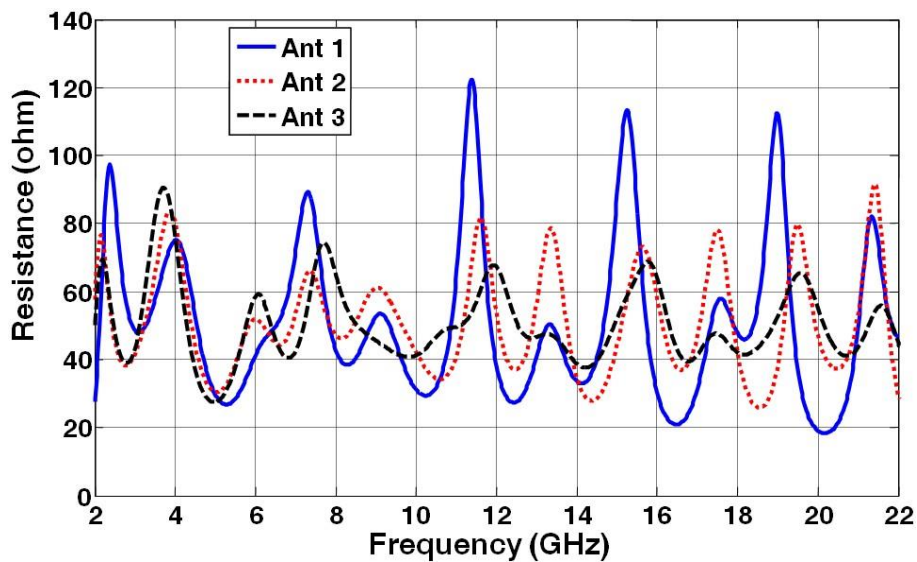
(b) Width of the slot

Fig. 3.13 The impedance performance of the three antennas (Ants 1, 2 and 3)

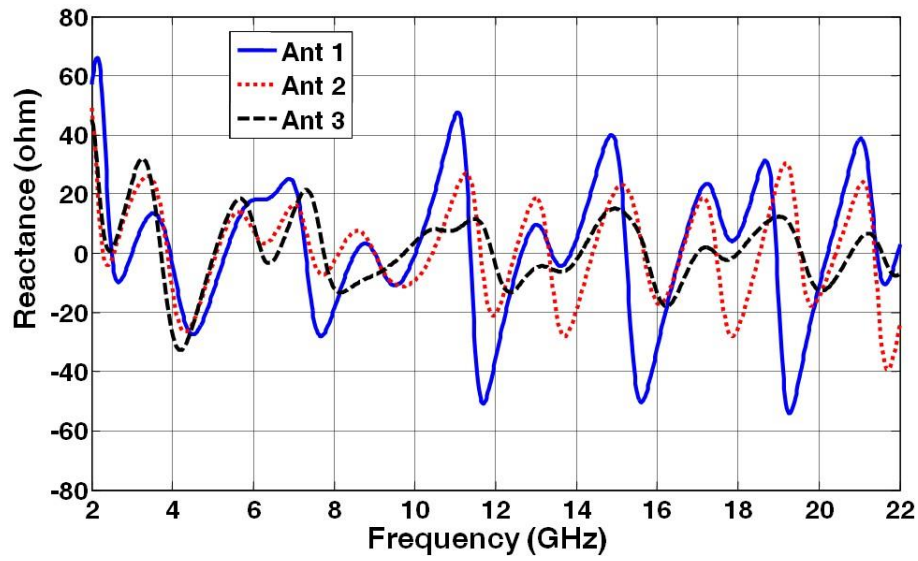
3.4 Modal Analysis

3.4.1 Impedance Performance

Using the fact that the input impedance of the antenna Z_a can be written as the summation of reactance (X_a) and resistance (R_a), which is $Z_a = R_a + jX_a$. The frequency bandwidth of the antenna is much enhanced when the reactance is reduced [13]. Fig. 3.14 shows the impedance performance of the three antennas from 2 to 22 GHz. It is obvious that the reactance of the proposed antenna is much reduced especially for the higher frequencies compared to Ants 1 and 2. This is because of the modified ground plane, which seems to introduce a capacitive load, and counteracts the inductive nature of the patch to produce nearly-pure resistive input impedance. Hence, Ant 3 can achieve a super wide frequency bandwidth. The summarised of the analysed performances for three antennas are listed in Table 3-2.



(a) Resistance



(b) Reactance

Fig. 3.14 The impedance performance of the three antennas (Ants 1, 2 and 3)

Table 3-2 Comparion of the analysed performanes for three antennas

Analyzed Parameters	Ant 1	Ant 2	Ant 3 (SWB)
Bandwidth (GHz)	2.45-10.42	2.1-21.40	2.1-200
Ratio bandwidth	4.25:1	10.19:1	100:1
Input impedance(Ω)	50-121	60-90	47-74

3.4.2 Current Distribution

Further investigation is conducted, the current distributions of the SWB antenna at the resonant frequencies of 2.5, 6.6, 9.6, 14.2, 18 and 20.8 GHz, which correspond to the first, second, third, fourth, fifth and sixth order harmonics are plotted in Fig. 3.15, respectively. It is obvious that at the first

resonant frequency they operate in an oscillating mode, i.e. a standing wave, which acts like a traditional quarter wavelength monopole and no nulls in the whole plane. With the increase of the frequency, nulls start to appear and the antenna becomes a travelling wave antenna. Thus, the proposed antenna is achieved a super wide bandwidth.

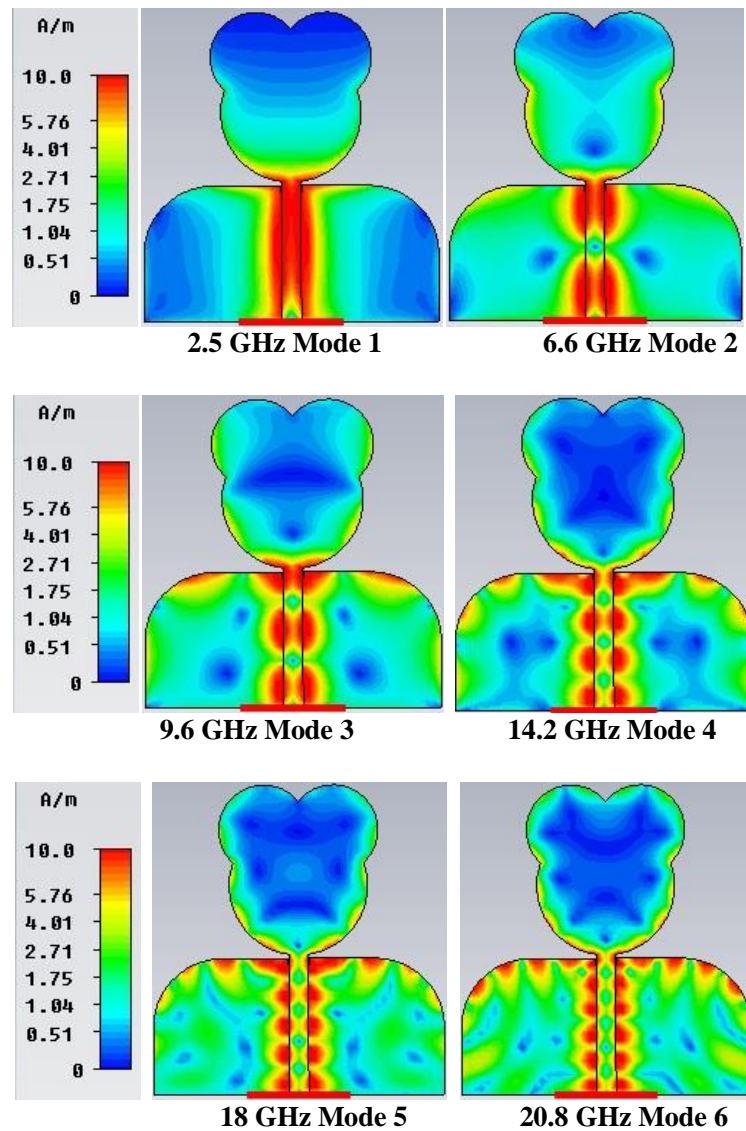


Fig. 3.15 Modes at resonate frequencies of the SWB monopole antenna

3.5 Experimental Results and Discussions

To validate our simulated results, the proposed SWB monopole antenna is built using standards FR4 laminate ($\epsilon_r = 4.3$) with a thickness of 1.5 mm and tested, the prototype of the SWB antenna is shown in Fig. 3.16.

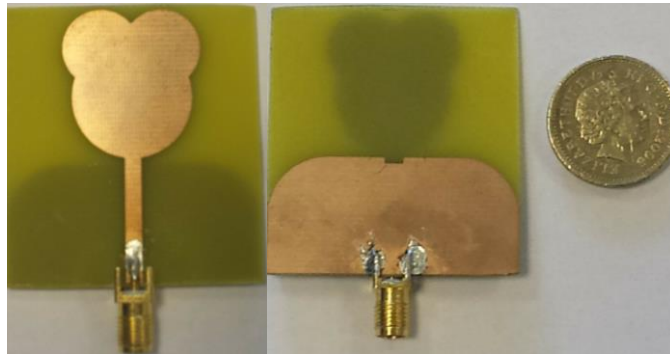


Fig. 3.16 Photo of the proposed SWB antenna

3.5.1 Reflection Coefficients

The proposed SWB antenna (Ant 3) is fabricated and measured. Fig. 3.17 shows the comparison of the simulated and measured reflection coefficients $|S_{11}|$. The measured bandwidth for 10 dB return loss covers the operation frequency range from 2 to 22 GHz and has good agreement with the predicted one; a small frequency shift at the lower frequencies and small deviation at the frequency higher than 19 GHz can be seen. This is believed to be due to fabrication errors when the antenna is printed on the substrate; Furthermore the simulation analysis did not take the SMA connector into account but in practice a SMA connector was used for the measurement which was suitable for up to 18 GHz max according to its specifications.

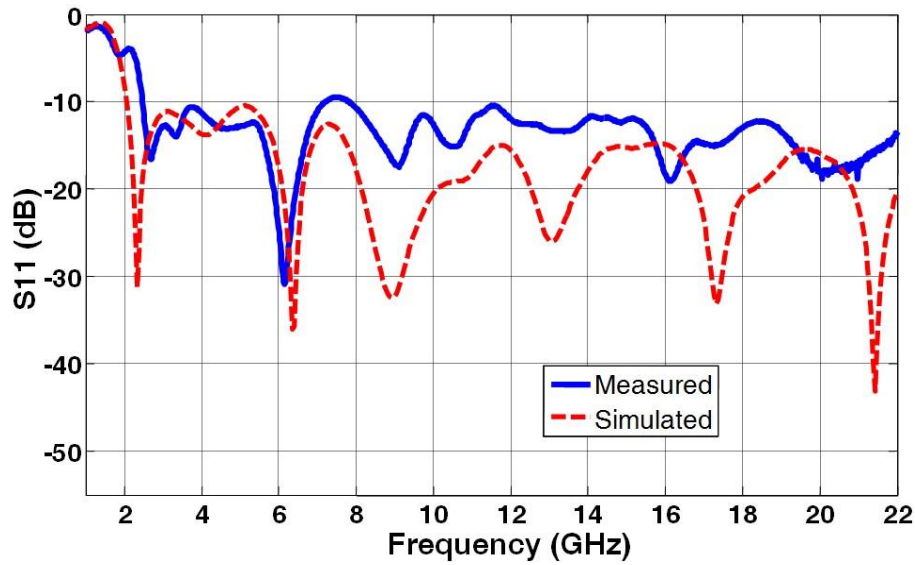


Fig. 3.17 Simulated and measured reflection coefficients of Ant 3

3.5.2 Radiation Patterns

Fig. 3.18 shows the simulated 3D radiation patterns of Ant 3. The plot indicates that the radiator exhibits a super wide band pattern characteristics, the usable spherical patterns are sustained in a wider bandwidth.

Fig. 3.19 shows the measured and simulated far-field radiation patterns of the proposed antenna in the H-plane (XZ-plane) and E-plane (YZ-plane) at 3.5 and 12.5 GHz, respectively. A reasonable agreement is demonstrated between the results. It can be seen that the radiation patterns in the XZ-plane are nearly omni-directional for the two frequencies. Fig. 3.19(a) shows the E-plane pattern at 3.5 GHz shows two nulls at y-direction, which is similar to the dipoles at the lower frequency, but degradation at higher frequency (12.5 GHz), as shown in Fig. 3.19(b). With the increase of the frequency to the much higher resonances (25, 50 and 150 GHz), the simulated results show that the patterns are become distorted, splitting into many minor lobes, as shown in Fig. 3.20.

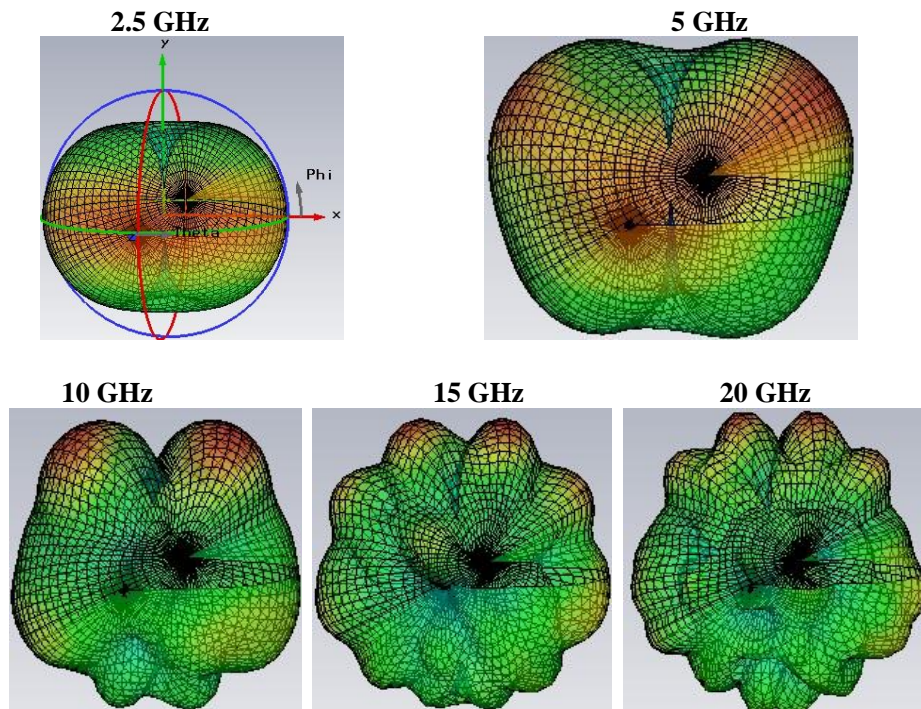
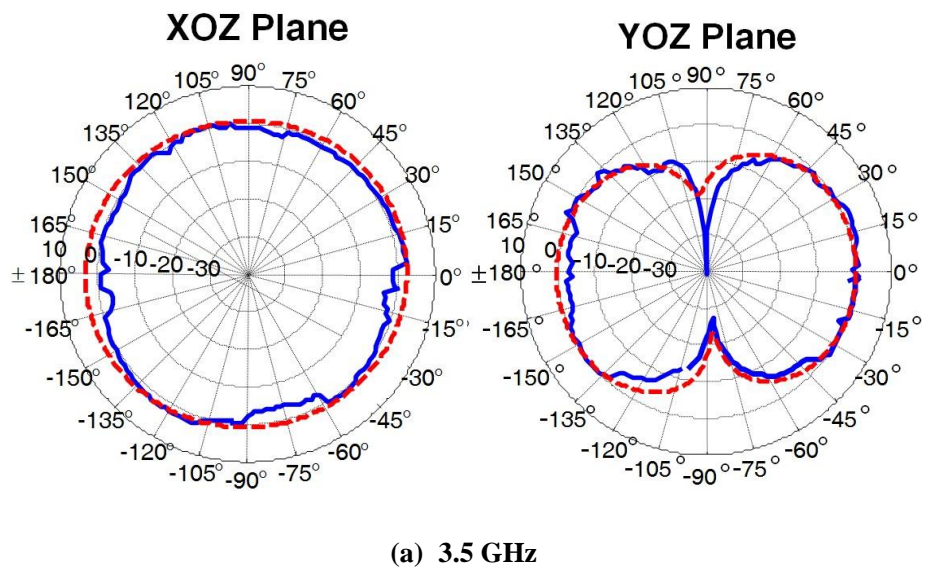


Fig. 3.18 3D-far-field co-polar radiation pattern performance of Ant 3



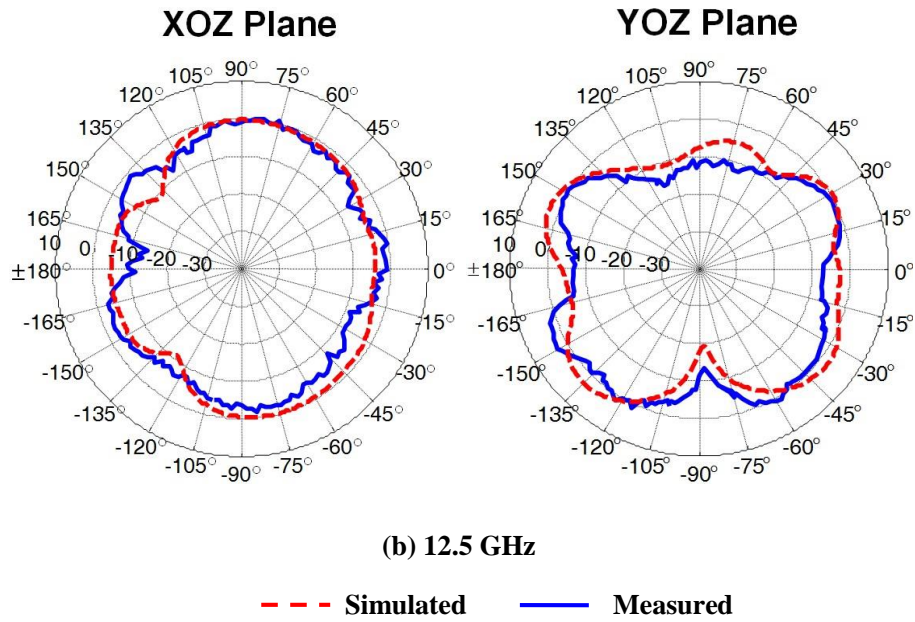


Fig. 3.19 Simulated and measured radiation patterns of the SWB antenna at (a) 3.5, and (b) 12.5 GHz

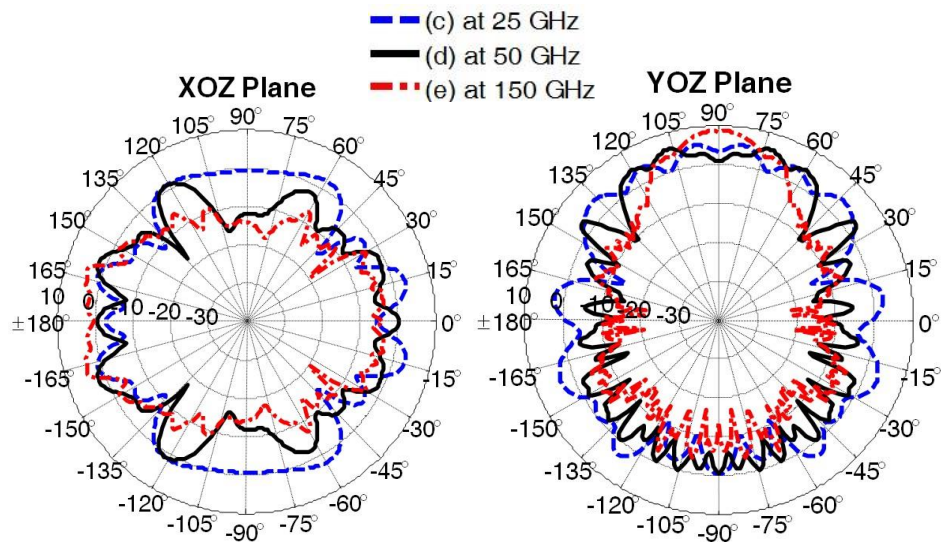


Fig. 3.20 Simulated radiation patterns of the SWB antenna at (c) 25, (d) 50, and (e) 150 GHz

3.5.3 Peak Gains

The simulated and measured peak gains of the SWB antenna from 2 to 18 GHz are shown in Fig. 3.21. A good agreement between the two results is found, the slight difference between the simulation and measurement may be caused by the cable effects in the measurement. It can be seen that the peak gains increase with the frequencies; this is because the radiation patterns become more directional at high frequencies, as can be seen in Fig. 3.8. The measured gain values vary within the range from 2 to 6 dBi and reach the maximum values at 15 GHz. In addition, the simulated gains of the antenna are illustrated for the rest of frequency bands (20 to 200 GHz), as shown in Fig. 3.22, the gain values vary within the range from 4.5 to 15 dBi.

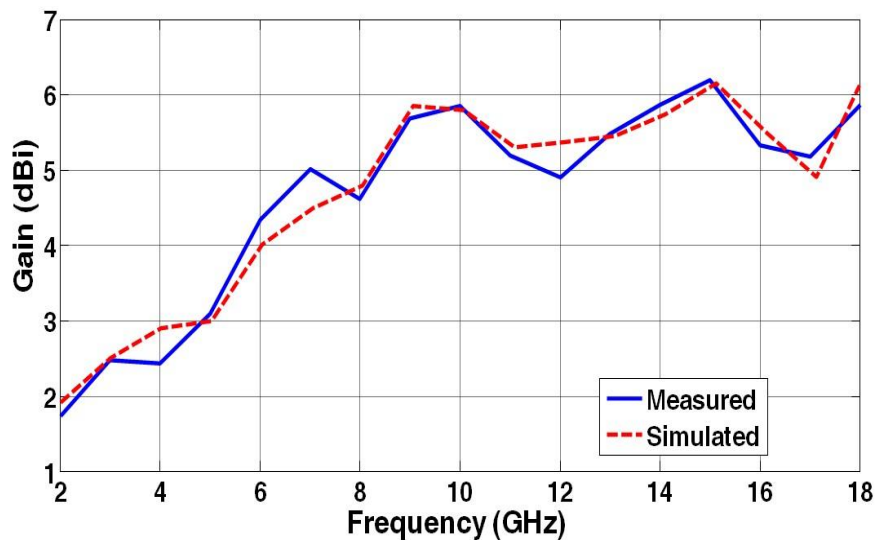


Fig. 3.21 Simulated and measured peak gains of Ant 3 (2 to 18 GHz)

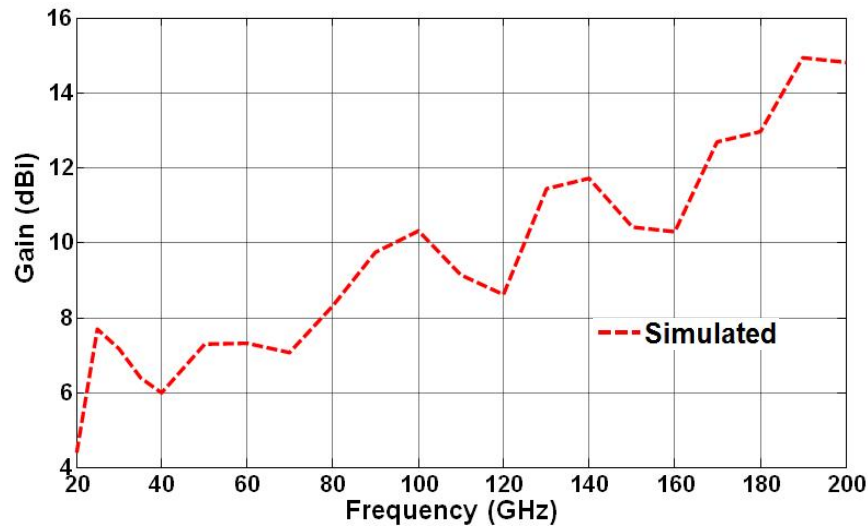


Fig. 3.22 Simulated peak gains of Ant 3 (20 to 200 GHz)

3.6 Summary

In this Chapter, a novel compact Mickey-mouse shaped monopole antenna with SWB performance has been proposed for future wireless communications. The proposed antenna has evolved from a simple circular monopole antenna. By implementing two ears to the radiator and truncating/smoothing ground plane, it has been observed that the impedance bandwidth of the proposed antenna is significantly improved. A reasonable agreement between simulation and measurement results has demonstrated, the antenna with a super wide bandwidth from 2 to 200 GHz for a return loss greater than 10 dB (i.e. a ratio of impedance bandwidth of 100:1) has achieved. Furthermore, the antenna has shown a stable radiation pattern over a wider bandwidth. The designed antenna has a simple configuration and easy for fabrication.

3.7 References

- [1] J. X. Liang, C. C. Chiau, X. D. Chen, C. G. Parini, "Study of a printed circular disc monopole antenna for UWB systems," *IEEE Trans. on Antennas and Propagation*, vol.53, no.11, pp. 3500-3504, Nov. 2005.
- [2] Y. Lu, Y. Huang, Y. C. Shen and H. T. Chattha, "A technique for minimising the effects of ground plane on the planar UWB monopole antennas," *Microwaves, Antennas & Propagation, IET*, vol.6, no.5, pp. 510-518, April 12 2012.
- [3] Z. N. Chen et al., "Planar Antennas," *IEEE Microwave Magazine*, vol. 7, no. 6, pp. 63-73, December 2006.
- [4] M. C. Fabres et al., "On the influence of the shape of planar monopole antennas in the impedance bandwidth performance," *Microwave and Optical Technology Letters*, vol. 44, no. 3, Feb 2005.
- [5] R. Giuseppe & M. J. Ammann, "A novel small wideband monopole antenna," *Loughborough Antennas & Propagation Conference (LAPC)*, Loughborough University, UK, 11-12th April 2006.
- [6] Y. Y. Sun, M. T. Islam, S. W. Cheung, T. I. Yuk, R. Azim, N. Misran, , "Offset-fed UWB antenna with multi-slotted ground plane," *2011 International Workshop on Antenna Technology (iWAT)*, pp. 432-436, 7-9 March 2011.
- [7] X. L. Bao, M. J. Ammann, "Investigation on UWB printed monopole antenna with rectangular slitted ground plane," *Microwave and Optical Technology Letters*, vol. 49, no. 7, pp. 1585-1587, 2007.
- [8] L. Liu, S. W. Cheung and T. I. Yuk, "Bandwidth improvements using ground slots for compact UWB microstrip-fed antennas," *Progress in*

- Electromagnetics Research Symposium (PIERS)*. Suzhou, China, pp. 12-16 September, 2011.
- [9] S. Jacob, V. A. Shameena, S. Mridula, C. K. Anandan, K. Vasudevan, P. Mohanan, "Planar UWB antenna with modified slotted ground plane," *Int J RF and Microwave Comp Aid Eng*, vol. 22, issue 5, pp. 594-602, September 2012.
- [10] C. C. Lin and H. R. Chuang, "A 3-12 GHz UWB planar triangular monopole antenna with ridged ground-plane," *Progress in Electromagnetics Research*, vol. 83, pp. 307-321, 2008.
- [11] N. P. Agrawall, G. Kumar, K. P. Ray, "Wide-band planar monopole antennas," *IEEE Trans. on Antennas and Propagation*, vol. 46, no.2, pp. 294-295, Feb 1998.
- [12] A. A. Eldek, "Numerical analysis of a small ultra wideband microstrip-fed tap monopole antenna," *Progress in Electromagnetic Research*, vol. PIER 65, 2006.
- [13] Y. J. Park and J. H. Song, "Development of ultra wideband planar stepped-fat dipole antenna," *Microwave and Optical Technology Letters*, vol. 48, pp. 1698-1701, 2006.

CHAPTER 4 DESIGN OF A PLANAR UWB ANTENNA WITH BAND-NOTCHED CHARACTERISTICS

4.1 Introduction

Since the UWB systems use a wideband spectrum, which could easily be interfered by the existing nearby communication systems such as the WLANs operating at the bands of 2.45-GHz (2.4-2.484 GHz), 5.25-GHz (5.15-5.35 GHz) and 5.75-GHz (5.725-5.825 GHz), the Worldwide Interoperability for WiMAX systems operating in the 3.3-3.8 GHz bands, downlink of X-band satellite communication system operating at the band of 7.25-7.75 GHz and ITU band of 8.01-8.5 GHz, respectively. Therefore, it is desire to design a UWB antenna with multiple-band-notched features (a combination of an

antenna and filters) to mitigate the potential interference at these frequency bands.

This Chapter presents a compact UWB planar monopole antenna to achieve quintuple-band-notched characteristics. By integrating five specially designed M-shaped resonators (MSRs) into the radiator, feed-line, and ground plane. Five notched bands behaviours are achieved. One of the key strengths of the antenna is that it provides excellent gain suppressions at the band-notched frequencies and the size is about 10% smaller compared to previous work reported in literature [75] where a similar performance is achieved by both antennas.

The dimensions and locations of the MSRs in defining the band-notched frequency are investigated. An equivalent circuit model is developed and the transmission line models are used for analysis. The performances of the proposed antenna in the frequency-domain and time-domain are also investigated using both numerically and experimentally methods.

The simulation results presented in this Chapter were performed using CST Microwave Studio.

4.2 Band-Notched Antenna Design

4.2.1 M-shaped Resonator (MSR)

As stated in Section 2.2, there were a number of different techniques to generate the band-notched function. The most popular one is to insert a simple slot (such as a U-shaped and inverted U-shaped slot as reported in [35]) in the antenna structure. In our design, a compact UWB antenna with multiple-band-notched characteristics is required; the half wavelength inverted U-shape slot investigated in [35] was too large and may not appropriate to generate a notch for the lower-frequency bands (such as WLANs at 2.45 GHz). By modifying the half-wavelength U-shaped slot to an M-shaped resonant (MSR) structure, a much more compact resonator structure can be formed. With the compact MSR, a multiple band-notched UWB antenna can be achieved by integrating several pairs of MSRs at different positions on the antenna. The geometries of the notch elements are shown in Figs. 4.1(a-c).

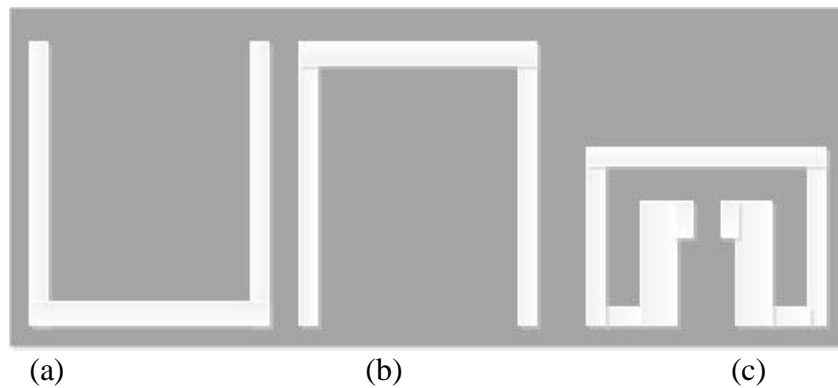


Fig. 4.1 Geometry of the notch elements: (a) U-shaped slot, (b) Inverted U-shaped slot, and (c) M-shaped resonant

In our proposed design, the notched frequency is mainly decided by the total length of the chosen MSRs to be approximately half/one-wavelength to

achieve the desired band-notched function. Its geometrical dimensions are defined by [1]:

$$f_{notch} \approx \frac{c}{2 \cdot L_{total} \cdot \sqrt{\epsilon_{eff}}} \quad (4.1)$$

$$\epsilon_{eff} \approx \frac{\epsilon_r + 1}{2} \quad (4.2)$$

$$L_{total} \approx \frac{\lambda}{2} \approx 2 \cdot (L1 + W1) - W2 \quad (4.3)$$

where c is the speed of light L_{total} is the total length around the MSR and ϵ_{eff} is the effective relative dielectric constant. Given a design resonance frequency, one can use Equations (4.1) to (4.3) to obtain the initial dimensions of the MSR and then adjust the dimensions for the final design. Generally speaking, increasing the length of the slot or narrowing the slot width is similar to increase the inductance value or the capacitance value of the slot. In other words, it has the effect of decreasing the centre notched frequency.

For the first notched frequency, which is determined by MSR #1; the notched frequency is decreased from 2.67 to 2.24 GHz when L_{total} is increased from 37 to 45 mm, as shown in Fig. 4.2. In addition, the numerical (using CST) and theoretical (Equations (4.1– 4.3)) predictions of the band-notched frequency for different total lengths (37 to 45 mm) of the MSR are compared and listed in Table 4-1, we can see that the results are in a reasonable agreement. The difference between numerical and theoretical frequencies is about 0.17 GHz, which may be caused by the approximation when calculating the effective relative dielectric permittivity ϵ_{eff} in Equation (4.1). Although MSR #1 may affect $|S_{11}|$ at other frequencies (especially at higher frequencies), the effects are relatively small. The same approach has been applied to other MRS to obtain the desired band-notched frequencies.

Table 4-1 Numerical and theoretical predictions for the band-notched frequency

L_{total} (mm)	Numerical Frequency (GHz)	Theoretical Frequency (GHz)
37	2.67	2.5
41	2.42	2.25
45	2.24	2.05

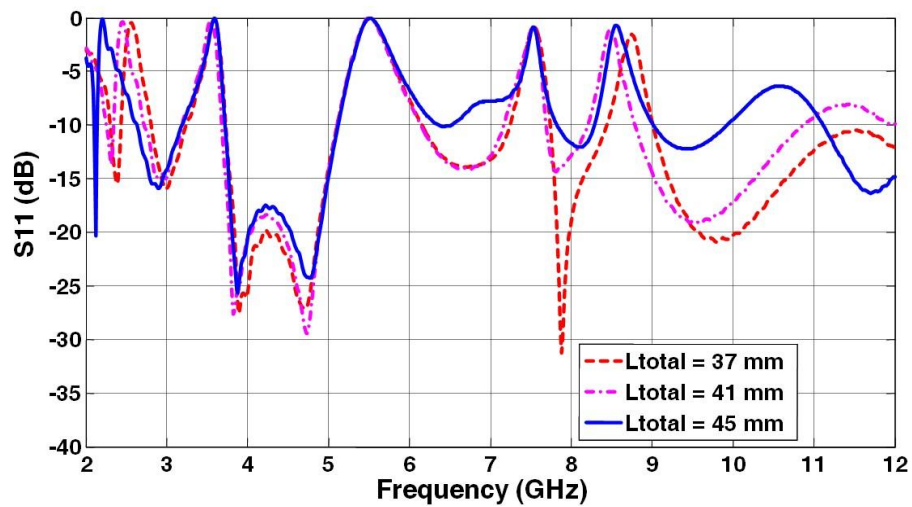


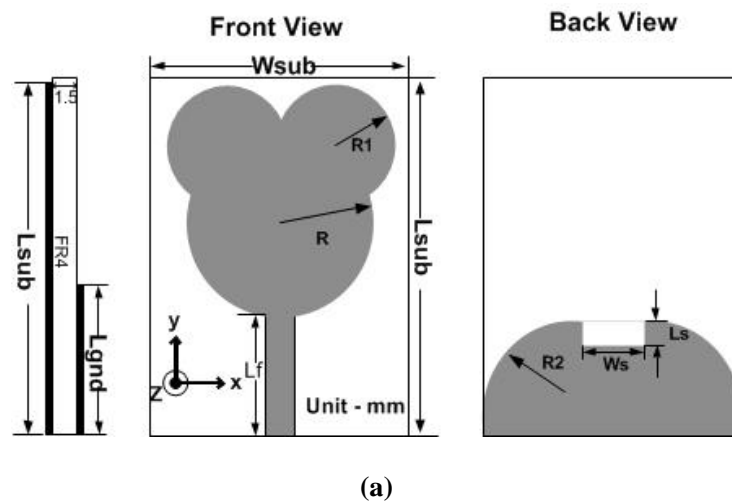
Fig. 4.2 Simulated reflection coefficients $|S_{11}|$ of the quintuple-band-notched antenna with different L_{total} values

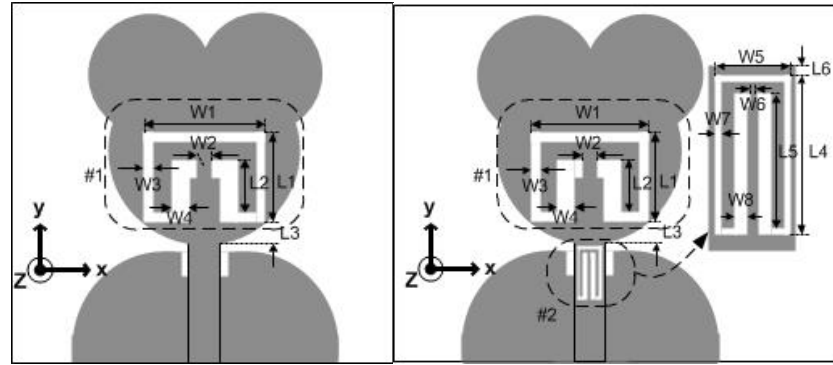
4.2.2 Structure of Antenna

The design procedure of our band-notched antenna is as follows: a UWB Mickey-mouse shaped antenna without any MSRs is designed and used as a reference antenna for comparison as shown in Fig. 4.2(a). A single/multiple pair of the MSRs is/are then added to the reference antenna to make it a single/multiple band-notched antenna. The dimensions of individual MSRs are adjusted to achieve the desirable center frequencies and bandwidths of the notches.

The reference antenna of our band-notched antenna design is based on the Mickey-mouse monopole antenna as described in previous chapter and has been modified to achieve a compact size over the desired frequency band of 3.1 to 10.6 GHz (UWB band), it can straightforward comparisons with the other numerous UWB band-notched antennas in the literature. The antenna is simulated and fabricated on FR4 substrate with a dimension of $22 \times 34 \text{ mm}^2$, which has a relative dielectric constant $\epsilon_r = 4.3$ and a thickness of 0.8 mm. The geometry of our design is shown in Fig. 4.3(a), which consists of a Mickey-mouse shaped radiator fed by a 50- Ω microstrip line and a truncated and smoothed ground plane on the other side of the substrate. The optimum dimensions of the reference antenna are listed in Table 4-2.

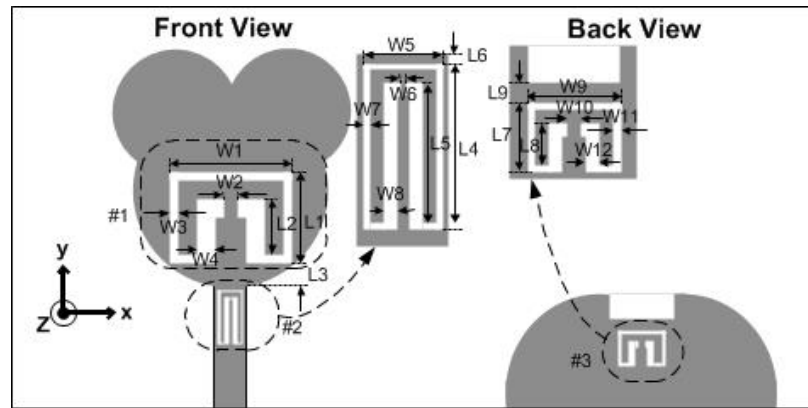
In principle, altering the current distributions along the antenna current path can change the radiation properties. The current on the reference antenna is mainly distributed in the feeding area of the radiator, the edges of the microstrip line and the upper edges of the ground plane. Therefore, a resonator to stop the current flow should be placed at any of these sensitive positions to create a single, dual, triple, quadruple, and quintuple-band-notched antennas as shown in Figs. 4.3(b-f), respectively.



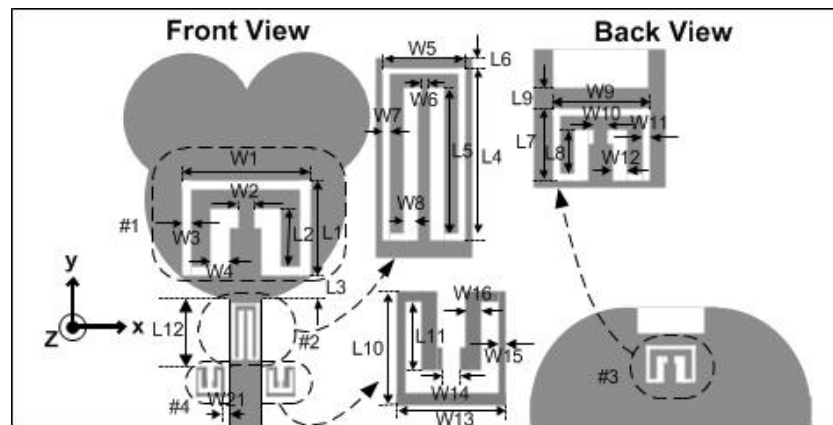


(b)

(c)



(d)



(e)

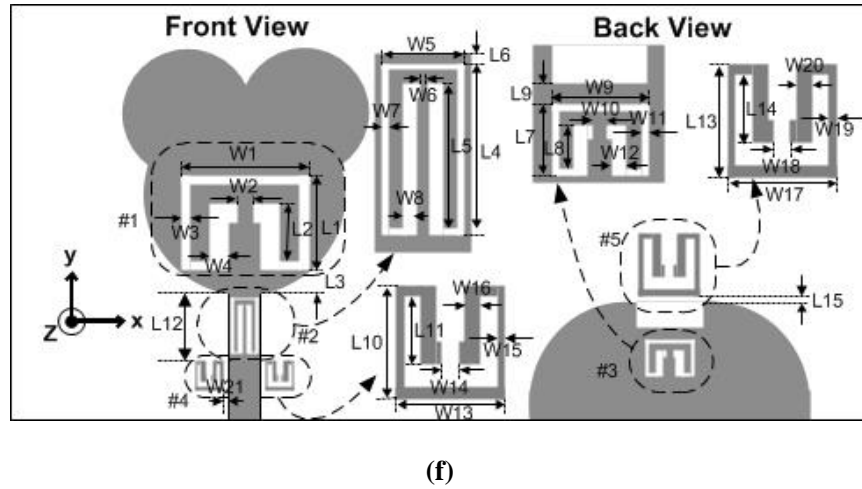


Fig. 4.3 Geometry of the proposed antenna: (a) UWB antenna, (b) Single, (c) Dual, (d) Triple, (e) Quadruple, and (f) Quintuple-band-notched antennas

The proposed quintuple-band-notched design in Fig. 4.3(f) is used to demonstrate the design principle of using the MSRs since it includes the other four designs in Figs. 4.3(b-e). Five MSRs, labelled as MSRs #1, #2, #3, #4, and #5, are designed to create the notches at the centre frequencies of 2.42, 3.53, 5.58, 7.53 and 8.48 GHz to suppress these frequency bands for some existing communication systems such as the WiMAX systems, the WLAN systems, downlink of x-band and satellite communication system and ITU band, respectively. The detailed optimum dimensions of MSRs #1, #2, #3, #4, and #5 of the quintuple-band-notched antenna are listed in Table 4-3.

Table 4-2 Dimensions in mm of the reference antenna shown in Fig. 4.3(a)

Parameters	Values	Parameters	Values
Wsub	22	R	9
Lsub	34	R1	5.5
Lgnd	12.7	R2	10
Lf	13.1	Ws	6
Ls	2	Wf	2.8

Table 4-3 Dimensions in mm of MSRs for the quintuple-band-notched antenna shown in Figs. 4.3(b-f)

MSR	W1	W2	W3	W4	L1	L2	L3
#1	10	1.2	0.75	1.5	7.5	4.5	1.5
MSR	W5	W6	W7	W8	L4	L5	L6
#2	2.4	0.15	0.2	0.4	5.1	4.48	1.9
MSR	W9	W10	W11	W12	L7	L8	L9
#3	4.4	0.66	0.33	0.66	3	2.08	0.5
MSR	W13	W14	W15	W16	L10	L11	L12
#4	2.43	0.37	0.18	0.27	2.54	1.52	7
MSR	W17	W18	W19	W20	L13	L14	L15
#5	4.6	0.7	0.35	0.68	4.8	2.88	0.1

4.2.3 Parametric Study

A parametric study of the quintuple-band-notched antenna is carried out to optimise the geometrical parameters of the MSRs (refer to Fig. 4). The results from the parametric study are summarised below:

4.2.3.1 Dimensions of the MSRs

The simulated reflection coefficients $|S_{11}|$ of the quintuple-band-notched antenna for different slot widths W_3 are illustrated in Fig. 4.4. The notched centre frequency increases from 2.15 to 2.63 GHz as the slot width W_3 is increased from 0.5 to 1 mm. This is because widening the slot width is similar to decreasing the inductance and the capacitance values. As a result, increasing the centre notched frequency.

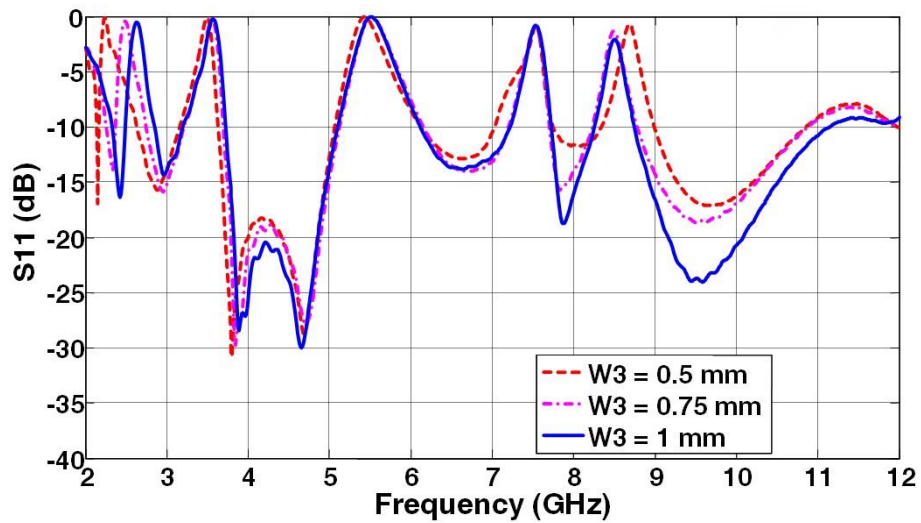


Fig. 4.4 Simulated reflection coefficients $|S_{11}|$ of the quintuple-band-notched antenna with different W_3 values

4.2.3.2 Location of the MSRs

The simulation results show that other important parameters in defining the notch bandwidth are the location of the MSRs. Fig. 4.5 shows the effects of varying L_3 on the first notch band. It can be clearly seen that, the location of the first notch (created by MSR #1) has a significant effect on the notch bandwidth and rejection level at 2.45 GHz. The coverage of MSRs #1 is increased notably while the centre frequency remains unchanged since the current density is higher in the region closer to the feed line. When L_3 is increased from 1.5 to 5.5 mm, the notch bandwidth is reduced from 0.38 to 0.16 GHz. Thus L_3 can be used to adjust the notch bandwidth and also the rejection level of MSR #1.

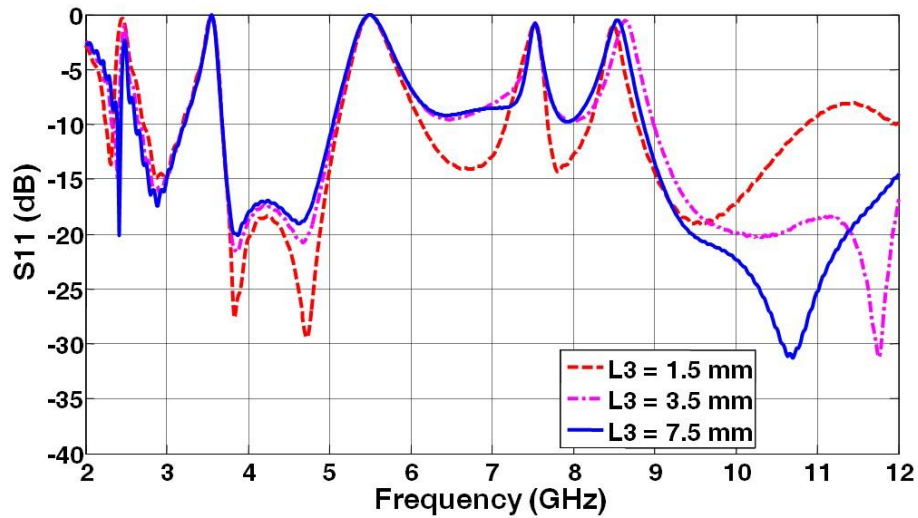


Fig. 4.5 Simulated reflection coefficients $|S_{11}|$ of the quintuple-band-notched antenna with different L_3

Similar to the case of MSR #1, the effects of different locations of L_6 , L_9 , W_{21} and L_{12} and L_{15} on the notch bandwidth of MSRs #2, #3, #4 and #5 are also investigated and shown in Fig. 4.6 to Fig. 4.10, respectively.

Fig. 4.6 illustrates the effects of varying L_6 on the third notch bandwidth; the behaviour is similar to changing L_3 but much less sensitive. When L_6 is increased from 0.4 to 3.4 mm (apart away from the feed point), the coverage of the second notch (created by MSR #2) is only slightly increased which means the location of the MSR is less sensitive to its location. From Fig. 4.7, it can be also observed that the coverage of the third notch (created by MSR #3) around 5.58 GHz is increased from 0.9 to 1.3 GHz with L_9 is varied from 1 to 3 mm. This change also affects the forth notch as shown in Fig. 4.7.

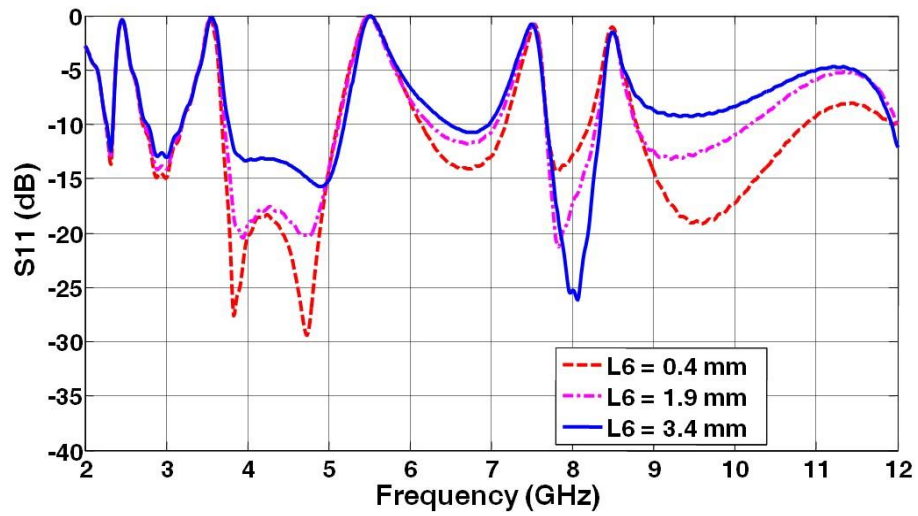


Fig. 4.6 Simulated reflection coefficients $|S_{11}|$ of the quintuple-band-notched antenna with different L_6 values

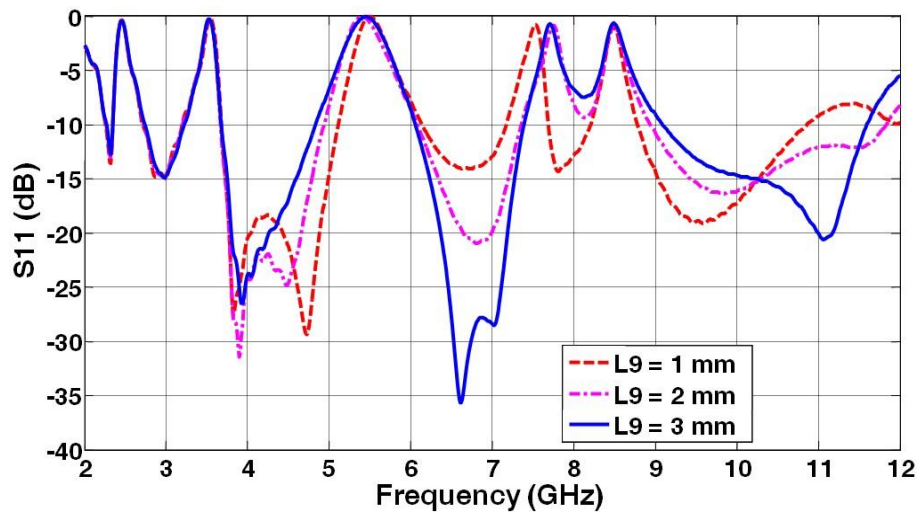


Fig. 4.7 Simulated reflection coefficients $|S_{11}|$ of the quintuple-band-notched antenna with different L_9 values

The fourth notch (created by MSR #4) around 7.53 GHz works due to capacitance between the feed line and the MRS. When W_{21} is decreased from 1.1 to 0.5 mm (the MSR is closer to the feed line), the increased coupling produces increased capacitance, which leads to a wider bandwidth and better

rejection level. From Figs. 4.8, it can be seen that with the -10 dB notch bandwidth of MRS #4 is significantly increased from 0.19 to 0.52 GHz. The figure also illustrates that W21 is much less sensitive on the notched centre frequency of MSR #4. The difference is only about 0.15 GHz. However, the fourth notch frequency is significantly affected by L12. From Fig. 4.9, it can be seen that when L12 is increased from 3.9 to 7.9 mm, the notched centre frequency is increased from 7.53 to 7.88 GHz. This change also affects the fifth notch as shown in Fig. 4.9.

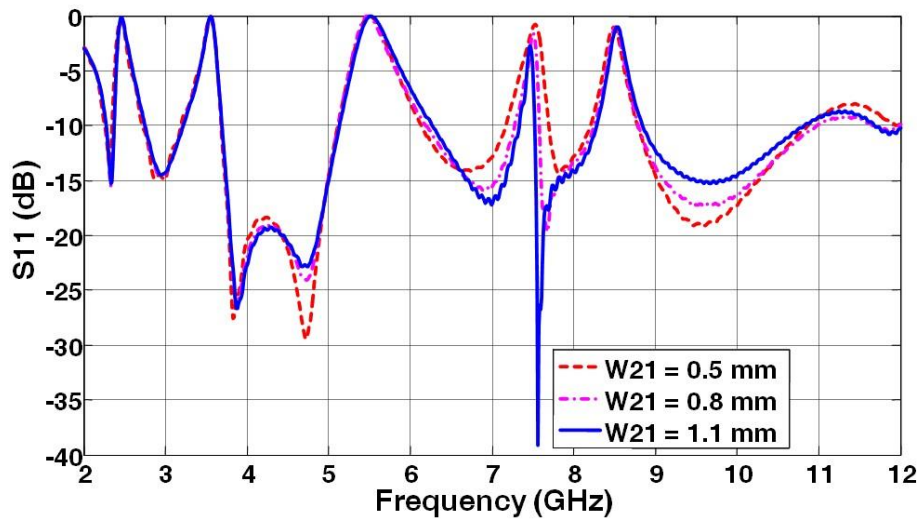


Fig. 4.8 Simulated reflection coefficients $|S_{11}|$ of the quintuple-band-notched antenna with different W21 values

The fifth notch (created by MSR #5) is printed on the reverse side of the substrate to generate a stop band at the frequency of 8.47 GHz. From Fig. 4.10, it can be observed that the location of this MSR has a significant effect on the notch bandwidth and rejection level, when L15 is increased from 0.1 to 1.1 mm (move away from feed line) the -10 dB notch bandwidth of MRS #5 is considerably reduced from 1.2 to 0.22 GHz. In addition, the notched centre

frequency is shifted about 0.3 GHz. Thus, this MSR is much sensitive to its location.

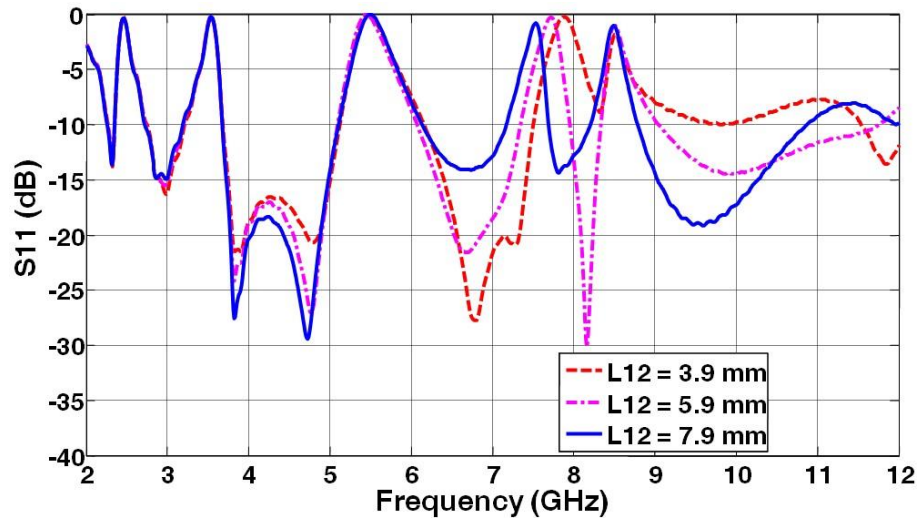


Fig. 4.9 Simulated reflection coefficients $|S_{11}|$ of the quintuple-band-notched antenna with different L_{12} values

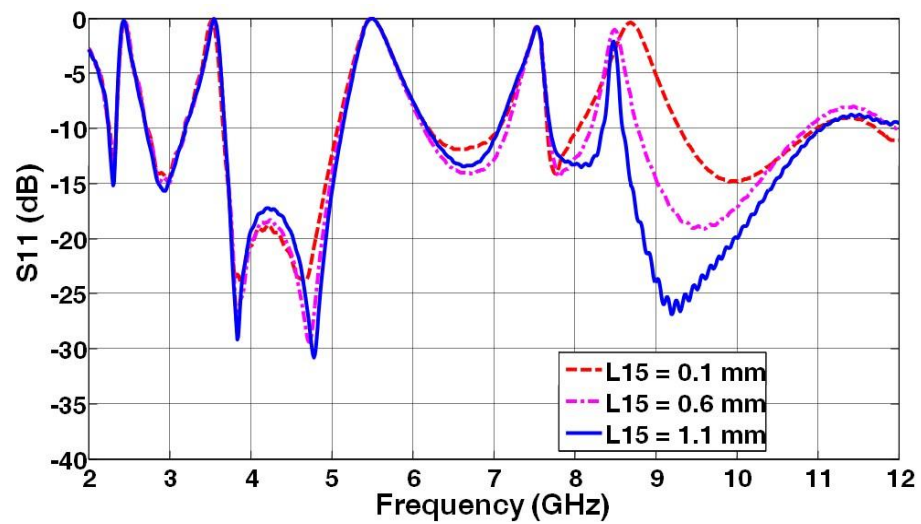


Fig. 4.10 Simulated reflection coefficients $|S_{11}|$ of the quintuple-band-notched antenna with different L_{15} values

The above results also show that the reflection coefficients in the rest of the UWB band remains about the same when the values of L3, L6, L9, L12, L15 and W21 are changed. It can be found that the location of the MSRs should be close to the feed point or feed line of the proposed antenna in order to maintain a good level of the notch performance. This property provides the designer with a great freedom to select the band-notched frequency and bandwidth of the antenna.

4.3 Theoretical Analysis

4.3.1 Current Distribution

To better understand the phenomenon behind the band-notched function of the proposed antenna, the current distributions on the quintuple-band-notched antenna are investigated at frequencies of 2.45, 3, 3.54, 5.49, 6, 7.53, 8.47 and 10 GHz, and are shown in Figs. 4.11(a)-4.11(h).

At the notched centre frequencies, i.e. 2.45, 3.54, 5.49, 7.53 and 8.47 GHz, Figs. 4.11(a) to 4.11(e) show that the current is mainly concentrated around the areas near the MSRs and much more than those in the main radiator of the antenna, as a result, the radiation of the antenna is limited and a band notched is achieved. But at the passband frequencies, the current mainly flow along the edge of the antenna while around the MSRs the current is very small as shown in Figs. 4.11(f) to 4.11(h), at frequencies of 3, 6 and 10 GHz, respectively.

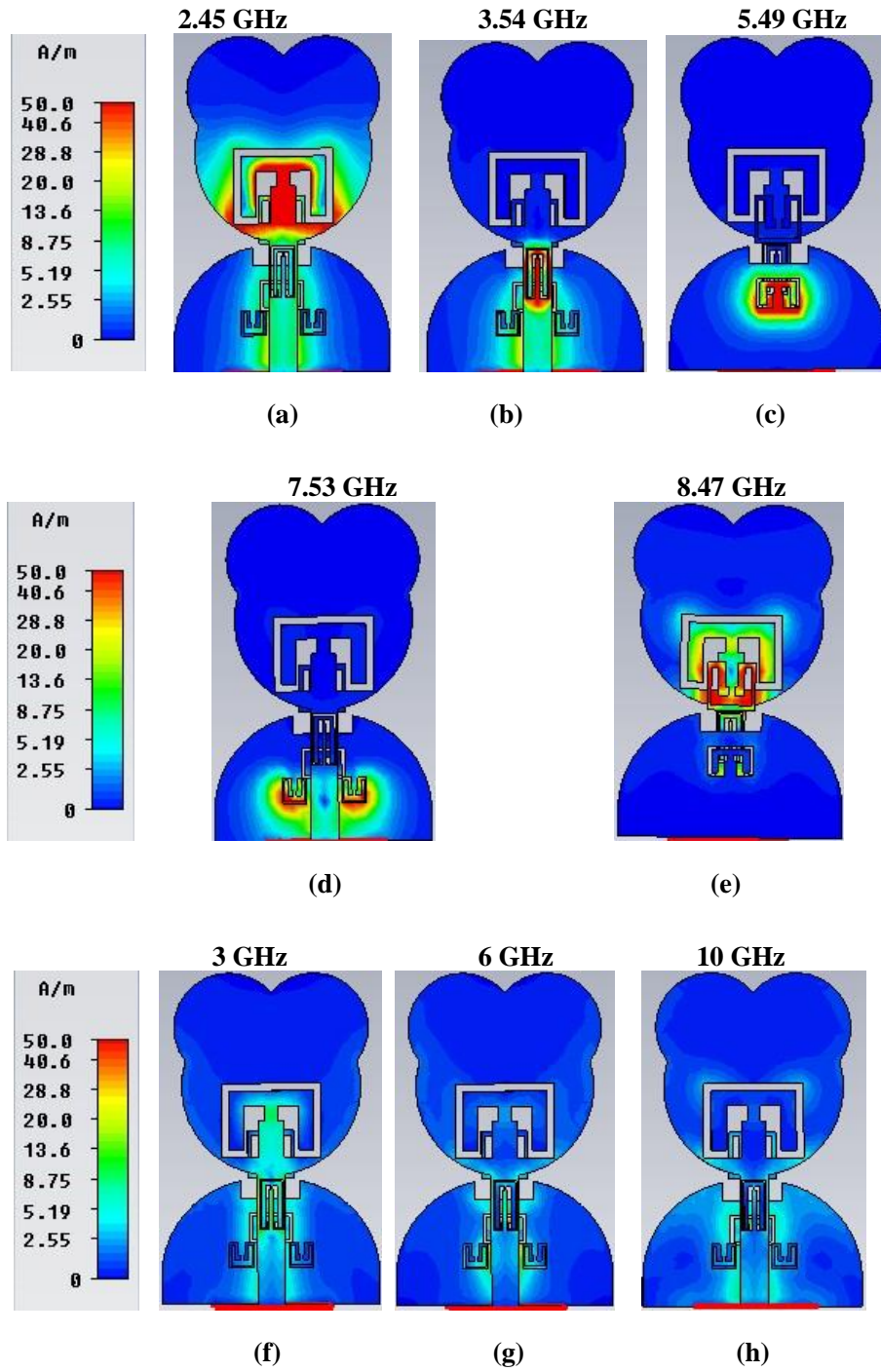


Fig. 4.11 Simulated surface current distributions of the quintuple-band-notched antenna at different frequencies (a) 2.45, (b) 3.54, (c) 5.49, (d) 7.53, (e) 8.47, (f) 3, (g) 6, and (h) 10 GHz

4.3.2 Equivalent Circuit

In order to further explain the principle of the MSRs for generating the band-notched characteristics. An equivalent circuit model of the proposed antenna is introduced and the transmission line models are used for the analysis. Generally speaking, the input impedance of a UWB monopole antenna can be considered as the first Foster canonical form [2]. In a complete Foster canonical form, each mode can be represented by a series of parallel RLC components. For the proposed quintuple-band-notched UWB monopole antenna, the rejection features are achieved by introducing five coupling resonance structures (MSRs), which contain five additional RLC resonators.

Fig. 4.12 shows the simulated input impedance of the quintuple-band-notched antenna. At the centre notch frequencies of 2.45, 3.54, 5.49 and 7.53 GHz(created by MSRs #1 to #4), It can be observed that the input impedance is quite similar to the impedance of a series RLC circuit, whose reactance is nearly zero and has a positive derivative, whereas the resistance has a local minimum. The impedance is nearly zero at the feeding point, which leads to the desired impedance mismatch at that frequency. At the fifth notch frequency 8.47 GHz (MSR #5), it can be seen that the reactance is nearly zero and has a negative derivative, whereas the resistance has a maximum. It is a parallel-type anti-resonance with significant changes in the values for both the resistance and the reactance parts.

As a result, the input impedance at the passband is represented by parallel RLC components (R_s , L_s and C_s) for the second and higher resonant frequencies and in series with C_0 and L_0 (represent the capacitance and inductance of the antenna when the antenna operates at the lower frequencies). Whereas at the rejection bands, four additional RLC-in-series resonator (created by MSRs #1 to #4) and a parallel RLC resonator R_5 , L_5 and C_5 (created by MSR #5) are incorporated to represent the band-notched structures (MSRs

#1 to #5). An approximated equivalent circuit model of Antenna 2 is depicted in Fig. 4.13.

In addition, the corresponding transmission line models of the proposed antenna, with quintuple-band-notched functions are shown in Fig. 4.14. Whereas the antenna consists of impedance Z_a and four parallel stubs and one series stub, which act like half-wavelength and full wavelength resonator, respectively. The five stub ends are short circuited and are modelled as $\lambda_{2.45}/2$, $\lambda_{3.54}/2$, $\lambda_{5.49}/2$, $\lambda_{7.53}/2$ and $\lambda_{8.47}$ long for the total length about 41, 28.1, 17.8, 9.57 and 18.1 mm which correspond to the rejection frequencies of 2.45, 3.54, 5.49, 7.53 and 8.47 GHz, respectively.

At the passband frequencies, as shown in Fig. 4.14(a), there is no (or little) effect from these three MSRs. But at the first notched band, as shown in Fig. 4.14(b), when $L_{total} \approx \lambda_{2.45}/2$, the impedance at the feeding point is zero (short circuited), which cause the antenna to be nonresponsive; therefore the first notched band is created. Correspondingly, the second, third, fourth and fifth band-notches are created when $L_{total} \approx \lambda_{3.54}/2$, $L_{total} \approx \lambda_{5.49}/2$, $L_{total} \approx \lambda_{7.53}/2$ and $L_{total} \approx \lambda_{8.47}$ as shown in Figs. 4.14(c) to 4.14(f), respectively.

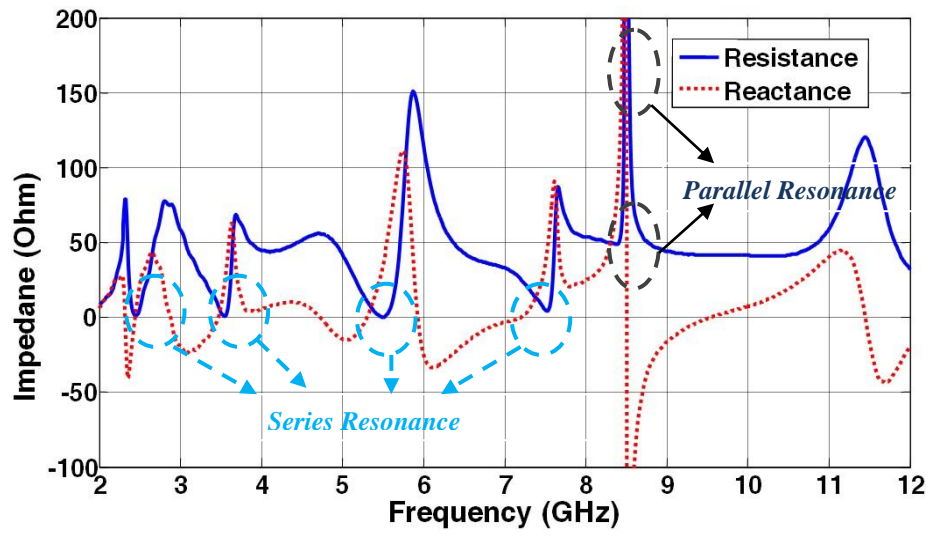


Fig. 4.12 Simulated input impedance of the quintuple-band-notched antenna

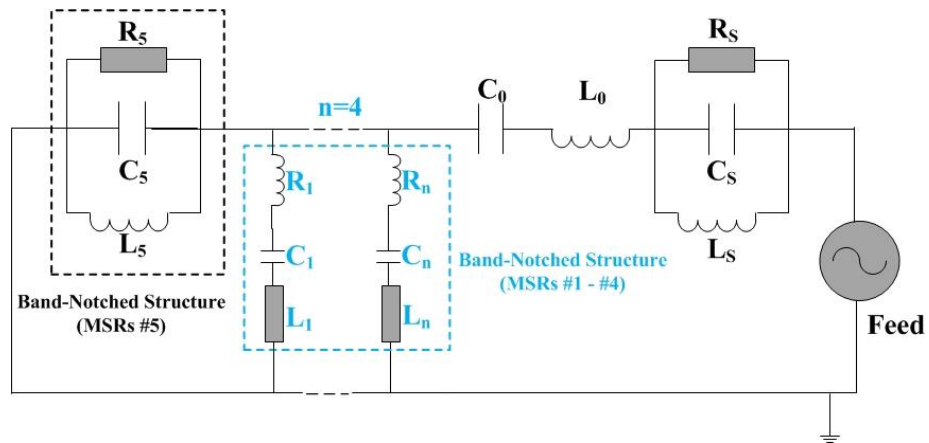
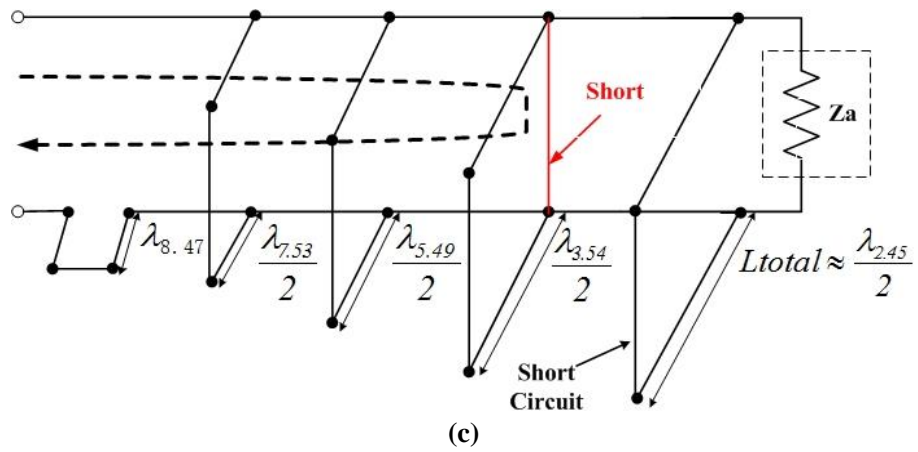
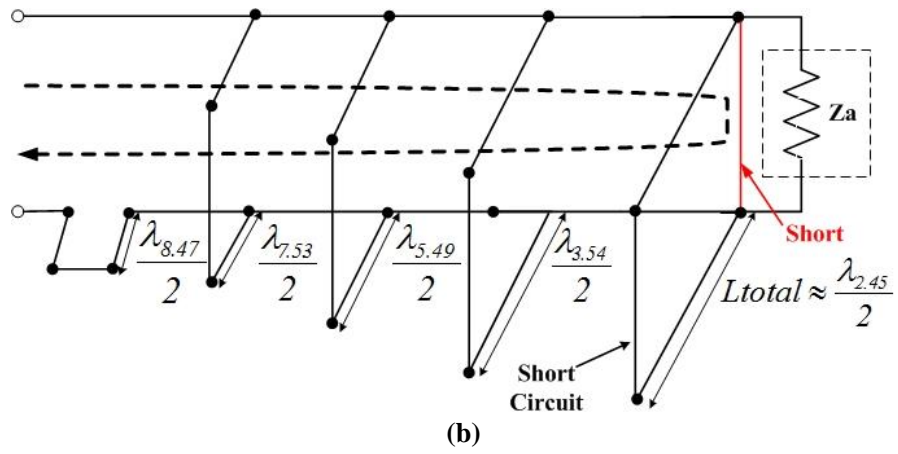
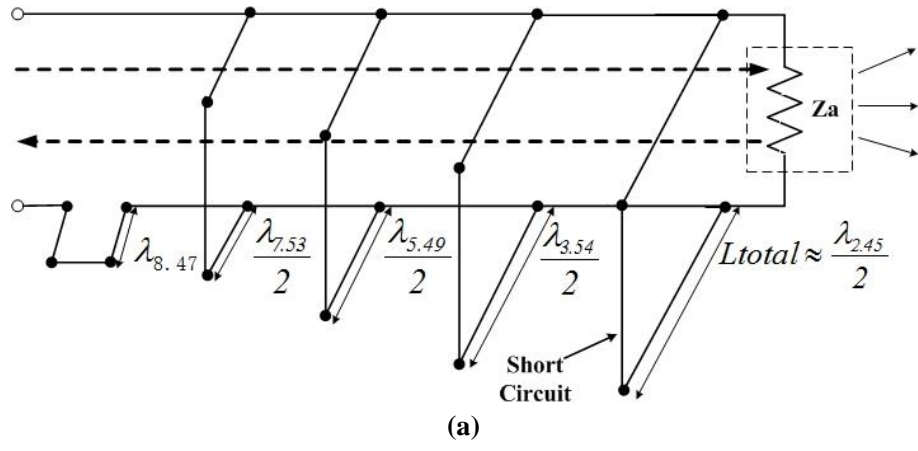


Fig. 4.13 An approximated equivalent circuit of the quintuple-band-notched antenna



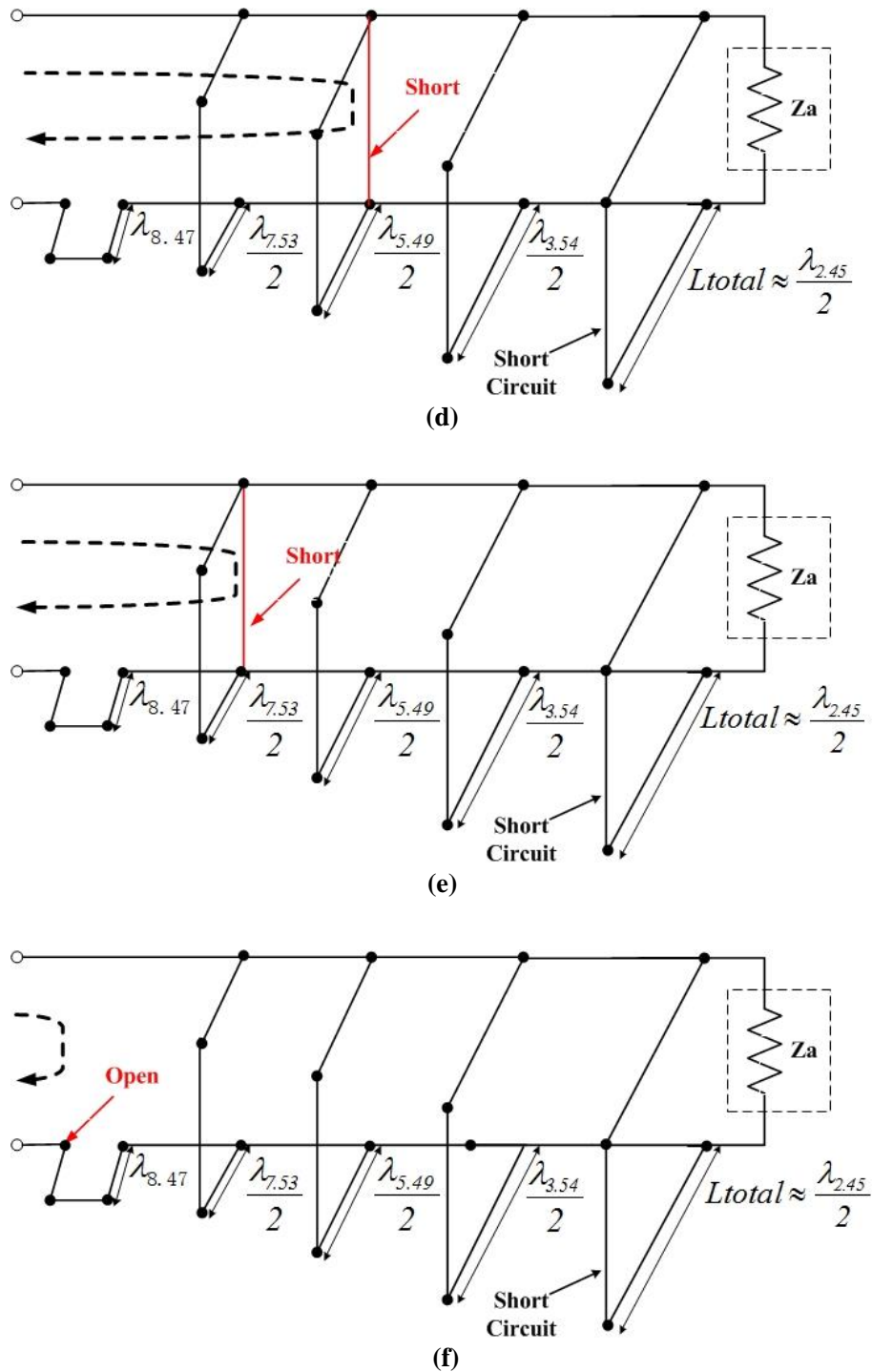


Fig. 4.14 Transmission line model of the quintuple-band-notched antenna at (a) Passband frequencies, (b) The first notched-band, (c) The second notched band, (d) The third notched band, (e) The fourth notched band, and (f) The fifth notched band

4.4 Results and Discussions

The return loss and realized gain across the UWB band, and the radiation patterns at the passband and also the notch frequencies of the quintuple-band-notched antenna are studied using computer simulation. To validate the simulation results, the proposed monopole antennas without and with band-notched characterizes are built and tested, the prototypes are shown in Fig. 4.15.

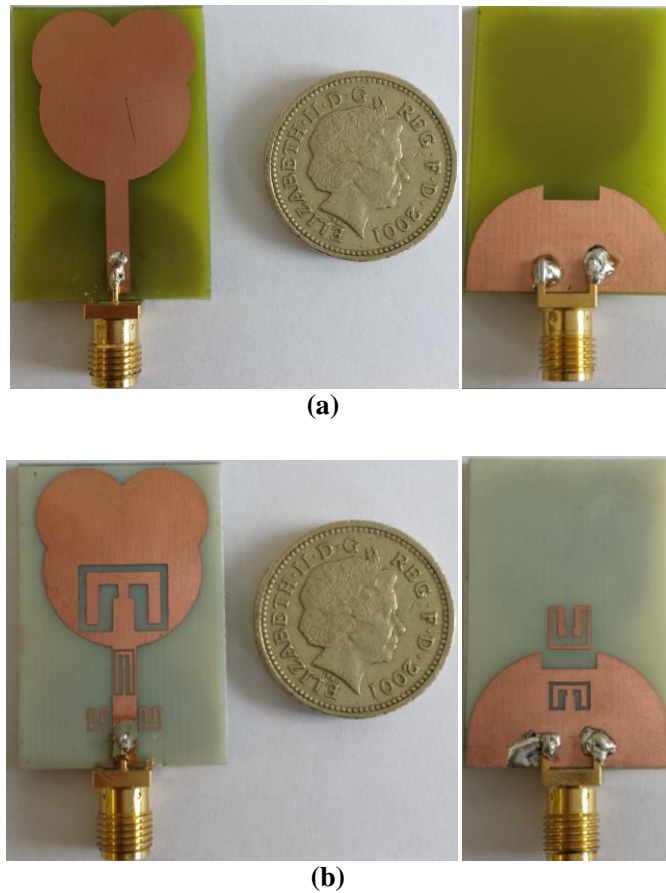


Fig. 4.15 Front and back view of the prototyped proposed UWB monopole antenna (a) Without, and (b) With band-notched

4.4.1 Frequency-Domain Performance

The simulated and measured reflection coefficients $|S_{11}|$ of the proposed antenna without band-notched function are shown in Fig. 4.16. They are in reasonable agreement while the difference at lower frequency around 2.7 GHz is probably caused by the cable effects due to the small ground plane of such a UWB antenna and the tolerance in manufacturing. It can be seen that, the antenna can operate from 2.7 to over 10.6 GHz for $|S_{11}| < -10$ dB.

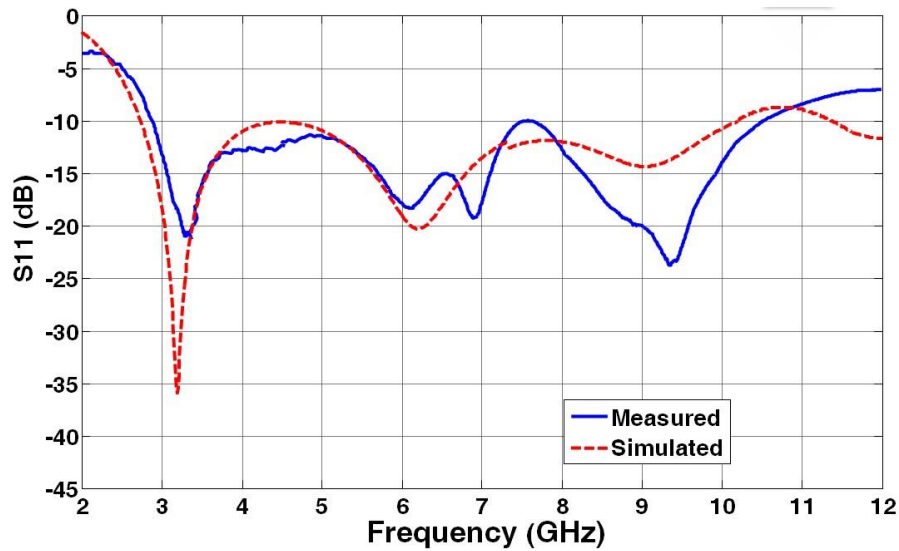


Fig. 4.16 Simulated and measured reflection coefficients $|S_{11}|$ of the proposed antenna without band-notched

The simulated and measured and reflection coefficients $|S_{11}|$ of the proposed antenna with five notched bands are also shown in Fig. 4.17. A reasonable agreement between the simulated and measured is obtained. The antenna with five MSRs is successfully designed with five desired notched bands: 2.35 to 2.73 GHz, 3.16 to 3.69 GHz, 5.0 to 6.1 GHz, 7.2 to 7.7 GHz and 8.1 to 8.74 GHz with very good levels of the rejection, while still maintaining the broadband performance from 2.24 to 10.8 GHz for $|S_{11}| < -10$ dB. The discrepancy performance between them is mostly attributed to the tolerance in

fabrication. The simulated -3 dB bandwidths of each notch are 130, 150, 420, 200, and 170 MHz; which correspond to quality (Q) factors of 18.82, 23.6, 13.39, 39.2 and 58.6 at the notched centre frequencies of 2.45, 3.54, 5.49, 7.53 and 8.47 GHz, respectively. In this respect, the antenna outperforms almost all other designs reported in the literature [60-75].

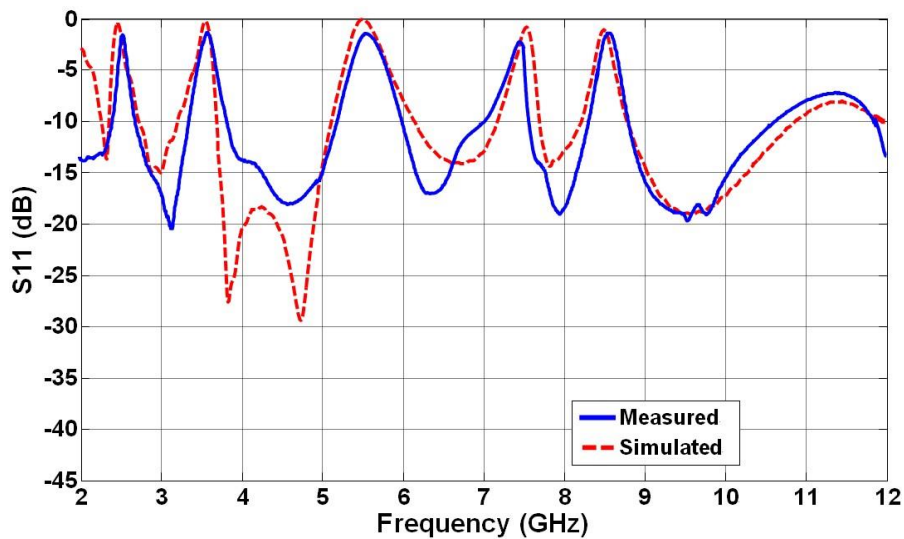
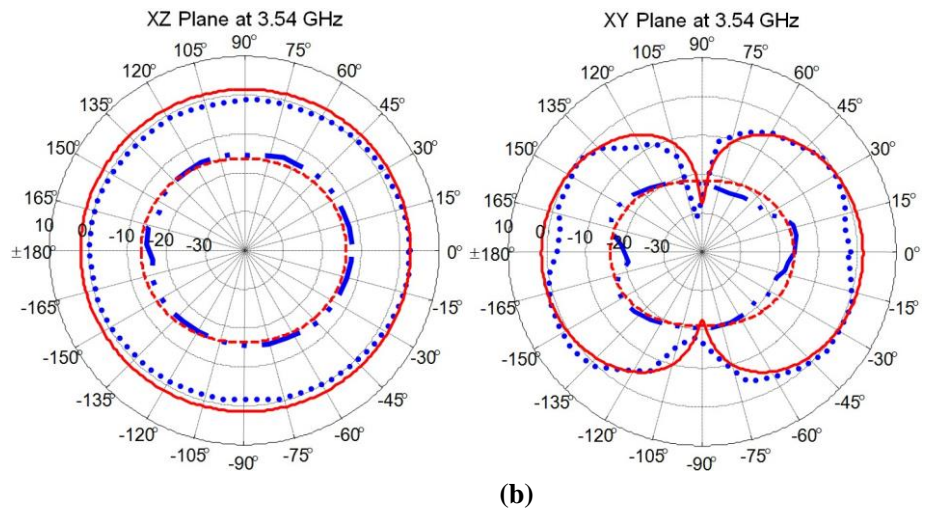
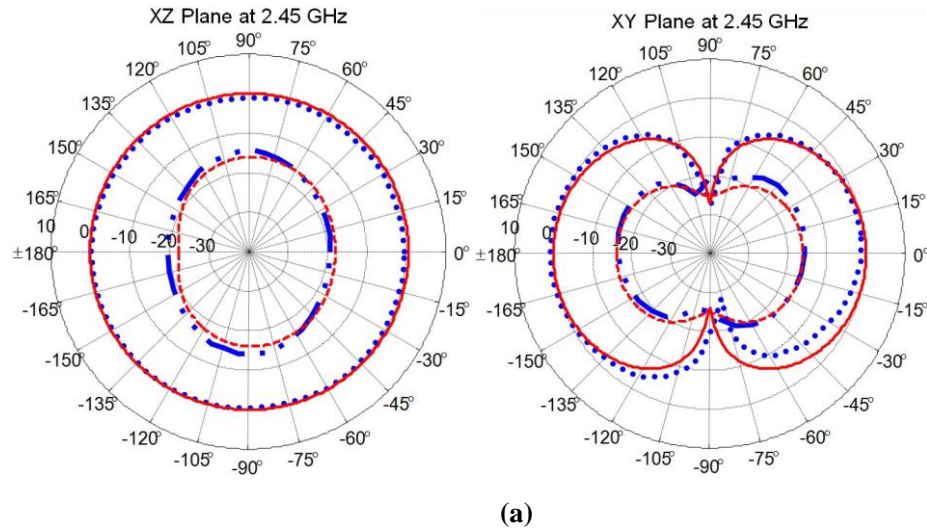


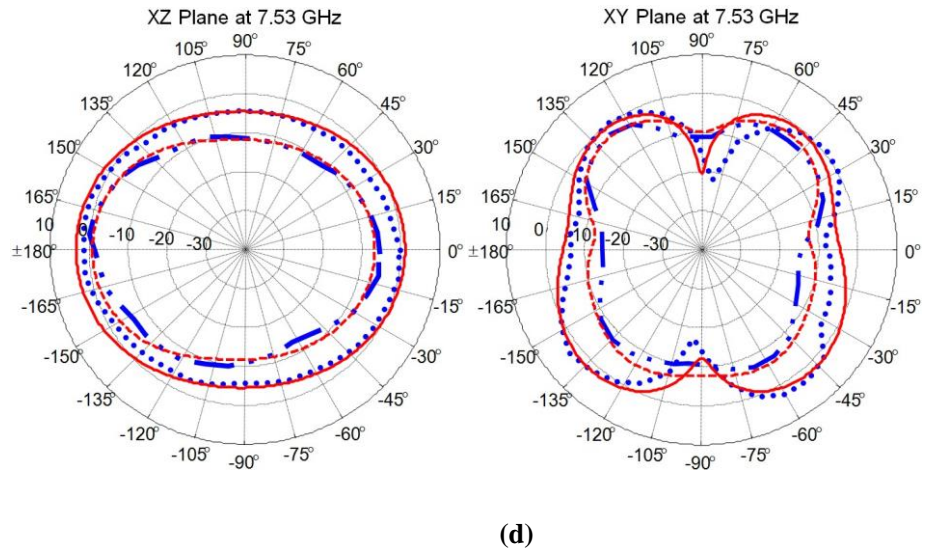
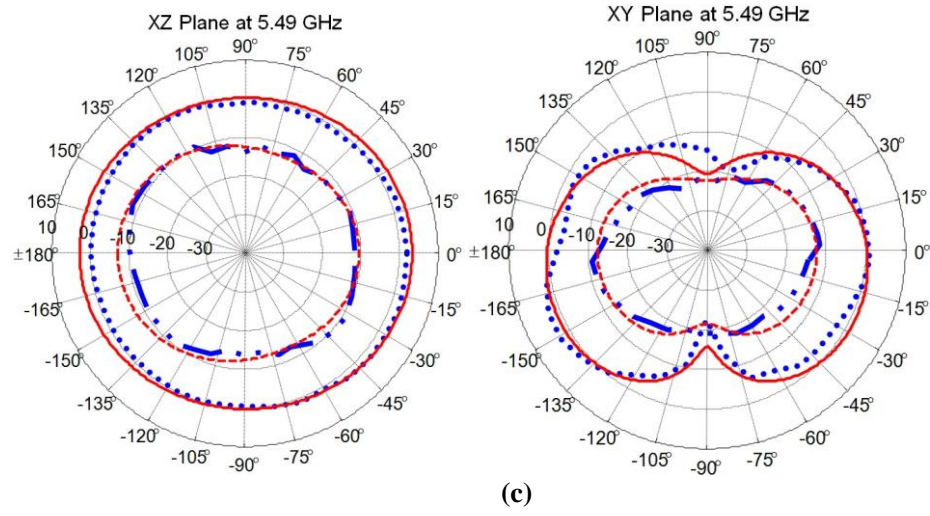
Fig. 4.17 Simulated and measured reflection coefficients $|S_{11}|$ of the quintuple-band-notched antenna

The radiation patterns of all the prototypes are simulated, measured and compared to investigate the effects of the MSRs. The simulated and measured radiation patterns of the proposed antenna without and with band-notched functions in the two principle planes, the H-plane (XZ-plane) and E-plane (XY-plane) at the frequencies of 2.45, 3.54, 5.49, 7.53 and 8.47 GHz are obtained and shown in Figs. 4.18(a) to 4.18(e), respectively. A reasonable agreement is demonstrated between the results. At all the tested frequencies without band-notched features, it can be found that the radiation patterns for co-polarisation are nearly omni-directional and stable in the H-plane. While in the E-plane, there are two nulls occurring in the positive and negative y-direction, which has typical monopole like patterns. For the antenna with the

band-notched functions, the figures show that the gains are almost evenly suppressed in all directions, and the average gain is dropped to about -10 dB.



UWB Antennas for Wireless Communications



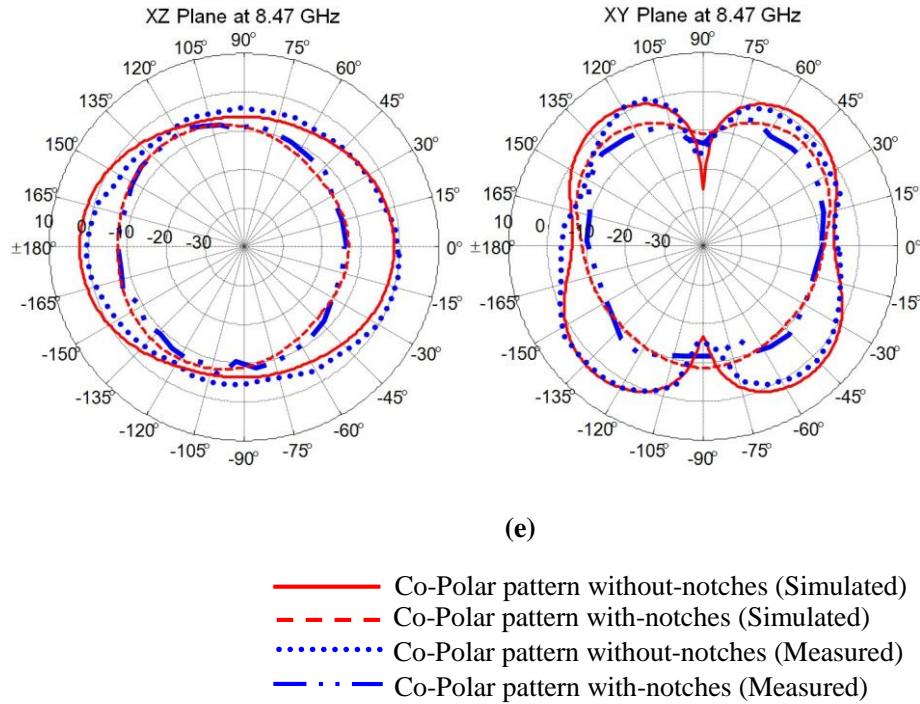


Fig. 4.18 Simulated co-polarized without (red solid line) and with band-notched (red break line), and Measured co-polarized without (blue dot line) and with band-notched (blue dot-dot break line) radiation patterns of the proposed antenna at (a) 2.45, (b) 3.54, (c) 5.49, (d) 7.53, and (e) 8.47 GHz

The simulated total efficiency of the proposed quintuple-band-notched antenna is shown in Fig. 4.19. A relatively constant efficiency of the antenna is observed over the UWB band, from 95% to 80%, except in those notched bands. At the notched frequencies of 2.45, 3.54, 5.49, 7.53, and 8.47 GHz, the corresponding efficiencies are substantially reduced to 9.1%, 7.2%, 5.5%, 13.2% and 16.8%. The low total efficiency indicates that the proposed antenna can provide a good average gain suppression of the notch band in all directions. Fig. 4.20 shows the simulated and measured maximum gain values of the proposed antenna. As expected, the antenna shows a stable gain throughout the operation band (2.24-10.8 GHz) from 1.2 to 5.1 dBi except at the notched bands. At the notch bands, gain suppressions of 15, 14, 16, 9 and 6 dB are observed. This

phenomenon indicates that the MSRs work effectively to introduce a quintuple-band-notched characteristic for the UWB antenna.

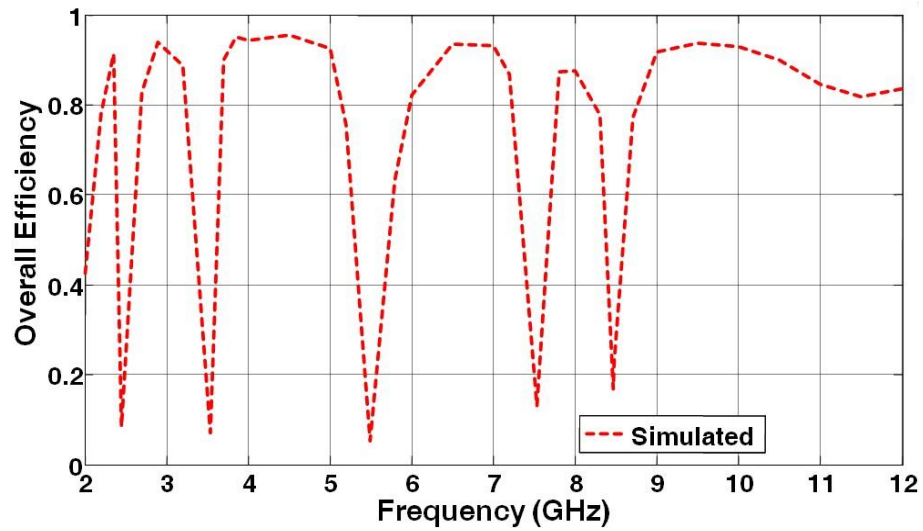


Fig. 4.19 Simulated overall/total efficiency of the quintuple band notched antenna

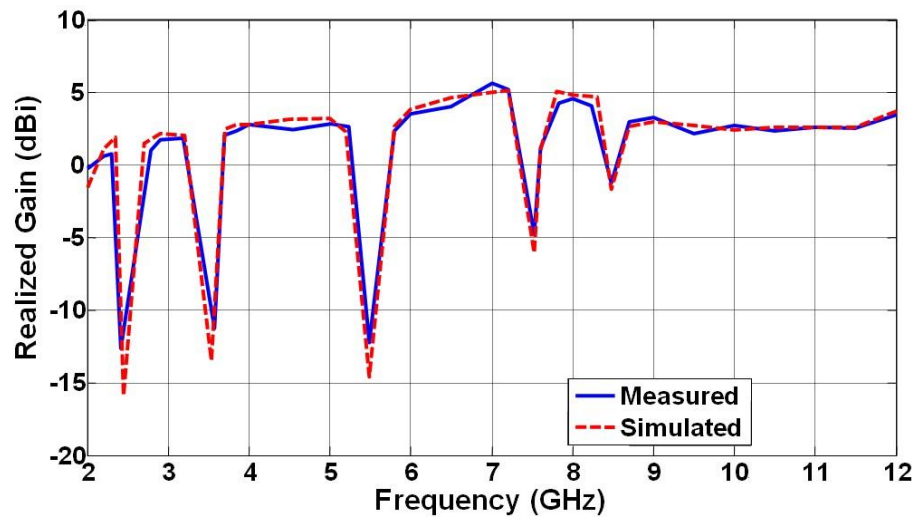


Fig. 4.20 Simulated and measured maximum realized gain values of the quintuple-band-notched monopole antenna

4.4.2 Time-Domain Performance

A good time domain performance is an essential requirement for the UWB antennas. Especially, the time-domain analysis for the UWB band-notched antennas is with great significance, because the waveform of the notched antennas can be easily distorted by the rejection characteristics. Therefore, the impulse response of the proposed antenna is investigated. Two identical antennas are placed face-to-face or side-by-side at a distance of 30 cm and the simulation step is shown in Fig. 4.21.

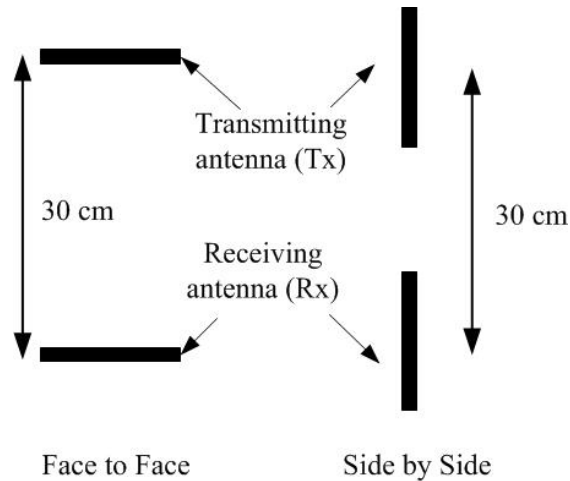


Fig. 4.21 Simulation setup of the antenna for the time-domian investigation

For comparison, the impulse responses of the UWB antenna without and with quintuple-band-notches in the cases of face-to-face and side-by-side are illustrated in Figs. 4.22 and 4.23, respectively. For the antenna with quintuple-band-notched funtion, the distroction of the received impulse is observed because of the existence of the notches in the frequency domain of the antenna. Figures also show that the magnitudes of the received signal are slightly larger in the face-to-face case than in the side-by-side case.

To evaluate the similarity between the transmitted and received impulses, the fidelity factor F is used, defined as [3, 4]

$$F = \max_{\tau} \int_{-\infty}^{\infty} f(t) r(t - \tau) dt \quad (4.4)$$

Where $f(t)$ and $r(t)$ are the transmitted and the received impulse signals, respectively, and τ is the time delay of the signal. By substituting the two normalized impulse signals in Equation (4.4). The fidelity factors F of the UWB antenna with and without band-notched are calculated, as shown in Table 4-4. Note that the antenna with $F = 1$ indicates an ideal scenario between the transmitted and received signals, without distortion in the transmission system of the impulse signal.

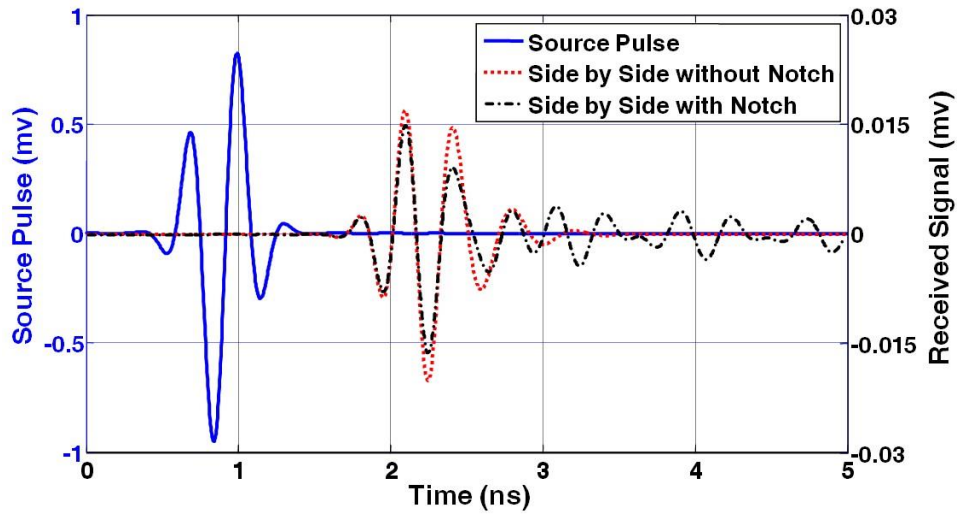


Fig. 4.22 Simulated signals of the antenna with/without notch with single impulse input signal for the side by side case

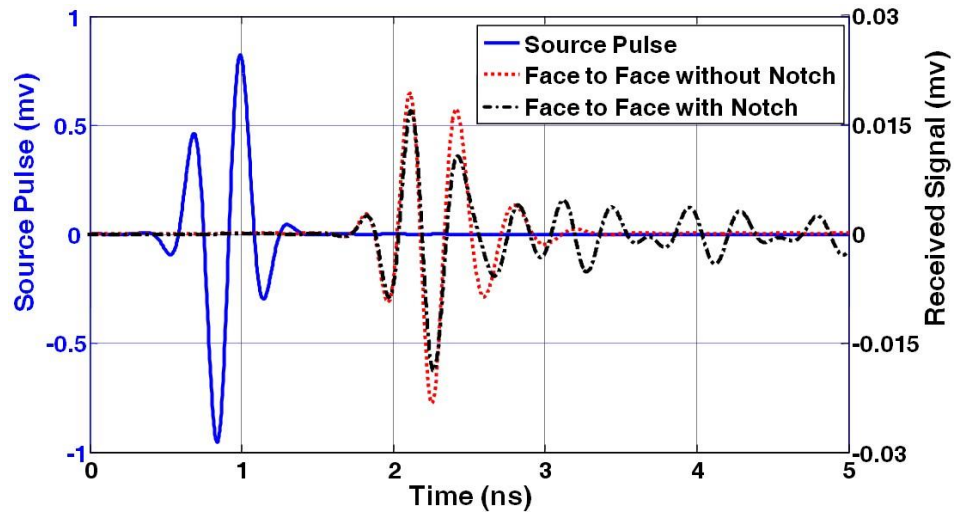


Fig. 4.23 Simulated signals of the antenna with/without notch with single impulse input signal for the face to face case

From Table 4-4, it can be seen that the differences of the fidelity in the two cases (face-to-face and side-by-side) for both antennas are very small. As expected, the UWB antenna without notches has the fidelity of more than 0.93. Although, the distortion of the received signal is expected (the fidelity F would drop) with notches, the proposed antenna with five notches still can achieve the fidelity of more than 0.855. The results reveal that the introduction of band-notched features has limited effect on the time-domain performance of the antenna.

Table 4-4 Calculated fidelity factor of the UWB antenna without and with band-notched function

Cases	UWB Antenna Without Band-Notched	UWB Antenna With Quintuple-Band-Notched
Face-to-Face	0.941	0.870
Side-by-Side	0.932	0.855

4.5 Summary

In this Chapter, a novel UWB planar monopole antenna with quintuple-band-notched characteristics has been proposed. The quintuple-band-notched functions have achieved by embedding five MSRs into the radiator, feedline, and ground plane. In the frequency-domain, the proposed antenna is able to operate from 2.24 to 10.8 GHz for $|S_{11}| < -10$ dB with five rejection bands performance in the frequency bands of 2.35 to 2.73 GHz, 3.16 to 3.69 GHz, 5.0 to 6.1 GHz, 7.2 to 7.7 GHz and 8.1 to 8.74 GHz with excellent levels of rejection. Good radiation patterns and gain values have also obtained. In the time-domain, the fidelity has used to evaluate the time-domain performance of the antennas. The results have shown that the quintuple-band-notched antenna has a good time-domain performance (i.e. the fidelity of more than 85% compared to 93% for the UWB antenna without notches). The proposed antenna is simple to design and fabricate and the integrated slots can provide tuning flexibility for a different desired frequency. Furthermore the proposed antenna can be easily integrated with other components of the system. It should be a very good candidate for UWB applications.

Table 4-5 compares our proposed band-notched antenna with one similar design as reported in [75], in terms of size, bandwidth (BW), number of notches and gain suppression. Both antennas have realised with five notches. However, the gain suppression of our design outperforms the design reported in [75] and the size of our antenna is about 10% smaller with a similar performance.

Table 4-5 Comparison with the design in [75]

	Techniques	Analyzed Parameters	Gain Suppression (dB)	Notch Bands (GHz)
Proposed design	M-shaped resonators	Size: $22 \times 34 \text{ mm}^2$ BW: 2.24-10.8 GHz	15	2.35-2.73
			14	3.16-3.69
			16	5.0-6.1
			9	7.2-7.8
			6	8.1-8.74
Design in [75]	C-shape slots and Open-circuit stubs	Size: $26 \times 31.8 \text{ mm}^2$ BW: 2.45-12 GHz	5	3.27-3.57
			6	5.01-5.45
			3	5.55-6.05
			3	7.05-7.45
			6	7.83-8.19

4.6 References

- [1] L. H. Lai, Z. Y. Lei, Y. J. Xie, G. L. Ning, and K. Yang, "UWB antenna with dual band rejection for WLAN/WIMAX bands using CSRRs," *Progress In Electromagnetics Research Letters*, vol. 26, pp. 69-78, 2011.
- [2] B. T. Wang, A. M. Niknejad and R. W. Brodersen, "Circuit Modelling Methodology for UWB Omni-directional Small Antennas", *IEEE Journal on Selected Areas in Comms*, vol. 24, pp.871-877, Apr. 2006.
- [3] Z. N. Chen, *et al.*, "Small printed ultra-wideband antenna with reduced ground plane effect," *IEEE Trans. on Antennas and Propagation*, vol. 55, pp. 383-388, 2007.
- [4] D. Lamensdorf and L. Susman, "Baseband-pulse-antenna techniques," *IEEE Antennas and Propagation Magazine*, vol. 36, pp. 20-30, 1994.

CHAPTER 5 DESIGN OF A PLANAR UWB ANTENNA WITH RECONFIGURABLE BAND REJECTION

5.1 Introduction

In Chapter 4, the UWB antenna with band-notched feature was realised to reduce the level of the interference from the RF front end at fixed notched bands. Considering future wireless applications, antennas are required to support multiple standards and application since the demand of compactness of the systems and devices. To achieve this, a UWB antenna with reconfigurable band notch operation could be a promising solution.

In this Chapter, a planar UWB monopole antenna is presented to achieve reconfigurable band-notched capability over the frequency band from 2.1 to 12

GHz to cover the UWB and other important mobile services. The band-notched function is realised by etching two co-directional split ring resonators (CSRR) structure on the radiator. The reconfigurability is achieved by implementing with three pairs of switches for the rejection frequencies. The simulation and measurement results demonstrate that the proposed antenna has the capability to switch between the UWB band and several narrow rejection bands. In addition, the effect of the position and length of the CSRR structures on the antenna impedance bandwidth are analysed. Both current distributions and transmission line models are used to interpret the radiation mechanism of the CSRR structures.

The simulation results presented in this Chapter were performed using CST Microwave Studio.

5.2 Band-Notched Antenna Design

5.2.1 Co-directional Split Ring Resonators (CSRR)

A Mickey-mouse shaped planar monopole antenna is selected as the reference antenna to be modified to produce the desired reconfigurable band-notched function as presented in Chapter 3. This is because the antenna can operate over a UWB band (3.1-10.6 GHz) and has good radiation performances. The two Mickey-mouse ears provide a longer current path to maximise the operational frequency for a given antenna size. It is now well-known that the SRR and CSRR structures can be considered as an electronically small LC resonator with a very high quality (Q) factor, which is able to produce a band-notched property for UWB antennas [1-3]. In this Chapter, the CSRR structures is used as a band-notched element in the planar UWB antenna because the CSRR is more suitable to be integrated on the planar structure than

the SRR [4]. In addition, the CSRR provides enough space on the conventional compact UWB antenna to embed the band-notched features due to the sub-wavelength resonant structure [5]. Commonly, the CSRR structures can act as filters to suppress the signal at the desired frequencies in order to create the band-notched performance. The total length of each CSRR is approximately $\lambda/2$ at the notched frequency, which is related to its geometry dimensions as defined by [6]:

$$f_{notch} \approx \frac{c}{2 \cdot L_{total} \cdot \sqrt{\epsilon_{eff}}} \quad (5.1)$$

$$\epsilon_{eff} = \sqrt{(\epsilon_{eff} + 1) / 2} \quad (5.2)$$

$$L_{total} \approx \frac{\lambda}{2} = 2 \cdot (L1 + W1) - r \quad (5.3)$$

where c is the speed of light, L_{total} is the total length of the CSRR structure and ϵ_{eff} is the effective relative dielectric constant. The length of the CSRR structure is the main parameter to determine the frequency of the rejection band once the substrate is given. For this study, we would like to form four band-stop filters. Fig. 5.1 shows the geometries of four different CSRR structures and their design dimensions on radiator. Four CSRR structures are designed to create the notches at the frequency bands of 2.4-2.464 GHz, 3.3-3.8 GHz and 5.15-5.825 GHz for the existing communication services (such as WLANs and WiMAX). The dimensions of the outer and inner CSRR structures are denoted as $L1 \times W1$ and $L3 \times W3$, and the gap lengths are $r1$ and r , respectively. The off-set distance to the bottom of the radiator and width of the CSRR structures are $L2$ and $W2$, respectively.

5.2.2 Length and Positions of the Resonator

The simulated reflection coefficients $|S_{11}|$ of Structures 1-4 are shown in Fig. 5.2. Structure 4 is the combination of Structures 2 and 3. Clearly, there is an inverse proportional relationship between the band-notched frequency and the total length of the CSRR structures. It can be seen that the notch frequency is decreased from 5.45 to 2.46 GHz when L_{total} is increased from 19.2 to 33.3 mm. In addition, the numerical and theoretical predictions of the band-notched frequency for different total lengths of the CSRR structure are compared and listed in Table 5.1. The results are in reasonable agreement with the results obtained using design Equations (5.1) and (5.2). The difference between the numerical and theoretical frequencies is about 0.2 GHz, which may be caused by the approximation of expression when calculating the effective relative dielectric permittivity ϵ_{eff} in Equation (5.1).

In addition, the simulation results indicate that other parameters, such as the width (W2) and position (L2) of the CSRR structures, can affect the frequency and bandwidth of the notch, as shown in Fig. 5.3. Take Structure 4 as an example, the effect of W2 on the notch frequency is shown in Fig. 5.3(a); and it can be observed that the band-notched frequency shifts upwards from 5.28 to 5.63 GHz with the increase of W2 from 0.2 to 0.6 mm. This is because widening the slot width is similar to decreasing the inductance and the capacitance values. In other words, it has the effect of increasing the centre notched frequency.

Furthermore, the level of rejection is dependent on the position of the CSRR structure. This is due to the strong current around the feeding point of the radiator (the current density is higher at this region). From Fig. 5.3(b), it can be observed that when L2 is increased from 1 to 3 mm, the -10 dB bandwidth is reduced from 0.65 to 0.21 GHz. Based on the above analysis, the final optimised parameters of the CSRR structures are: $W1 = 8$ mm, $W2 = 0.4$ mm,

$W3 = 5$ mm, $L1 = 9.5$ mm, $L2 = 1$ mm, $L3 = 4.6$ mm, $r = 0.8$ mm and $r1 = 6.6$ mm.

Table 5-1 Numerical and theoretical predictions for the band-notched frequency

Ltotal (mm)	Numerical Frequency (GHz)	Theoretical Frequency (GHz)
33.3	2.46	2.63
28.4	3.57	3.28
19.2	5.45	5.26

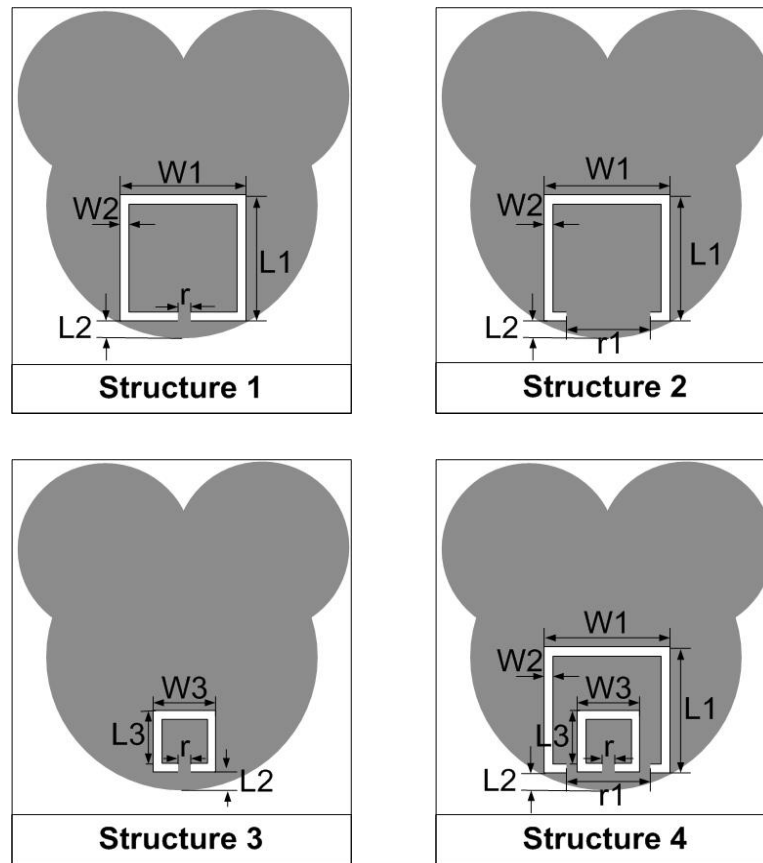


Fig. 5.1 Geometries of Four different CSRR filter structures

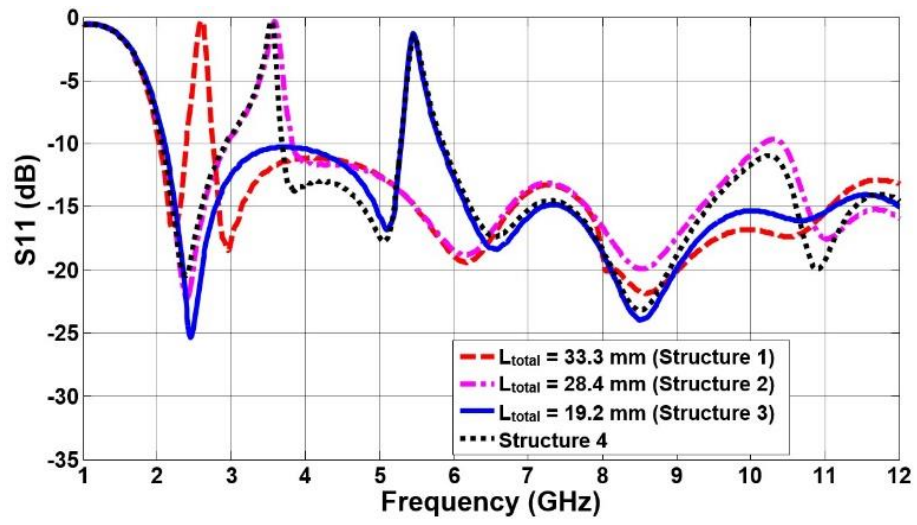
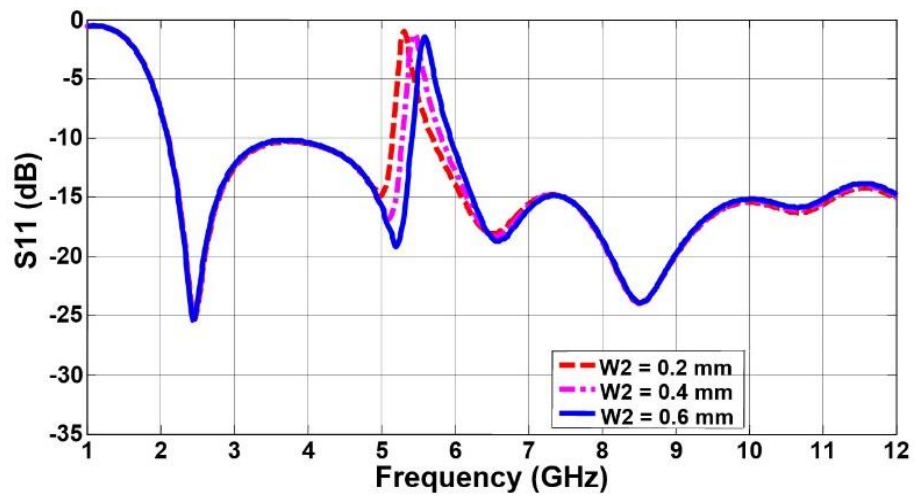


Fig. 5.2 Simulated reflection coefficients $|S_{11}|$ of the antenna for different structures



(a)

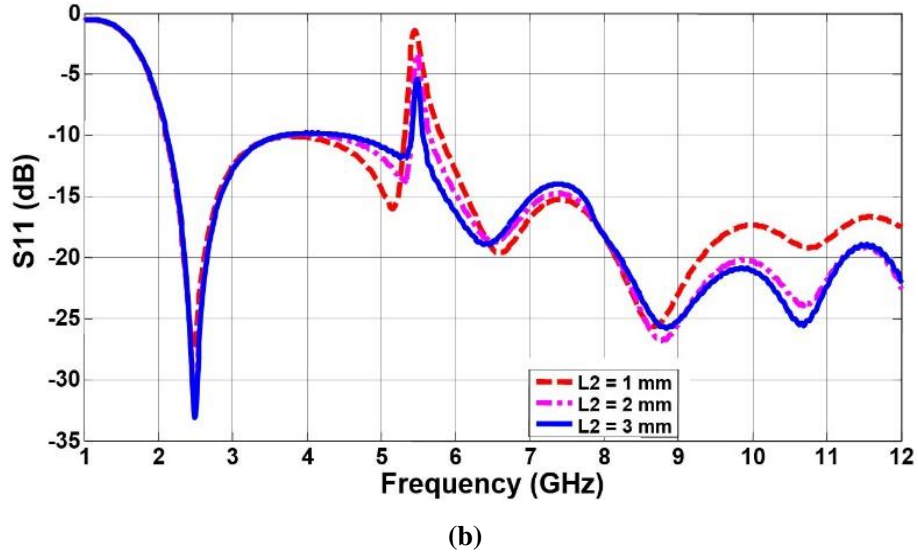


Fig. 5.3 Simulated reflection coefficients $|S_{11}|$ of the antenna for different values (a) W_2 , and (b) L_2

5.3 Antenna Integration with Switches

To achieve the reconfigurable functions, the CSRR structures are integrated with three pairs of switches (S1, S2 and S3) as shown in Fig. 5.4. In the simulation, these switches were modelled as a gap with the dimension of $0.8 \text{ mm} \times 0.4 \text{ mm}$ (the same width as W_2) for the OFF state and the gap filled with a small copper strip for the ON state. Thus, ON and OFF states of a switch are achieved by short-circuit and open-circuit of the copper strip, respectively. For implementation, the gaps are obtained as switches in the CSRR structures. The positions of switches S1-S3 are placed at distances $L_2 = 1 \text{ mm}$, $L_4 = 4.8 \text{ mm}$ and $L_5 = 8 \text{ mm}$ (from the bottom point of the radiator) to create Structures (1-4) for the desired rejection bands, respectively. For example, when switches S1 and S3 are in the ON state and S2 is OFF, it creates Structure 3, where the effective length of the outer CSRR structure is 19.2 mm corresponding to the band-notched frequency at 5.45 GHz .

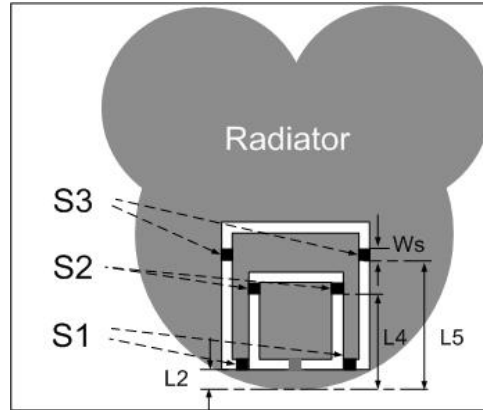


Fig. 5.4 Topology of three pairs of switches on the radiator: $W_s = 0.8$ mm

5.4 Theoretical Analysis

5.4.1 Current Distribution

In order to better understand the phenomenon behind the band-notched characteristics, the current distributions on the antenna (Structure 3) are investigated. Fig. 5.5 shows that how the inner CSRR structure resonates at 5.45 GHz and how its behaviour is changed when the switches are integrated (S2 is OFF and the other two switches are ON). In Fig. 5.5(a), at the notch frequency of 5.45 GHz, it can be seen that the majority of the current is confined around the bottom edge of the inner CSRR structure. In which, the directions of the current in the interior and exterior of the inner CSRR structure are opposite which results in small combined radiation fields (a high attenuation near resonate frequency [7]). Hence, the rejection at the frequency of 5.45 GHz is created. By contrast, the current on the inner CSRR structure is weak and does not resonate at the frequency of 8.5 GHz, even when switch S2 is in the OFF state as shown in Fig. 5.5(c). On the other hand, when switch S2 is ON, the total length of the inner CSRR structure is divided into three parts

and no currents flow through the CSRR structure, as shown in Fig. 5.5(b). Therefore, it cannot achieve the desired band-notched performances.

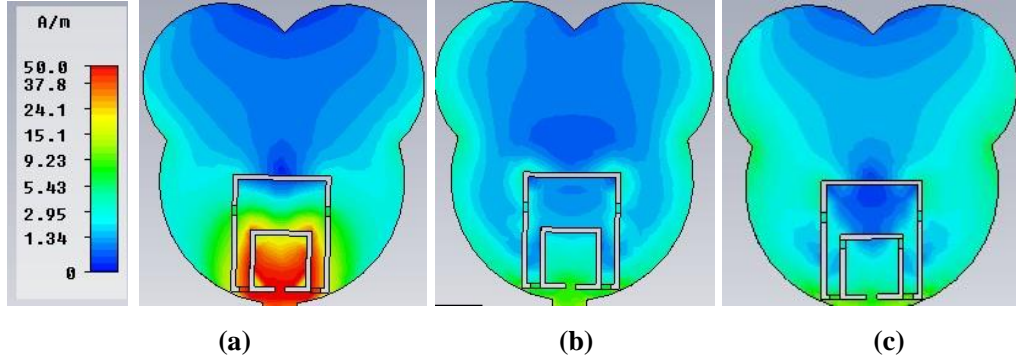


Fig. 5.5 Simulated current distributions: (a) S2 OFF at 5.45 GHz, (b) S2 ON at 5.45 GHz (UWB state), and (c) S2 OFF at 8.5 GHz

5.4.2 Transmission Line Model

In order to further understand the mechanism of the CSRR structures with integrating the switches. The transmission line models are used for analysis [8]. Fig. 5.6 shows the simulated input impedance of the antenna (Structure 3), it can be observed that the reactance is nearly zero and has a positive derivative, whereas the resistance has a local minimum at the notch frequency of 5.45 GHz - it is similar to the impedance of a series resonance.

Therefore, the corresponding transmission line models for different switching states are shown in Fig. 5.7. Whereas the antenna consists of impedance Z_a and three series stubs. Each stub (CSRR structure) is modelled as a $\lambda/4$ long and short-circuit terminated stub. Three pairs of switches (S1, S2 and S3) are across the input to the series stub. When all switches are turned ON, the stubs are disconnected from the circuit as shown in Fig. 5.7(a) and it has no or little effect on the incident power, which is radiated from the antenna. Nevertheless, when switch S3 is in the OFF state and the other two pairs of

switches are ON, the antenna is similar to Structure 2 in Fig. 5.1. The effective stub total length is $\lambda_{3.57}/4$ long for the total length of 28.4 mm which corresponds to the rejection frequency at 3.57 GHz. As a result, the incident power is reflected as appears in Fig. 5.7(b). Correspondingly, when switch S2 is OFF and the other two pairs of switches are ON (Structure 3) or S2 and S3 are OFF and S1 is ON (Structure 4), a single (5.25-5.81 GHz) and dual-band (2.94-3.68 GHz and 5.33-5.84 GHz) notches are created as shown in Figs. 5.7(c) and 5.7(d), respectively.

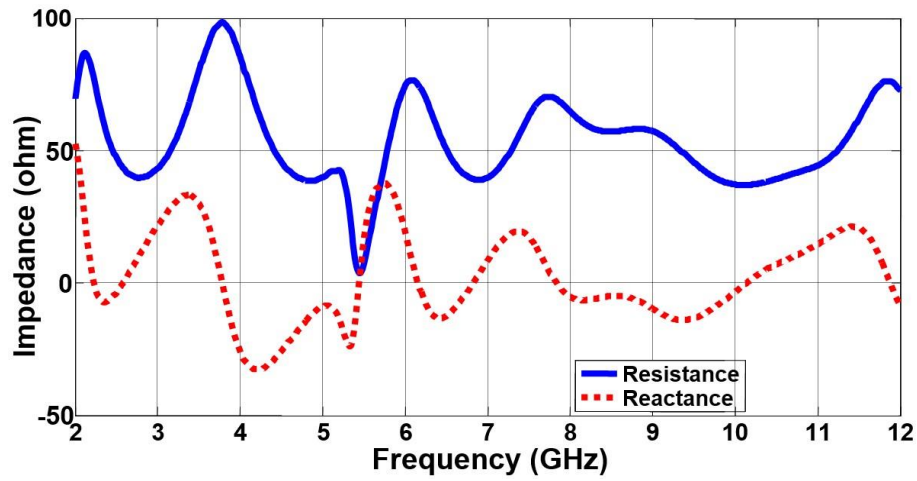
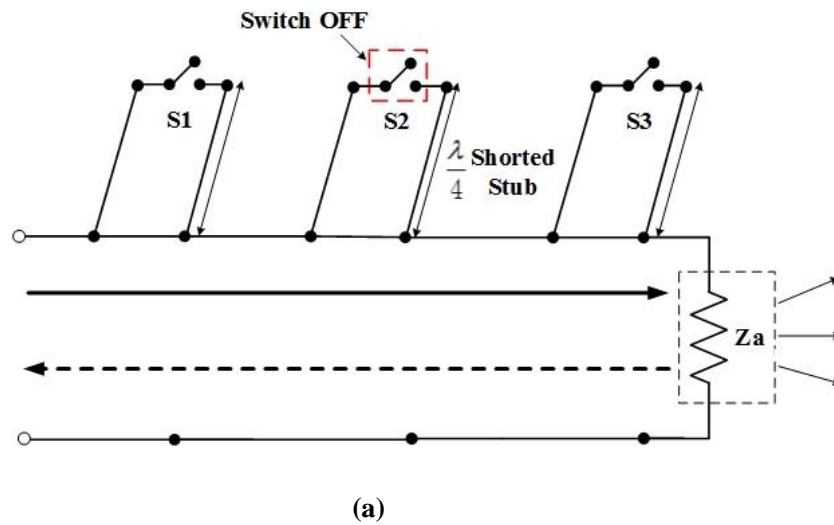
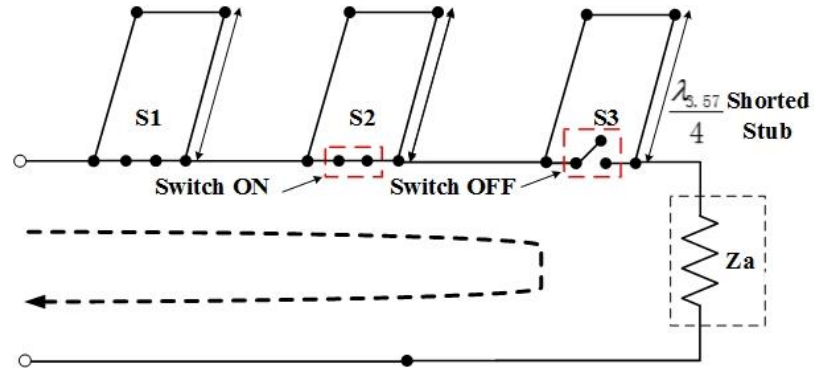
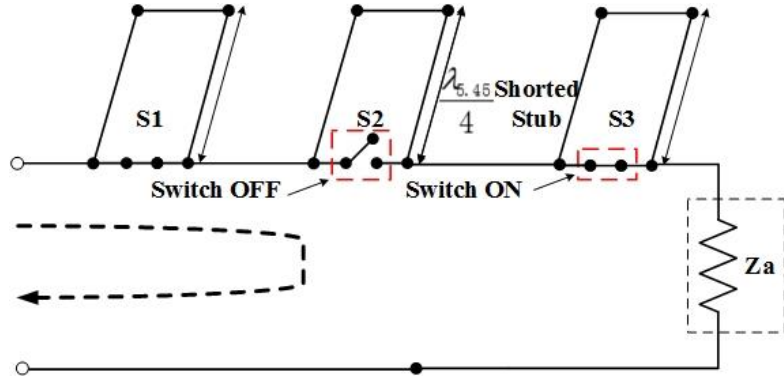


Fig. 5.6 Simulated input impedance of the antenna (Structure 3)

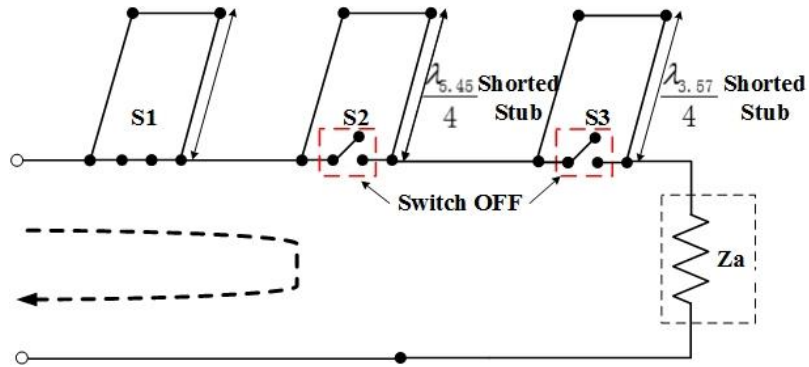




(b)



(c)



(d)

Fig. 5.7 Transmission line model for (a) CSRR structures with switches ON (passband), (b) CSRR structures with switch S3 OFF, (c) CSRR structures with switch S2 OFF, and (d) CSRR structures with switches S2 and S3 OFF

5.5 Results and Discussions

To evaluate the performance of the proposed antenna, the impedance, radiator characteristics and bandwidth behaviour are analysed. For the proposed design, a total of eight operating states are investigated as shown in Table 5-2. For the return loss measurement, five structures linked to five operating states are selected, fabricated and tested to validate the design and the prototypes of these antennas are shown in Fig. 5.8.

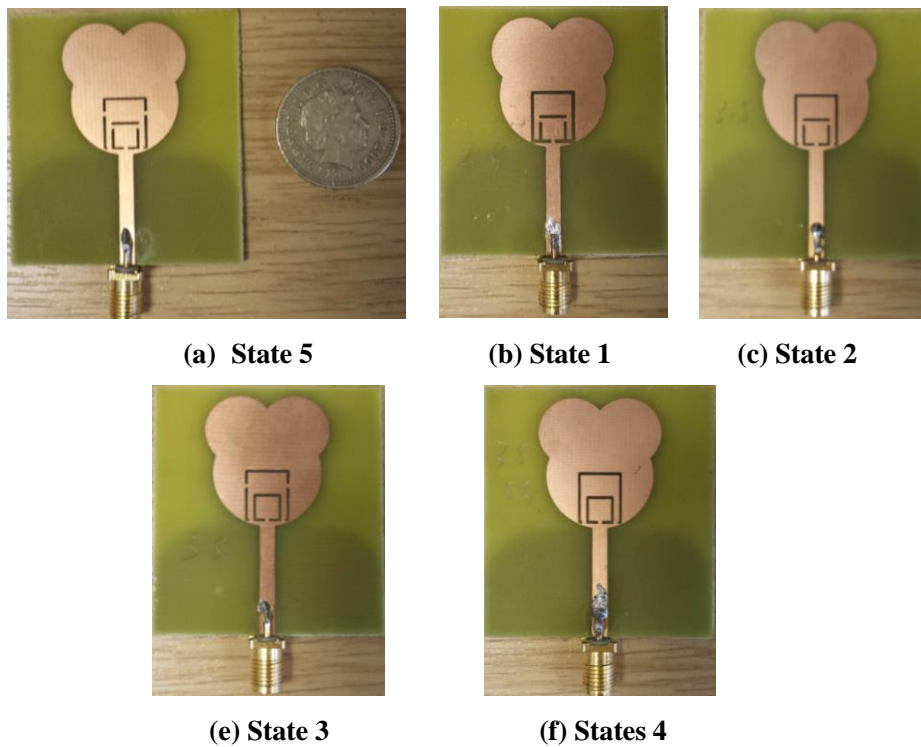


Fig. 5.8 Selected prototypes of the proposed antenna for five switching states

5.5.1 Frequency-Domain Performance

5.5.1.1 Reflection Coefficients

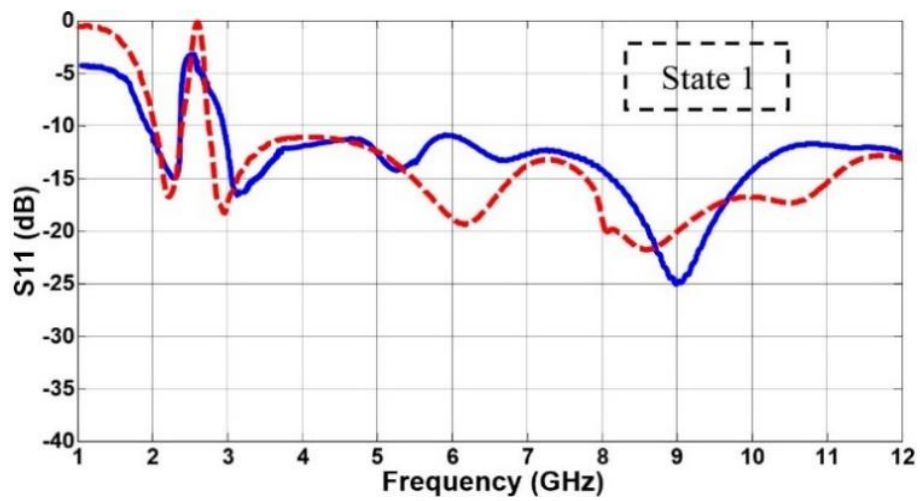
The simulated and measured reflection coefficients S_{11} for different switching States (1-5) are shown in Fig. 5.9. A reasonable agreement is demonstrated between them, a small shift in the lower frequency bands are consistently observed and the measured rejection levels of the notches are lower than the simulated ones, it is probably due to the cable and connector effects (the cable and connector are not included in the simulation but presented in the measurements); or a gap is not a good switch since it is a capacitor in practice for RF/MW. The discrepancies at higher frequencies (around 5.5 GHz) are mostly likely caused by the loss of the connector.

In addition, it can be observed from these figures that when all the switches are turned into ON states (State 5), the band-notched characteristics effects are all eliminated, because no current flows into the CSRR structure which effectively disconnected the CSRR structure from the antenna, resulted in the proposed antenna working in its UWB state. The same performance is also obtained for the antenna in State 6. To reject the WLAN band, switch S2 is in the ON state while switches S1 and S3 are turned OFF, the effective length of the inner CSRR structure is 33.3 mm which corresponds to a rejection frequency at 2.46 GHz (State 1). Furthermore, from Table 5-2, it can be seen that when switch S1 is in the ON state, the antenna operating frequencies are 2.87-3.83 GHz for S2 is ON and S3 is OFF and 5.25-5.81 GHz for S2 is OFF and S3 is ON, respectively. In the meantime, in State 4 only when switch S1 is ON, the antenna operates in a dual-band notched state at the frequency bands: 2.94-3.68 GHz and 5.33-5.84 GHz, respectively. For the other switch combinations, the simulated results of the reflection coefficients S_{11} for states 6-8 are shown in Fig. 5.10.

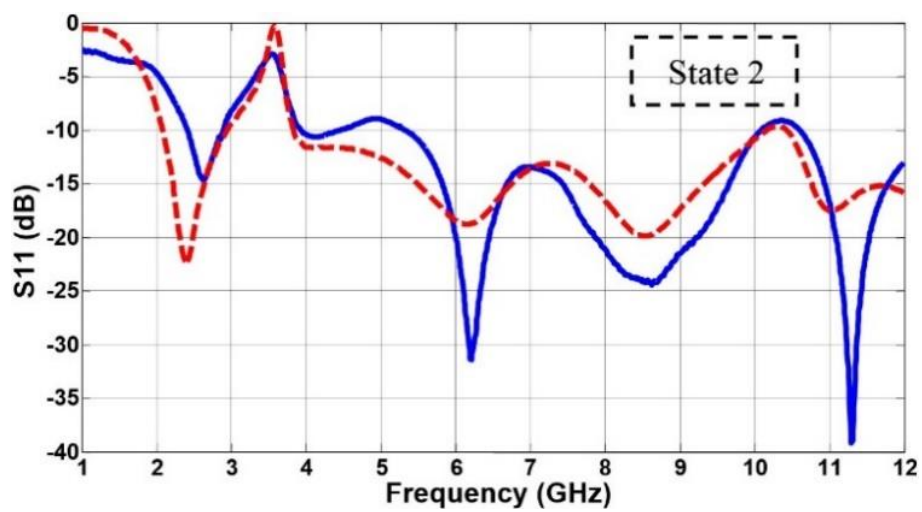
The results demonstrate that the proposed antenna can successfully block the WLAN bands (2.4-2.464 GHz, 5.155.825 GHz), and WiMAX band (3.3 - 3.8 GHz) while maintaining a good impedance matching for the rest of the band from 2.1 to 12 GHz for $|S_{11}| < -10$ dB. It also indicates that the band-notched frequency is controllable by electronically changing the condition of the switches on the radiator.

Table 5-2 Switch combinations and operational frequency bands for each state

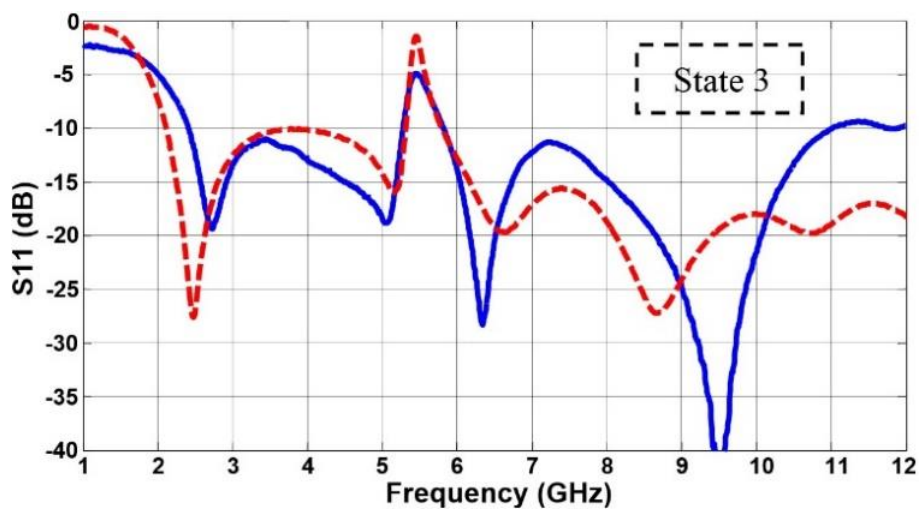
Switches	S1	S2	S3	Frequency Bands (GHz)
State 1	OFF	ON	OFF	2.31-2.72 Rejected
State 2	ON	ON	OFF	2.87-3.83 Rejected
State 3	ON	OFF	ON	5.25-5.81 Rejected
State 4	ON	OFF	OFF	2.94-3.68 & 5.33-5.84 Rejected
State 5	ON	ON	ON	2.1-12
State 6	OFF	ON	ON	2.1-12
State 7	OFF	OFF	ON	2.86-4.8 & 8.48-8.79 Rejected
State 8	OFF	OFF	OFF	3.12-5.31 & 8.2-8.42 Rejected



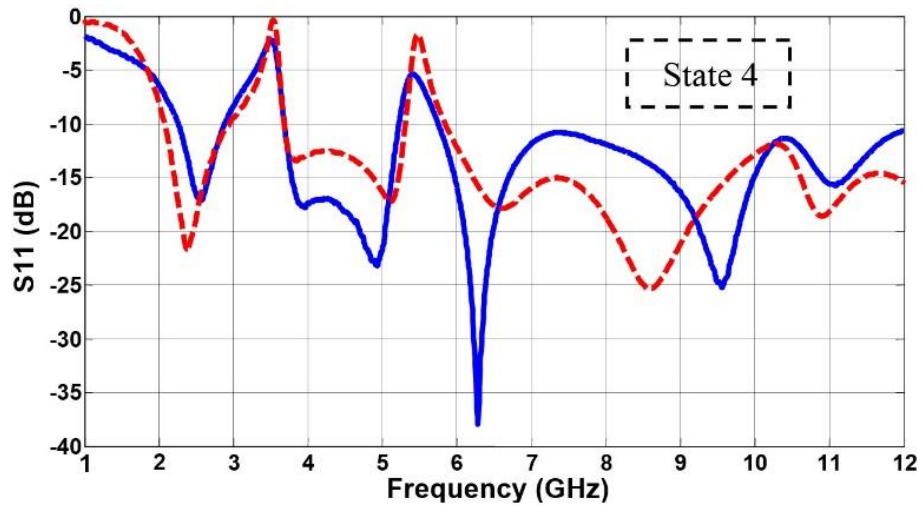
(a) State 1



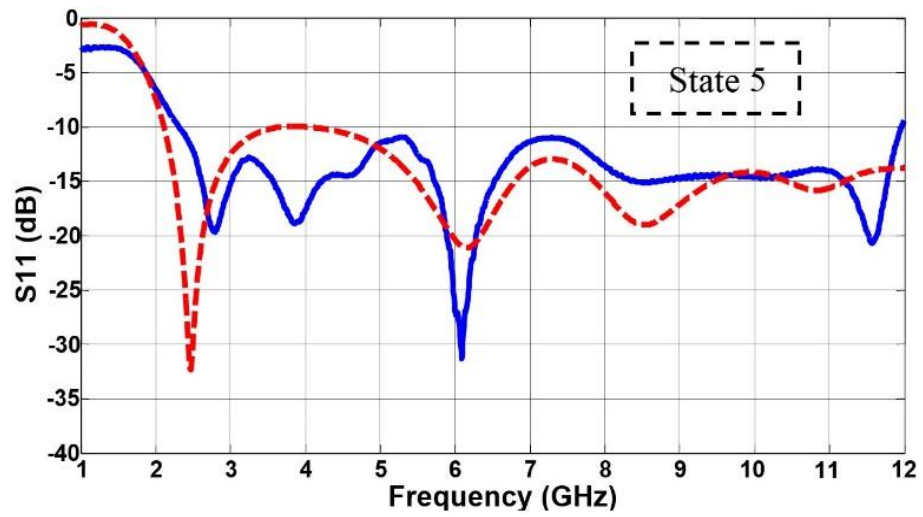
(b) State 2



(c) State 3



(d) State 4



(e) State 5

--- Simulated — Measured

Fig. 5.9 Simulated and measured reflection coefficients $|S_{11}|$ of the proposed antenna for switching States 1-5

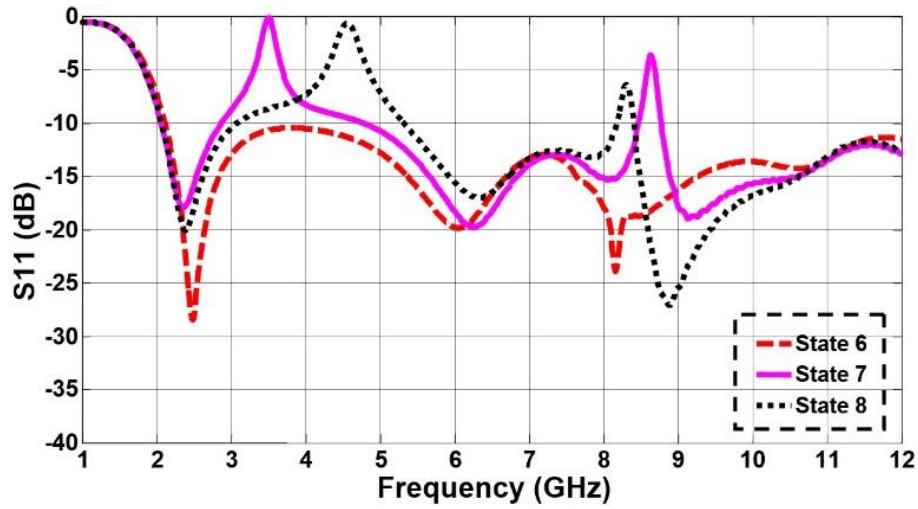
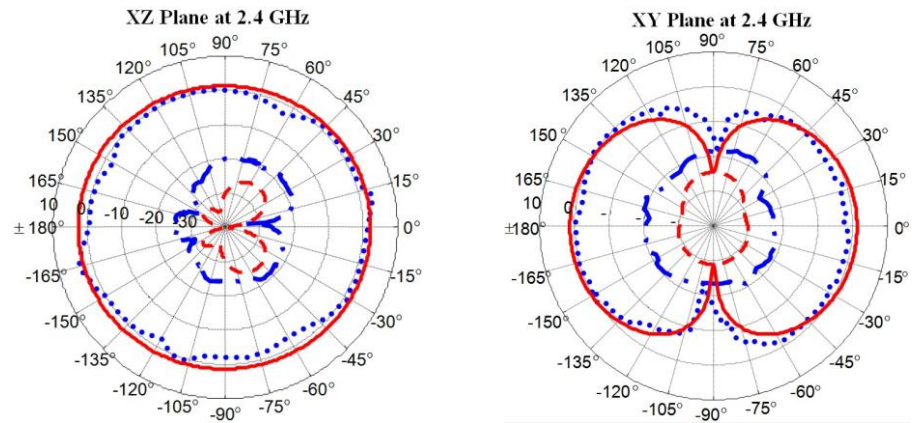


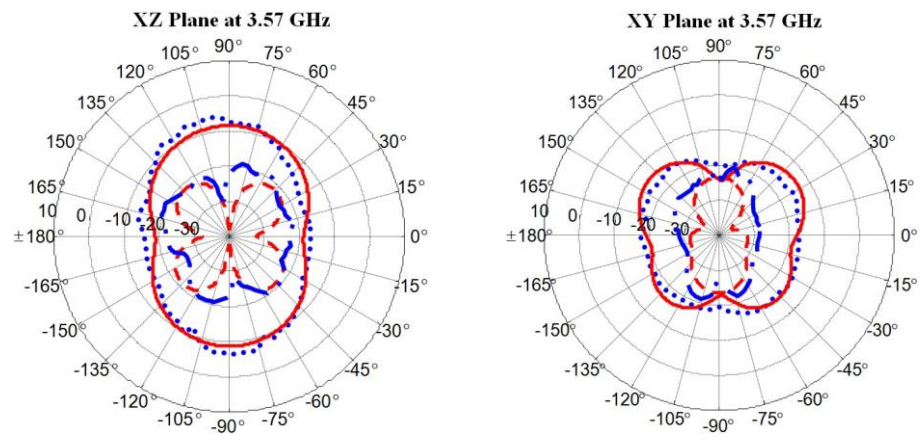
Fig. 5.10 Simulated reflection coefficients $|S_{11}|$ of the proposed antenna for switching States 6-8

5.5.1.2 Radiation Patterns

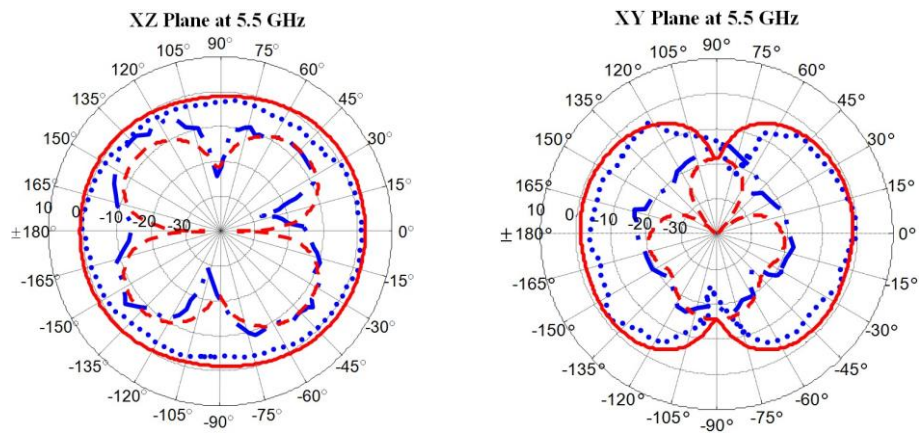
The simulated and measured radiation patterns of the propose antenna in the H-plane (XZ-plane) and E-plane (XY-plane) in two operation states (States 2 and 5) at the frequencies of 2.4, 3.57, 5.5 and 8.5 GHz are shown in Fig. 5.11. As observed, a good agreement is demonstrated between the results. It can be seen that the embedded CSRR structure has little effect on the radiation performances for Sate 5 (UWB state). Nearly omni-directional patterns are observed in the XZ-plane and the XY-plane, at the frequencies of 2.4, 5.5 and 8.5 GHz, there are two nulls in the y-direction, the same as a typical planar monopole antenna as shown in Figs. 5.11(a), 5.11(c) and 5.11(d), respectively. For the band-notched structure (State 2) at 3.57 GHz, the radiated field is significantly degraded as shown in Fig. 5.11(b).



(a)



(b)



(c)

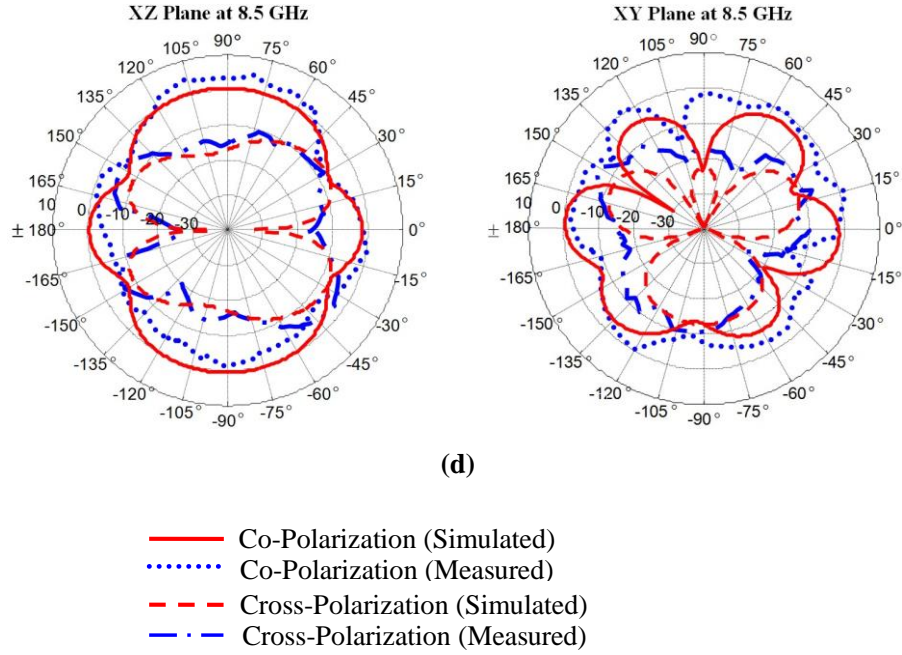


Fig. 5.11 Simulated co-polarization (red solid line) and cross-polarization (red break line), and measured co-polarization (blue dot line) and cross-polarization (blue dot break line) radiation patterns of the proposed antenna at (a) 2.4 GHz (State 5), (b) 3.57 GHz, (c) 5.5 GHz, and (d) 8.5 GHz

5.5.1.3 Gains

The measured gain values of the proposed antenna for five different switching States (1-5) are shown in Fig. 5.12. The measurement was conducted in an anechoic chamber using the reference antenna method. As expected, the antenna shows a gain from 1.8 to 5.8 dBi throughout the operation band (2.1 to 12 GHz) for State 5. For other switching States (1-4), the gain drastically decreases at the notched bands, and the measured gain suppression of 15, 9.5, 7.5, 9 and 7 dB are observed at frequencies of 2.45 GHz, 3.57 GHz, 5.45 GHz, 3.55 and 5.46 GHz, respectively. Fig. 5.13 shows the simulated total efficiency of the proposed antenna. It can be found that a relatively constant efficiency of the antenna is observed for State 5, from 95% to 80%. However, for switching States (1-4), the corresponding total efficiencies are substantially reduced to

3.4%, 4.6%, 21.7%, 4% and 23.5%, respectively. The results further demonstrate that the proposed antenna has effectively generated the band-notched characteristics in a reconfigurable way.

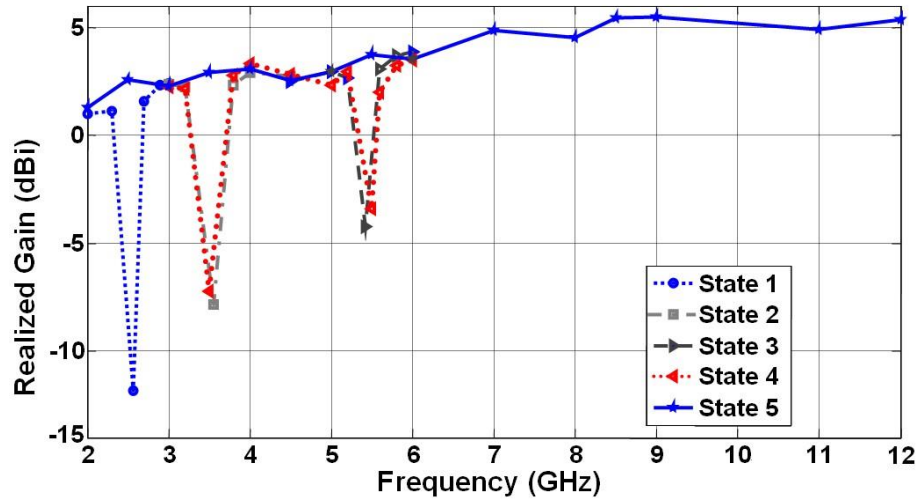


Fig. 5.12 Measured gains of the proposed antenna for five different switching states

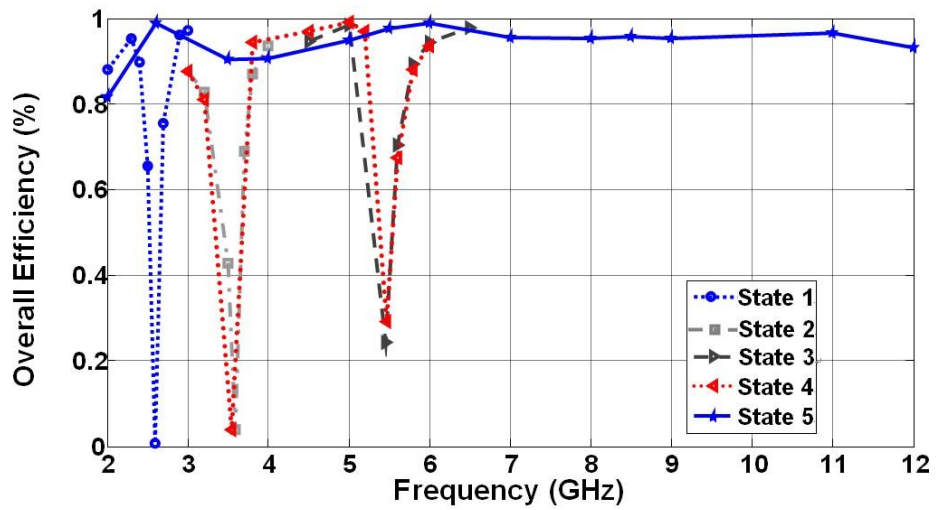


Fig. 5.13 Simulated overall/total efficiency of the antenna for five different switching states

5.5.2 Time-Domain Performance

The impulse responses of the UWB antenna for different switching States (4 and 5) are investigated and shown in Figs. 5.14 and 5.15. The simulation setup is the same as described in Section 4.4.2. From the figures, it can be seen that the amplitudes of the received signals are slightly higher in the face to face case compared to those in the side by side case. In addition, the impulse responses of the antenna for switching State 5 (UWB band) are also a little larger than State 4 (two rejection bands) in the same case. Furthermore, the late distortion) and lower power are observed in the received signals for the antenna in State 4, this is due to the existence of the notches in the frequency domain of the antenna.

To evaluate the similarity between the transmitted and received impulses, the fidelity factors F (as defined in Equation (4.4)) are calculated and shown in Table 5-3. It can be seen that the fidelity is slightly larger in the face to face than side by side case. As expected, the antenna for switching State 5 has the fidelity of more than 0.955. The results also show that the antenna has the fidelity of more than 0.829 for switching State 4. This further demonstrates that the introduction of band-notched features has limited effect on the time-domain performance of the antenna.

Table 5-3 Calculated fidelity factor of the UWB antenna for switching States 4 and 5

Cases	UWB Antenna for Switching State 4	UWB Antenna for Switching State 5
Face-to-Face	0.850	0.970
Side-by-Side	0.829	0.955

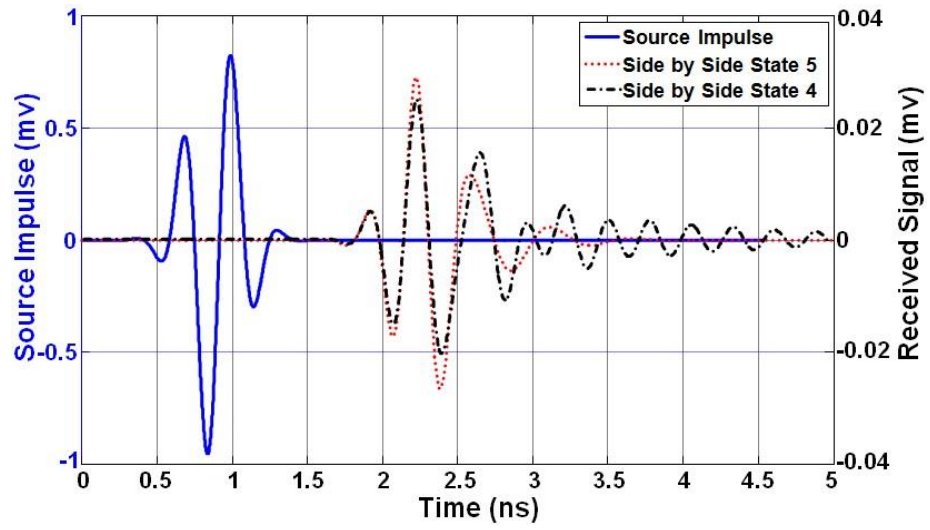


Fig. 5.14 Simulated signals of the antenna with single impulse input signal for switching States 4 and 5 in the side by side case

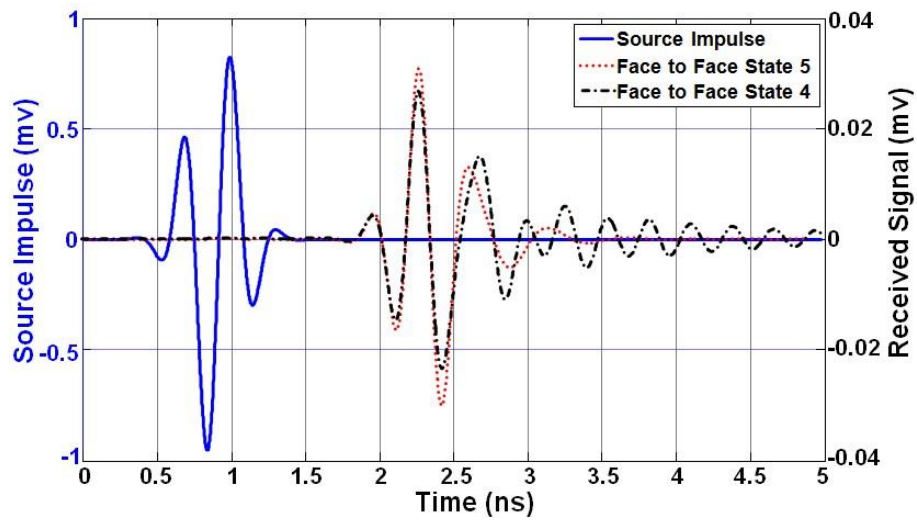


Fig. 5.15 Simulated signals of the antenna with single impulse input signal for switching States 4 and 5 in the face to face case

5.6 Summary

In this Chapter, a new planar monopole antenna with reconfigurable band-notched characteristics has been proposed for UWB applications. The band rejection has realised by incorporating two CSRR structures on the radiator element. To achieve the reconfigurability, the switches have added to the CSRR structures. The simulated and measured results have shown that the antenna is able to operate from 2.1 to 12 GHz for $|S_{11}| < -10$ dB for different switching states including a UWB state (2.1-12 GHz), three narrower band-notched states (2.31-2.72 GHz, 2.87-3.83 GHz and 5.25-5.81 GHz), and a dual band-notched state (2.94-3.68 and 5.33-5.84 GHz), with good levels of rejection. Furthermore, the surface current distributions and transmission line modes have been used to analyse the effect of the added resonating structures. Good radiation patterns and gain values have also been measured for different switching states. In addition, the proposed antenna has achieved a good time-domain performance, i.e. the fidelity of more than 0.829 for switching State 4 (with dual band-notches). This compact wideband antenna can be a very good candidate for a wide range of mobile portable applications from 2.1 to 12 GHz.

5.7 References

- [1] J. B. Pendry, A. J. Holden, D. J. Robbins, and W. J. Stewart, "Magnetism from conductors and enhanced nonlinear phenomena," *IEEE Transactions on Microwave Theory and Techniques*, vol. 47, pp. 2075-2084, 1999.
- [2] J. Kim, et al., "5.2 GHz notched ultra-wideband antenna using slot-type SRR," *Electronics Letters*, vol. 42, pp. 315-316, 2006.

- [3] L. Li, Z. L. Zhou, J. S. Hong, and B. Z. Wang, "Compact dual-band-notched UWB planar monopole antenna with modified SRR," *Electronics Letters*, vol. 47, pp. 950-951, 2011.
- [4] J. D. Baena, J. Bonache, F. Martin, R. Marques, F. Falcone, T. Lopetegi, M. A. G. Laso, J. G. Garcia, I. Gil, M. F. Portillo, and M. Sorolla, "Equivalent-circuit models for split-ring resonators and complementary split-ring resonators coupled to planar transmission lines," *IEEE Transaction on Microwave Theory and Techniques*, vol. 53, no. 4, pp. 1451-1461, 2005.
- [5] W. Wang., S. Gong, Z. Cui, J. Liu, and J. Ling, "Dual band-notched ultra-wideband antenna with co-directional SRR," *Microwave and Optical Technology Letters*, vol. 51, no. 4, pp.1032-1034, 2009.
- [6] L. H. Lai, Z. Y. Lei, Y. J. Xie, G. L. Ning, and K. Yang, "UWB antenna with dual band rejection for WLAN/WIMAX bands using CSRRs," *Progress in Electromagnetics Research Letters*, vol. 26, pp. 69-78, 2011.
- [7] L. Wang-Sang, K. Dong-Zo, K. Ki-Jin, and Y. Jong-Won, "Wideband planar monopole antennas with dual band-notched characteristics," *IEEE Transactions on Microwave Theory and Techniques*, vol. 54, pp. 2800-2806, 2006.
- [8] S. Nikolaou, N. D. Kingsley, G. E. Ponchak, J. Papapolymerou, and M. M. Tentzeris, "UWB elliptical monopoles with a reconfigurable band notch using MEMS switches actuated without bias lines," *IEEE Trans. on Antennas and Propagation*, vol. 57, pp. 2242-2251, 2009.

CHAPTER 6 DESIGN OF A UWB-MIMO ANTENNA FOR WIRELESS APPLICATIONS

6.1 Introduction

Due to the advantages of combination of MIMO and UWB technologies, this may extend the communication range as well as offer higher reliability. In this Chapter, a compact UWB-MIMO antenna for wireless applications is presented. A novel isolation technique is firstly introduced and implemented to reduce the mutual coupling between two antenna elements. The size of the proposed antenna is about 30% smaller than one reported in literature [106], where similar performance is achieved by both antennas.

In addition, the effect of the technique (slots) on the impedance matching and isolation of the antenna is also studied extensively for optimising the geometry. The performances of the antenna in terms of the frequency-domain

and MIMO characteristics are also investigated both numerically and experimentally.

The simulation results presented in this Chapter were performed using CST Microwave Studio.

6.2 UWB-MIMO Antenna

6.2.1 Antenna Configuration

Fig. 6.1 illustrates the geometry of the initial design of the UWB-MIMO antenna. The antenna (referred to as Antenna 1 in this thesis) is fabricated on an inexpensive FR4 substrate with a thickness of 1.5 mm and relative permittivity of 4.3. The Mickey-mouse shaped radiator is adopted due to its excellent performance, which is the same as that in Fig. 3.7. The radiator is fed by a microstrip line of the characteristic impedance of 50-ohm, the length of the feedline is denoted as L_f and its width (W_f) is fixed at 2.8 mm. The distance between the two identical radiators (centre to centre) is denoted as W_d . A shared partially truncated ground plane is implemented and placed on the back side of the substrate, which ensures a good impedance matching over a broad frequency range. The overall size of the substrate is $L_{sub} \times W_{sub}$.

The wide impedance bandwidth characteristics of a single element of Antenna 1 can be realized by implementing a Mickey-mouse shaped radiator as discussed in previous chapters [1]. The parameters of Antenna 1 are optimised in terms of the reflection coefficient through a parametric study and determined as follows: $W_{sub} = 60$ mm, $L_{sub} = 45$ mm, $L_{gnd} = 19.7$ mm, $L_f = 21.4$ mm, $L_r = 18$ mm, $W = 4$ mm, $L = 2$ mm, $R = 10$ mm. The simulated and measured S parameters $|S_{11}|$ and $|S_{21}|$ of Antenna 1 are displayed in Figs. 6.2(a) and 6.2(b), respectively. They are in a reasonable agreement while the difference between

them around 2.1 GHz is mainly due to the cable effects in the measurement. An important feature is that this antenna can operate from 2.1 to 10.6 GHz (including ISM 2.45 GHz and UWB bands) for $|S_{11}|$ and $|S_{21}| < -10$ dB. However the isolation is very close to -10 dB at lower frequencies (due to the electrically smaller separation) which is not good enough for many applications - normally over 15 dB isolation is required, thus further improvements are needed. It is worth mentioning that $|S_{22}|$ and $|S_{12}|$ are not presented here since they are the same as $|S_{11}|$ and $|S_{21}|$ due to the symmetric geometry of the antenna.

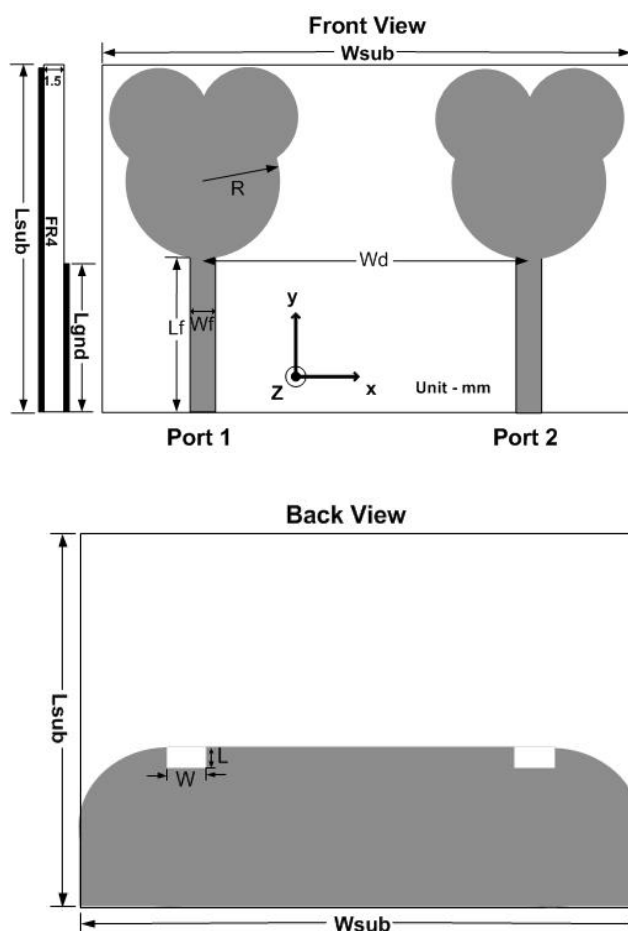
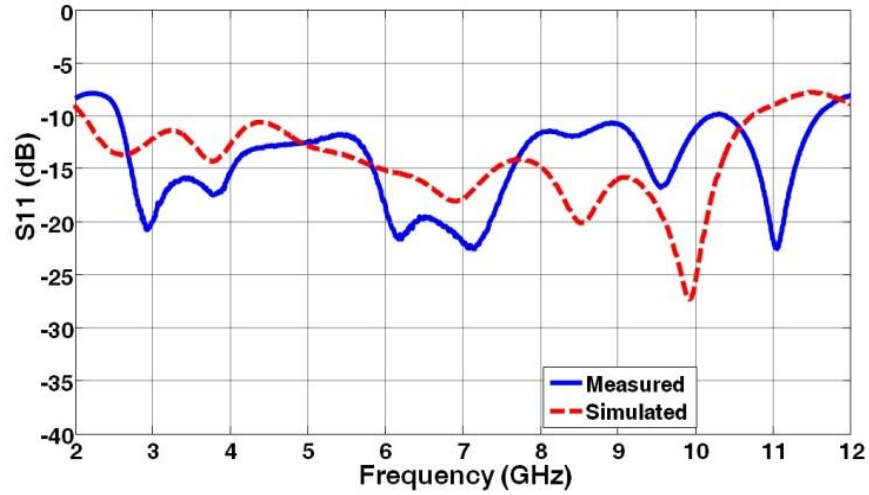
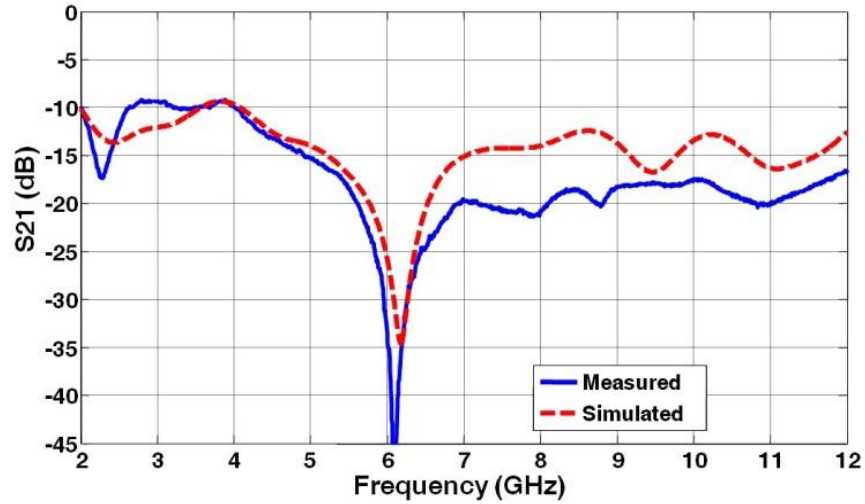


Fig. 6.1 Geometry of a UWB-MIMO monopole antenna (Antenna 1): Front view (up) and Back view (down)



(a) S11



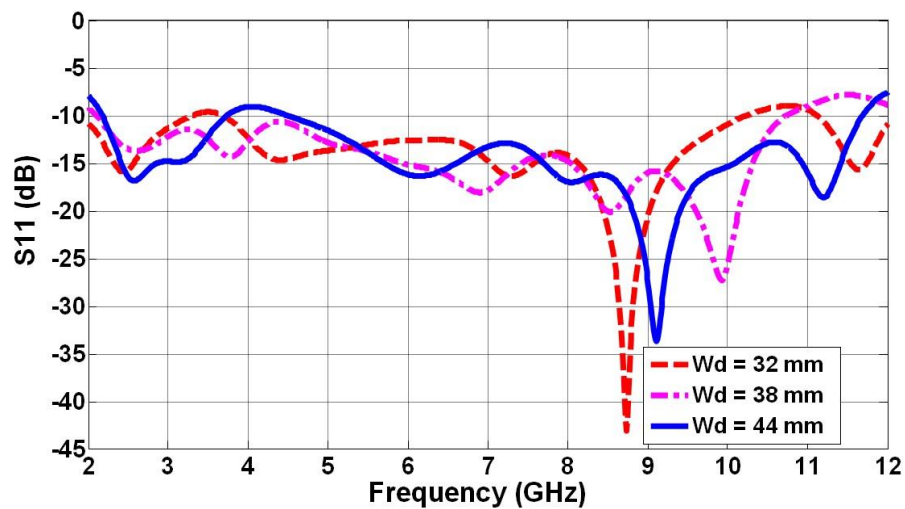
(b) S21

Fig. 6.2 Simulated and measured S parameters of Antenna 1 (without slots)

6.2.2 Effects of the Distance between Two Elements

From the simulated results, it can be found that the separation W_d of the two ports/elements is a critical parameter for achieving a good impedance matching and isolation. The simulated reflection coefficients $|S_{11}|$ and the mutual coupling coefficients $|S_{21}|$ with different values of W_d (from 32 to 44 mm) are obtained and shown in Figs. 6.3(a) and 6.3(b), respectively. From Fig.

6.3(a), it can be observed that the -10 dB $|S_{11}|$ bandwidth is sensitive to the separation of the two antenna elements. The impedance matching becomes worse (larger S_{11}) at lower frequencies around 4 GHz when the W_d is either too large or too small. When W_d is chosen to be 38 mm, a resonance around 4 GHz is generated, which extends the lowest frequency to 2.3 GHz. Nevertheless the effects on the mutual coupling coefficients $|S_{21}|$ are relatively small as shown in Fig. 6.3(b). It can be seen that the smaller coupling is achieved with the larger separation (W_d is 44 mm) over a UWB, however it cannot satisfy the requirement for UWB operation and maintaining a small overall size for MIMO antenna.



(a) S_{11}

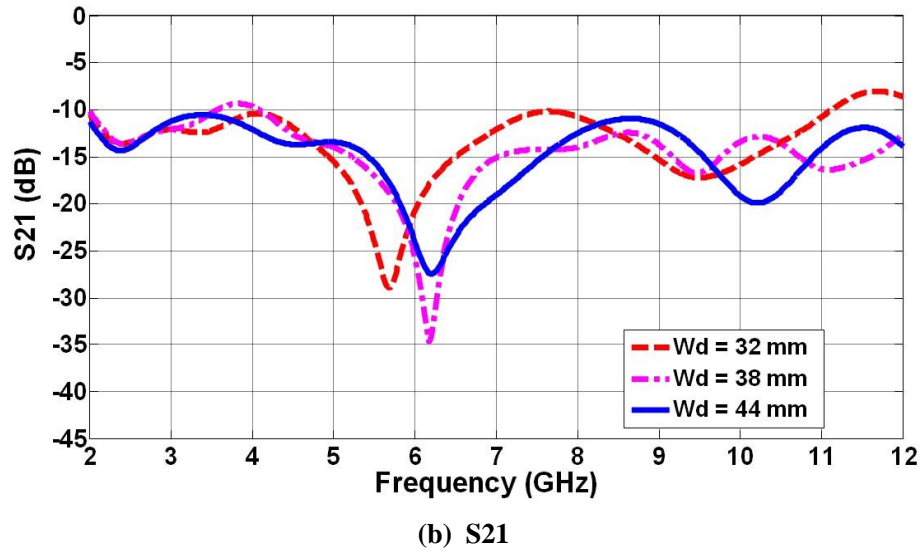


Fig. 6.3 Simulated S21 of Antenna 1 with different Wd values

6.2.3 Current Distribution

To better understand how the two ports/elements of the antenna are linked to each other, the current distributions of Antenna 1 are investigated. The simulated current distributions of Antenna 1 at the frequencies of 3.1 and 10.6 GHz are shown in Figs. 6.4(a) and 6.4(b), respectively. When Port 1 is excited, Port 2 is terminated with a $50\ \Omega$ load. It can be seen that the surface current in the excited radiator Port 1 induces currents in the second radiator at all frequencies through the common ground plane. This introduces a strong mutual coupling between the two closely antenna elements and it agrees well with other investigations reported in such as [2-3] and it has actually become a common knowledge now. For MIMO antennas to work well, they should be independent with little coupling, thus a better isolation is needed. A simple and effective approach is to work on the common ground plane to limit the current flow from one port to the other, ultimately to reduce mutual coupling between the two ports.

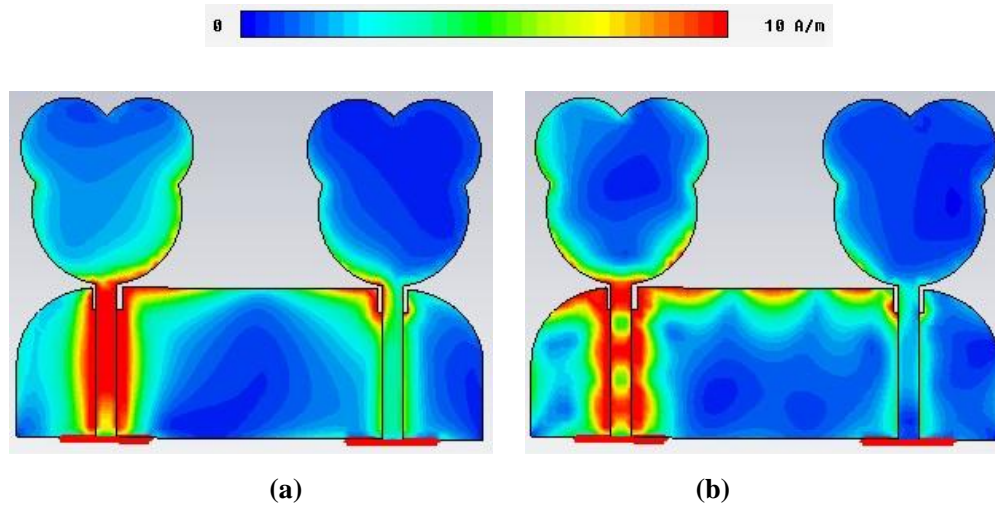


Fig. 6.4 Simulated current distributions of Antenna 1 at: (a) 3.1, and (b) 10.6 GHz.
Port 1 is excited; Port 2 is terminated with a 50 Ω load

6.3 Mutual Coupling Reduction

6.3.1 Trident-Like Slot Configuration

For both diversity and MIMO applications, it is crucial to reduce the mutual coupling between any two antennas elements while still maintaining a good impedance matching over the band of interest. In order to further reduce the mutual coupling between the ports of Antenna 1, a new trident-like slot is introduced and etched on the common ground plane. Fig. 6.5 shows the geometry of the modified UWB-MIMO antenna with the trident-like slot on the ground plane (denoted as Antenna 2).

The trident-like slot is modified based on the isolation techniques described in [4] and [5]. It is formed by a pair of the quarter-wavelength slot (Slot 1) and two inverted L-shaped slots (Slot 2), i.e. symmetrically placed with respect to Slot 1. The design principle is by implementing a structure to provide filtering

properties to eliminate the original coupling current. Consequently, the mutual coupling between two elements can be weakened. The parameters of the trident-like slot are optimised through a parametric study. The resultant parameters are: $L1 = 7$ mm, $L2 = 12$ mm, $L3 = 1$ mm, $W1 = 0.8$ mm, $W2 = 2$ mm and $W3 = 0.8$ mm.

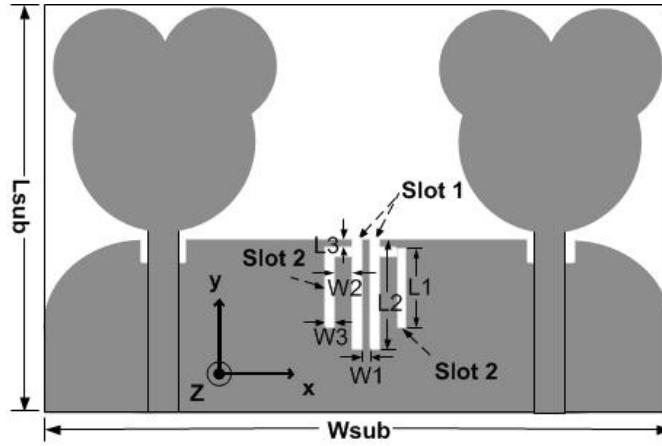
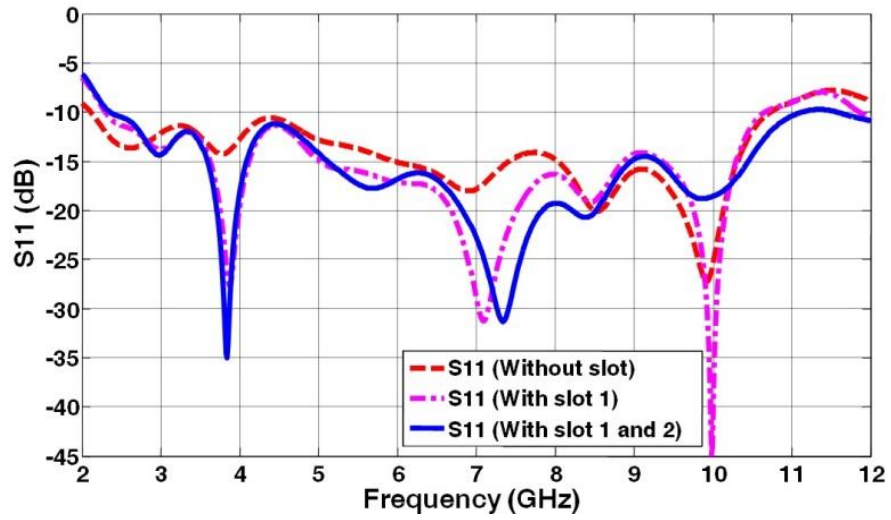


Fig. 6.5 Geometry of the modified UWB-MIMO monopole antenna with the trident-like slot (Antenna 2)

6.3.2 Effectiveness of the Trident-like Slot on its Performance

To evaluate the effectiveness of the trident-slot, the simulated reflection coefficient $|S_{11}|$ and mutual coupling coefficient $|S_{21}|$ of the proposed antenna with and without the slots obtained and are shown in Figs. 6.6(a) and 6.6(b), respectively. Fig. 6.6(a) shows that with the introduction of Slot 1 alone or Slots 1 and 2, the effect on the impedance bandwidth for $|S_{11}|$ is mainly at the lower frequencies, while a better matching can be obtained at the higher frequencies around 11 GHz, nevertheless the overall effects are relatively small.

However, the mutual coupling coefficient $|S_{21}|$ is now significantly improved and is less than -15 dB over the UWB band. Fig. 6.6(b) shows that the -15 dB $|S_{21}|$ bandwidth is about 4 GHz (4-8 GHz) for the case using Slot 1 and 9.2 GHz (2.3-11.5 GHz) for the case using both Slots 1 and 2, while the case without using any slot, it is 1.8 GHz (2.2-4 GHz). It indicates that more than 15 dB isolation is successfully achieved across the operating frequency band of 2.3-12 GHz in the case of using Slots 1 and 2.



(a) S11

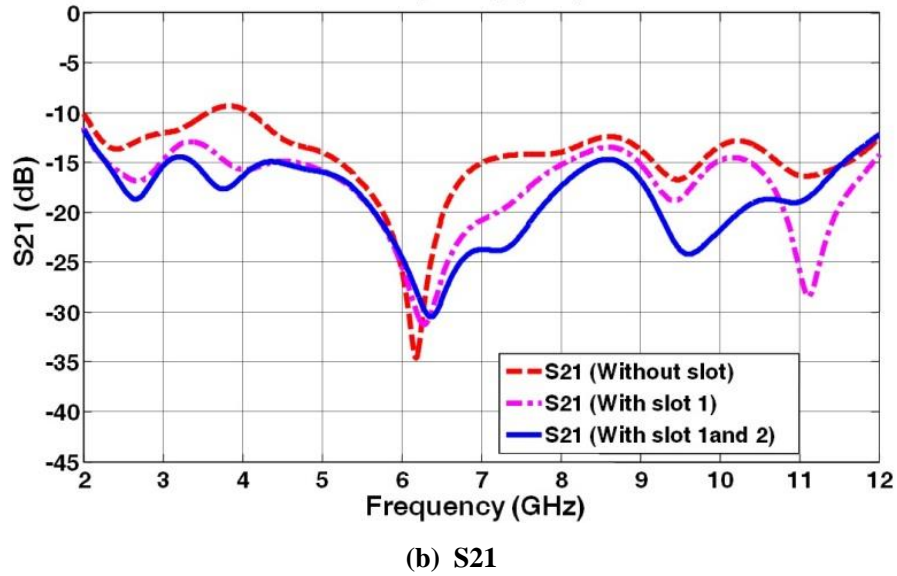


Fig. 6.6 Simulated S parameters of Antenna 2

6.4 Theoretical Analysis

6.4.1 Current Distribution

To further understand the effect of the embedded trident-like slot, the simulated current distribution of the UWB-MIMO antenna with the trident-like slots at the frequencies of 3.1 and 10.6 GHz are illustrated in Figs. 6.7(a) and 6.7(b), respectively. When Port 1 is excited, Port 2 is terminated with a $50\ \Omega$ load, it can be seen that the current from Port 1 is trapped in the slot and cannot flow to Port 2 through the common ground plane at all these frequencies. Since the radiators are of symmetrical geometry, the effect is the same when Port 2 is excited and Port 1 is terminated with a $50\ \Omega$ load. This confirms that the trident-like slot can efficiently enhance the isolation between the two ports/elements. Note that Fig. 6.7 only shows the snap shots of the continuously changing current distributions.

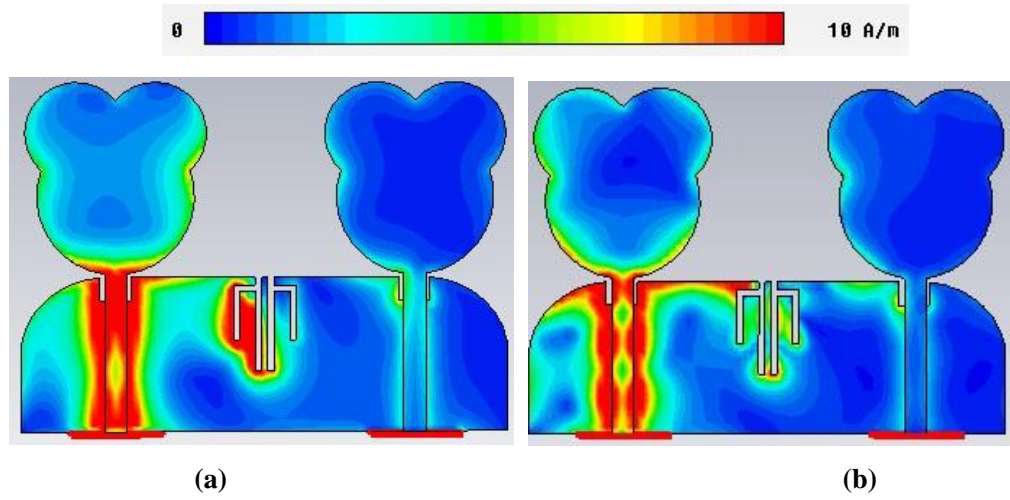


Fig. 6.7 Simulated surface current distributions of Antenna 2 with at the frequencies of: (a) 3.1 GHz, (b) 10.6 GHz.

6.4.2 Equivalent Circuit

As stated in previous section, the isolation between the two closed-placed ports/elements is achieved by inserting a trident-like slot on the ground plane to stop the current flow between the two ports. To better understand how the isolation is improved by this modification on the ground plane, an approximate equivalent circuit is derived based on the degenerated foster canonical form [6]. In a complete Foster canonical form, higher order modes can be represented by a series of parallel RCL components.

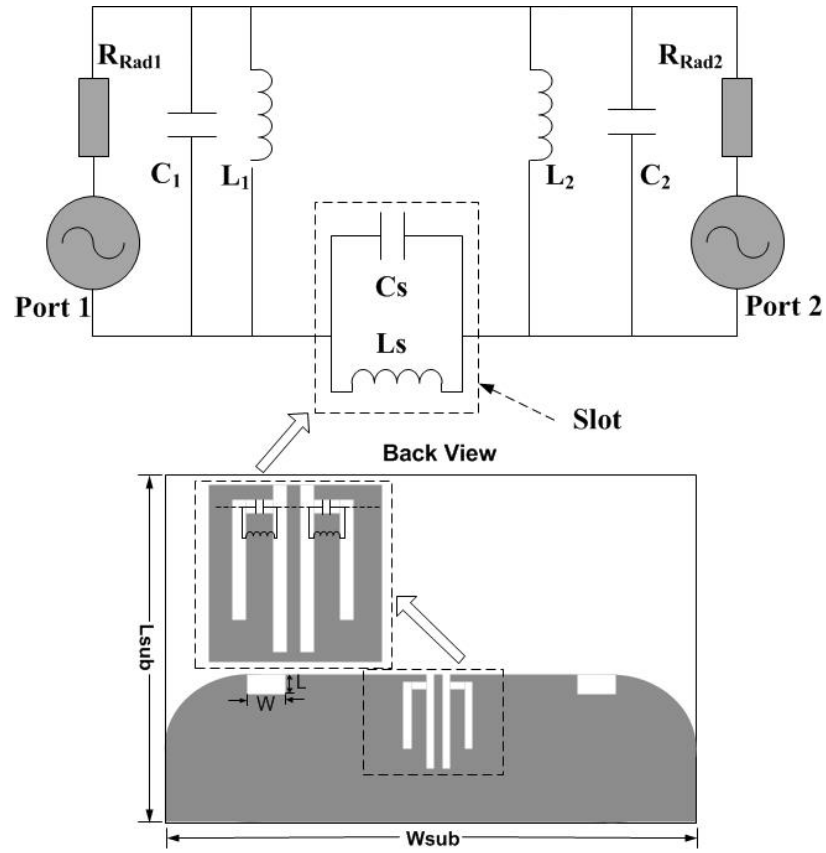


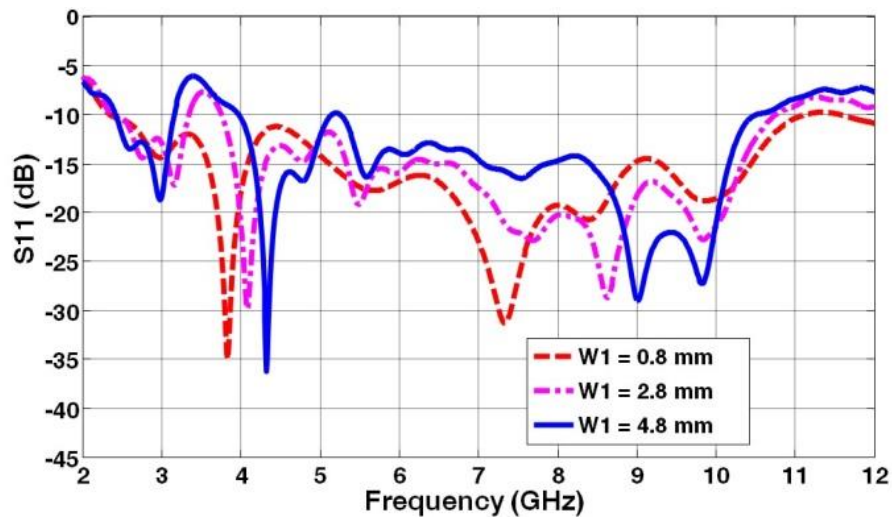
Fig. 6.8 The approximate equivalent circuit of Antenna 2

After the trident-like slot is inserted on the ground plane, anti-resonance is introduced to the equivalent circuit of Antenna 1 as a two-port network containing parallel LC circuits with an inductance L_s and a capacitance C_s . Thus the approximated equivalent circuit of Antenna 2 is formed and shown in Fig. 6.8. The slots on the ground plane act as capacitor and the gaps between the slots behave like inductors. In fact, the capacitance value C_s can be increased by reducing the slot width or increasing the slot length. To further understand this concept, the parameters of the trident-like slot are studied in the next section.

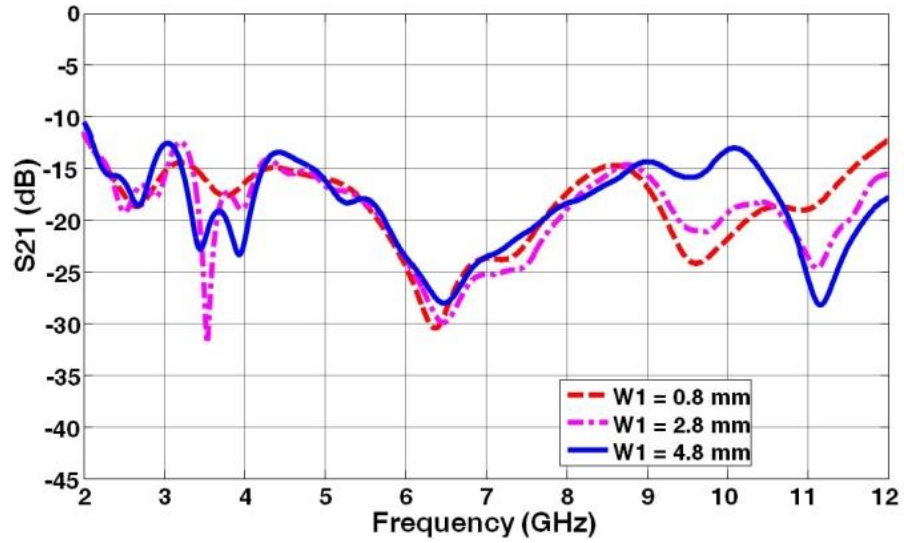
6.4.3 Parametric Study

From above investigations, it can be seen that the embedded trident-like slot on the ground plane is a very effective on improving the isolation of the two antenna elements. To further understand the decoupling mechanism, a parametric study is carried out to analyse the effect of some major parameters. The study is based on the antenna geometry given in Fig. 6.5. The results from the parametric study are illustrated in Fig. 6.9 to Fig. 6.12.

Firstly, the width $W1$ is varied from 0.8 to 4.8 mm while the other parameters are not changed. Its effects on the S parameters $|S_{11}|$ and $|S_{21}|$ are shown in Fig. 6.9. It can be clearly seen that increasing the width $W1$ from 0.8-4.8 mm, both $|S_{11}|$ and $|S_{21}|$ are affected significantly; i.e. the impedance bandwidth for $|S_{11}| < -10$ dB is reduced from 2.3-12 GHz to 4-10.5 GHz and the decoupling bandwidth for $|S_{21}| < -15$ dB is reduced from 2.3-11.5 GHz to 5-4 GHz, as shown in Figs. 6.9(a) and 6.9(b), respectively. The major impact seems to be at lower frequencies (around 3.5 GHz), especially on S_{11} , this is understandable since the electrical length of the ground plane is small.



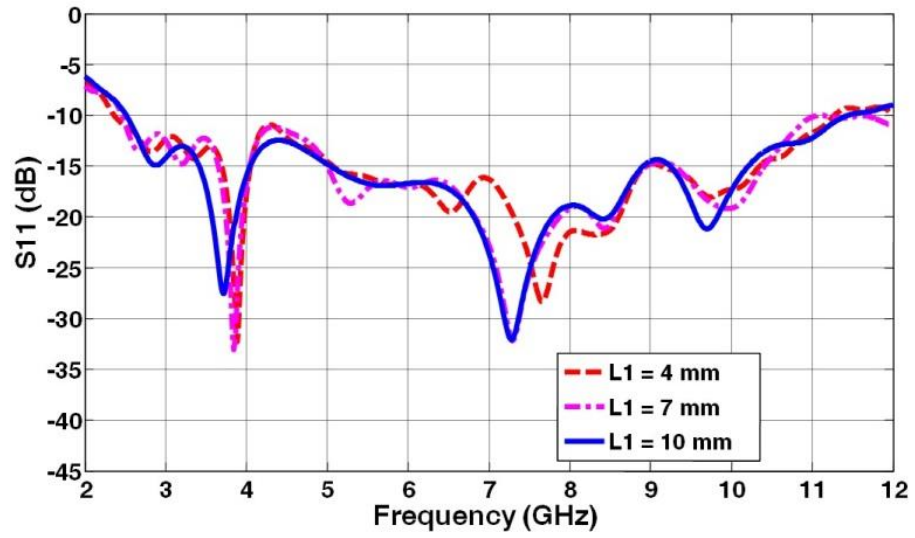
(a) S_{11}



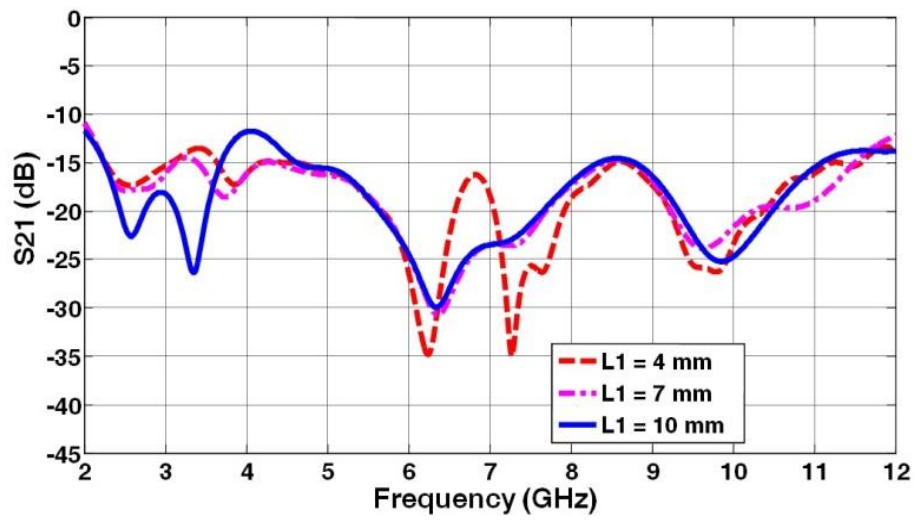
(b) S21

Fig. 6.9 Simulated S parameters of Antenna 2 for different W1 values

Secondly, the effect of the parameter L1, which determines the length of Slot 1 on Antenna 2 is investigated. When the length L1 is increased from 4 to 10 mm, the decoupling slot becomes longer; this has little impact on the impedance bandwidth for $|S_{11}| < -10$ dB, as shown in Fig. 6.10(a). However, the -15 dB $|S_{21}|$ bandwidth of the two ports/elements is affected when the length L1 is either too long or too short, as shown in Fig. 6.10(b). Overall, L1 has limited effects the antenna performance.



(a) S_{11}



(b) S_{21}

Fig. 6.10 Simulated S parameters of Antenna 2 for different $L1$ values

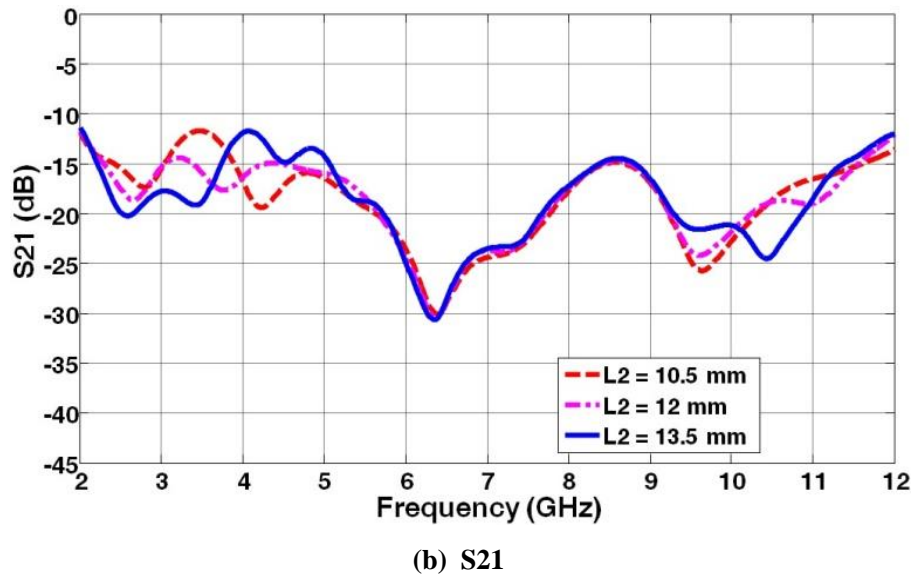
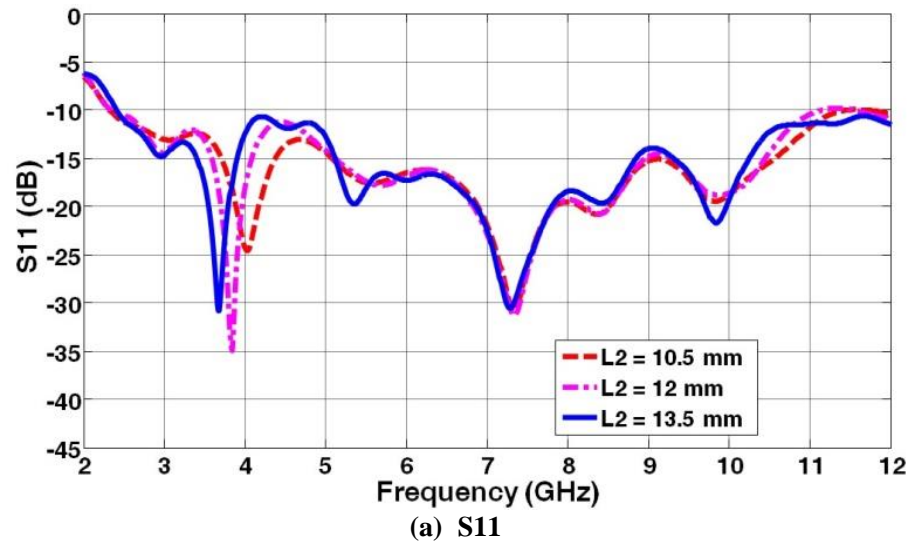
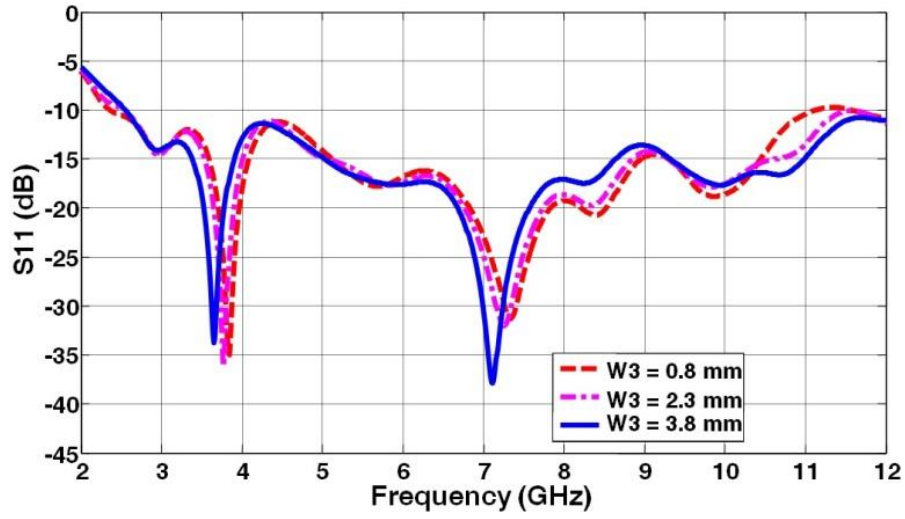
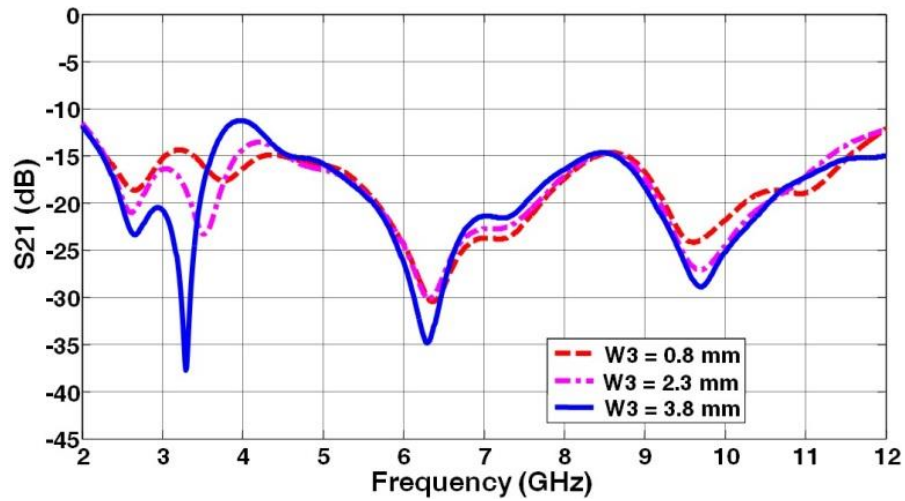


Fig. 6.11 Simulated S parameters of Antenna 2 for different L_2 values



(a) S11



(b) S21

Fig. 6.12 Simulated S parameters of Antenna 2 for different W3 values

Finally, the effects of all other parameters of the slots are investigated. Similar performances can also be observed when the length of Slot 1 L_2 and the width of slot W_3 are increased from 10.5 to 13.5 mm and 0.8 to 3.8 mm, as shown in Figs. 6.11 and 6.12, respectively. The effects of the slot parameters on the S parameters of Antenna 2 are summarized in Table 6-1. Their major effects are at the lower frequencies

Table 6-1 Summary of the effects of the slot parameters in mm on the S parameters of Antenna 2

Parameters (mm)		Bandwidth (GHz) (S11 < -10 dB)	Bandwidth (GHz) (S11 < -15 dB)
W1	0.8	2.3-11	2.3-11.5
	2.8	3.7-10.6	3.4-12
	4.8	4-10.5	4.9-8.9
L1	4	2.3-11.3	3.7-11.2
	7	2.3-11	2.3-11.6
	10	2.4-11.5	4.62-11
L2	10.5	2.3-12	3.90-11.7
	12	2.3-12	2.3-11.6
	13.5	2.3-12	5.1-11.3
W3	0.8	2.3-11.2	2.3-11.6
	2.3	2.5-12	4.6-11.3
	3.8	2.6-12	4.5-11.8

From above analysis, it can be found that the -10 dB |S11| bandwidth is less sensitive to the length and width of the slot compared to the -15 dB |S21| bandwidth. The optimum values of W1, L1, L2 and W3 are found to be 0.8, 7, 12 and 0.8 mm, respectively. The observed effects are mainly due to the change in the values of Cs and Ls as discussed in the previous section.

6.5 Measurement Results and Discussions

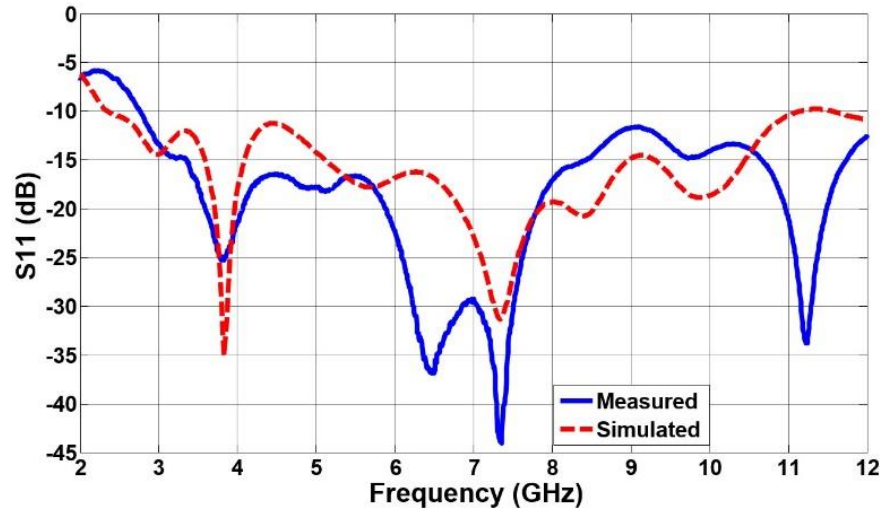
In this section, the performances of the proposed UWB-MIMO antenna (Antenna 2) are verified through the measurement. A prototype of Antenna 2 is fabricated as shown in Fig. 6.13.



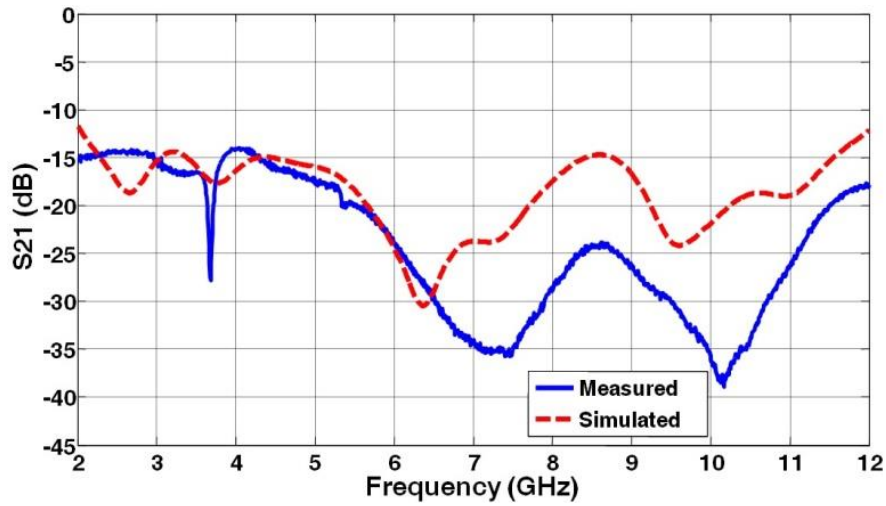
Fig. 6.13 Prototype of the proposed UWB-MIMO antenna (Antenna 2)

6.5.1 Reflection Coefficients

The simulated and measured results of $|S_{11}|$ and $|S_{21}|$ of Antenna 2 (with slots) are plotted in Fig. 6.14. A reasonable agreement is obtained between them while the discrepancies can be attributed to the connector and cable effects in the measurement which were not included in the simulation but presented in the measurements. It can be seen that Antenna 2 can operate from 2.3 to 12 GHz for $|S_{11}| < -10$ dB, as shown in Fig. 6.14(a). The bandwidth achieved can cover for a wide range of services including WiFi (2.4-2.5 GHz), WiMAX (2.5-2.7 GHz), LTE (2.5-2.7) and UWB (3.1-10.6 GHz). More importantly, the isolation of Antenna 2 is better than 15 dB over the UWB band, as shown in Fig. 6.14(b). It should be noted that mutual coupling coefficient $|S_{21}|$ of less than -15 dB is considered as a good isolation performance.



(a) S11



(b) S21

Fig. 6.14 Simulated and measured S parameters of Antenna 2

6.5.2 Radiation Characteristics

The measured radiation patterns of Antenna 2 in the H-plane (XZ-plane) and E-plane (XY-plane) at frequencies of 3.1, 5 and 8 GHz for two ports are shown in Figs. 6.15(a) to 6.15(c), respectively. In the measurement, Port 1 or 2 is excited, while Port 2 or 1 is terminated with a 50 Ω load, respectively. It can be demonstrated that the radiation patterns of the two ports/elements are mirror

transformations. As expected, the spacing diversity is achieved and the patterns are relatively stable across the operating band of Antenna 2

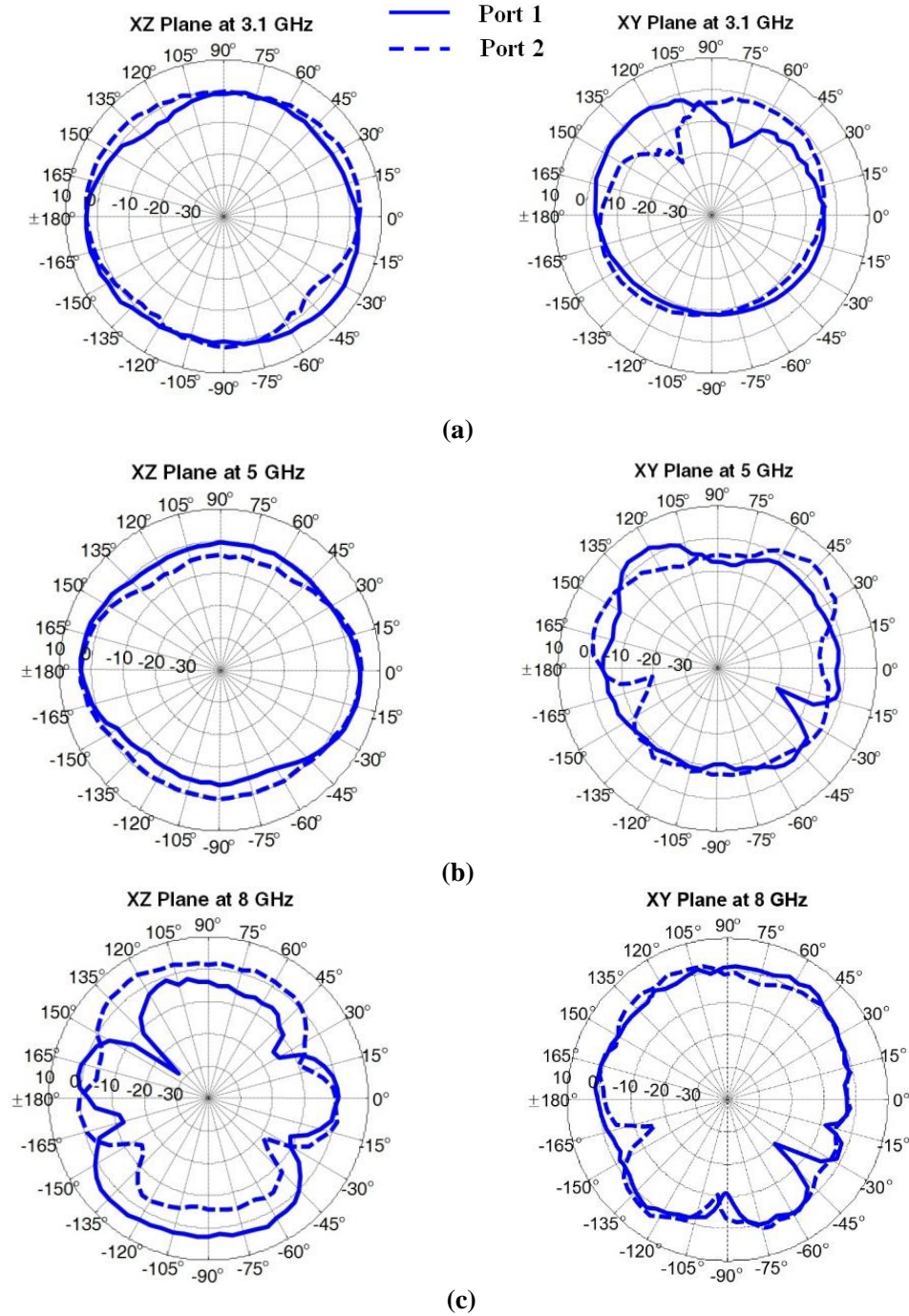


Fig. 6.15 Measured radiation patterns of Antenna 2 at the frequencies of 3.1 GHz, (b) 5 GHz, and (c) 8 GHz

Fig. 6.16 shows the simulated and measured gain values of Antenna 2 (with slot) compared to Antenna 1 (without slot). A reasonable agreement is demonstrated between the simulated and measured results while the reasons attributed to the differences are believed due to the cable loss and presence of the SMA connector in the measurement which was not considered in the simulation. As expected, the measured gains of Antenna 2 show a stable gain throughout the operation band (2.3 to 12 GHz) from 3.2 to 5.6 dBi and the variation of the gains is about 2.4 dB. In addition, the gain is reduced by an average of about 0.5 dB when the trident-like slot is implemented.

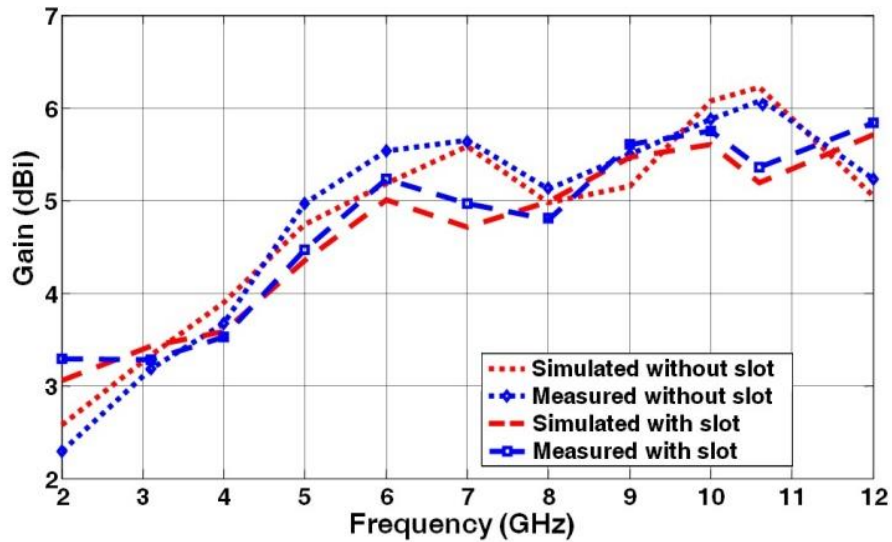


Fig. 6.16 Simulated and measured gains of the antenna with and without slot

6.5.3 MIMO Characteristics

The envelope correlation is a crucial parameter for evaluating the diversity performance of the antenna. In general, the envelop correlation coefficient of an antenna array can be computed by using the far-field radiation pattern [7] or scattering parameters from the antenna system [8] which is only suitable for antennas with little loss. In this thesis, the S-parameters method is utilised due to the complication of the 3D far-field measurement and the low loss of the

antenna. The envelope correlation coefficient is denoted as ρ_e and can be calculated by Equation (6.1) in [9].

$$\rho_e = \frac{|S_{11}^* S_{11} + S_{21}^* S_{22}|^2}{(1 - |S_{11}|^2 - |S_{21}|^2)(1 - |S_{22}|^2 - |S_{12}|^2)} \quad (6.1)$$

For the antenna diversity, the practically acceptable envelope correlation is less than 0.5. The variation of the envelope correlation coefficient across the desired frequency band is shown in Fig. 6.17. Both simulated and measured results are in reasonable agreement. It can be observed that the maximum value of the envelope correlation coefficient is less than 0.01 across the band of interest. This indicates that the proposed antenna has a good diversity performance.

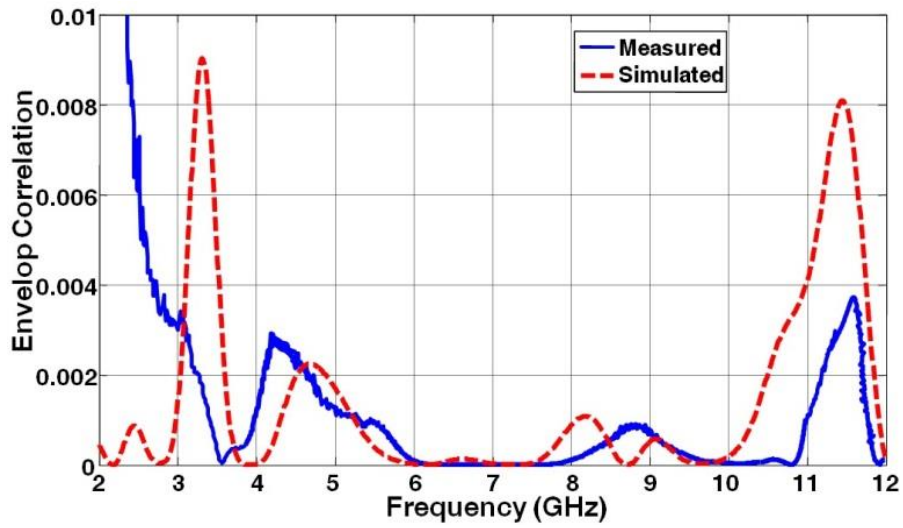


Fig. 6.17 Simulated and measured envelope correlation coefficient of Antenna 2

6.6 Summary

In this Chapter, a novel UWB-MIMO antenna has been proposed for wireless applications over the frequency band from 2.3 to 12 GHz. The size of the proposed antenna is 45 mm by 60 mm, about 30% smaller than the one reported in literature [106], where similar performance has achieved by both antennas. The wideband isolation between the two antenna elements has been achieved by etching a trident-like slot on the common ground plane over a wideband. The simulated and measured results have shown that the proposed antenna can operate from 2.3 to 12 GHz for $|S_{11}| < -10$ dB with the mutual coupling coefficient of less than -15 dB. In addition the current distributions have been investigated and an equivalent circuit have been introduced for analysis. A comprehensive parametric study has also been carried out to analyse the effect of the coupling element. Furthermore the antenna spacing diversity has been studied and a good diversity performance has obtained, i.e. an envelope correlation coefficient of less than 0.01 across the bands of interest. This indicates that the proposed UWB-MIMO antenna is a very good candidate for wireless applications.

6.7 References

- [1] P. Cao, Y. Huang, J. W. Zhang and R. Alrawashdeh, "A compact super wideband monopole antenna," in *7th European Conference on Antennas and Propagation (EuCAP)*, Sweden, pp. 3107-3110, 2013.
- [2] H. T. Chattha, Y. Huang, S. J. Boyes and Z. Xu, "Polarization and pattern diversity-based dual-feed planar inverted-F antenna," *IEEE Trans. on Antennas and Propagation*, vol. 60, pp. 1532-1539, 2012.

- [3] K.-L. Wong, S.-W. Su and Y. L. Kuo, "A printed ultra-wideband diversity monopole antenna," *Microwave and Optical Technology Letters*, vol. 38, pp. 257-259, 2003.
- [4] F. Jolani, A. M. Dadgarpour, and G. Dadashzadeh, "Reduction of mutual coupling between dual-element antennas with new PBG techniques," *13th International Symposium on Antenna Technology and Applied Electromagnetics and the Canadian Radio Science Meeting, ANTEM/URSI 2009*, pp. 1-4, 2009.
- [5] S. Zuo, Y.-Z. Yin, W. J. Wu, Z.-Y. Zhang, and J. Ma, "Investigations of reduction of mutual coupling between two planar monopoles using two $\lambda/4$ slots," *Progress in Electromagnetics Research Letters*, vol. 19, pp. 9-18, 2010.
- [6] B. T. Wang, A. M. Niknejad and R. W. Brodersen, "Circuit modeling methodology for UWB omni-directional small antennas," *IEEE Journal on Selected Areas in Comms*, vol. 24, pp.871-877, Apr. 2006.
- [7] M. A. Jensen and Y. R. Samii, "Performance analysis of antennas for hand-held transceivers using FDTD," *IEEE Trans. on Antennas and Propagation*, vol. 42, pp. 1106–1113, Aug. 1994.
- [8] S. Blanch, J. Romeu, and I. Cotbella, "Exact representation of antenna system diversity performance from input parameter description," *Electronics Letter.*, vol. 39, no. 9, pp. 705–707, May 2003.
- [9] I. Salonen, P. Vainikainen, "Estimation of signal correlation in antenna arrays," *Proceedings of 12th International Symp. on Antennas*, vol. 2, pp. 383-386, Nov. 2002.

CHAPTER 7 CONCLUSIONS AND FUTURE WORK

7.1 Summary

This thesis has described four inter-related research topics into “UWB Antennas for Wireless Communications” and several novel PMA antennas have been shown, each of which has addressed a specific issue for current and future wireless communication systems, in terms of SWB coverage, band-rejection, frequency reconfigurable and channel capacity. Accordingly, these antenna designs could be good candidates for implementation in a wide range of wireless communication applications.

In Chapter 3, a compact planar monopole antenna with SWB performance has been presented, for use in current and future wireless communication

systems. The simple planar UWB circular monopole antenna with microstip-fed has firstly designed to investigate the operation mechanism. It has found that the resonate frequency and impedance bandwidth of the circular monopole antenna are mainly affected by the feeding gap and the width of the ground plane. The impedance bandwidth of the proposed antenna has then significantly improved by implementing a pair of ears on the top of the radiator and a top-corner rounded ground plane with a one-step staircase slot compared to a conventional circular monopole antenna. As a result, an antenna with SWB performance from 2 to 200 GHz with an impedance bandwidth of 100:1 for a return loss greater than 10 dB has achieved. The designed antenna has a simple configuration and easy for fabrication.

In Chapter 4, a compact planar UWB monopole antenna has been proposed to achieve quintuple-band-notched characteristics. The quintuple-band-notched function has achieved by embedding five m-shaped resonators into the radiator, feedline, and ground plane. The integrated slots can provide tuning flexibility for a different desired notch frequency. In the frequency domain, the measured simulated return loss of the antenna agrees well. The proposed antenna is able to operate from 2.24 GHz to 10.8 GHz for $|S_{11}| < -10$ dB with excellent levels of rejection in the frequency bands of 2.3 to 2.7 GHz, 3.2 to 3.7 GHz, 5.1 to 6.1 GHz, 7.2 to 7.7 GHz and 8.1 to 8.74 GHz with gain suppression of 15, 14, 16, 9 and 6 dB, respectively. In addition, the surface current distributions and transmission line models are employed. Good radiation patterns and gain values are obtained. In the time domain, the fidelity has used to evaluate the time-domain performance of the antennas. The results have shown that the quintuple-band-notched antenna has the fidelity of more than 85%. This indicates that introduction of band-notched feature has limited effect on the time-domain performance of the antenna.

In Chapter 5, a UWB monopole antenna with reconfigurable band-notched characteristics has been presented. The band rejection has realised by incorporating two CSRR resonators on the radiator element. To achieve the reconfigurability, the switches have added to the CSRR structures. The measured and simulated results have shown that the proposed antenna can operate at different switching states including a UWB state, single and dual band-notched states with good rejection behaviours. Good radiation patterns and gain values have also been obtained for different switching states. The performances have verified the proposed design concept.

In Chapter 6, a UWB-MIMO antenna with size of 45 mm by 60 mm has been proposed for wireless applications. A trident-like slot has introduced and inserted on the common ground plane to enhance the isolation over a wideband. The simulated and measured results have shown that the proposed antenna can operate from 2.3 to 12 GHz for $|S_{11}| < -10$ dB with mutual coupling coefficient of less than -15 dB. To better understand the underlying mechanism, the surface current distributions and an equivalent circuit have employed. A comprehensive parametric study has also carried out to optimise the coupling element. The antenna patterns and MIMO characteristics have been studied. The results have shown that the MIMO antenna can achieve a envelop correlation coefficient of less than 0.01 across the bands of interest. This indicates that the proposed UWB-MIMO antenna could be a very good candidate for wireless applications.

7.2 Future Work

Regards to the conclusions drawn and the limitations of the work presented, future work can be carried out in the following areas:

- Investigation on the integration of real RF switches for band-rejection re-configurability, e.g. PIN diodes and Microelectromechanical Systems (MEMS) switches. While the tunable band-notched antenna designed could be realized using varactor diodes. However, there are still many potential challenges ahead such as how to bias the RF switches and varactor diodes without affecting the antenna performance and to minimize the effects on the antenna impedance matching and efficiency.
- The antenna miniaturisation is always the demand due to the fact that the future wireless devices and systems are becoming more compact. How to further significantly reduce the size of the MIMO antenna, while still maintaining the UWB performance and high isolation between the two closely-packed elements, are still need to be investigated.
- In the design of electrical small monopole antennas, the measurement results very often do not agree well with the simulation ones, particular at the lower frequencies. This is may be due to that in the measurement, a coaxial cable with the SMA connector is always used, while in the simulation, the signal is fed directly to the input port of the antenna without using any cables. Thus, it is interesting to see cable effects on the antenna performance.

END